

Cover Page



Universiteit Leiden



The handle <http://hdl.handle.net/1887/69726> holds various files of this Leiden University dissertation.

**Author:** Azadi Chegeni, F.

**Title:** Towards in-cell structural study of light-harvesting complexes : an investigation with MAS-NMR

**Issue Date:** 2019-03-12

# Towards *in-cell* structural study of light-harvesting complexes

An investigation with MAS-NMR

Fatemeh Azadi Chegeni

**ISBN:** 978-94-6380-239-0

**Printed by:** Proefschrift Maken || [www.proefschriftmaken.nl](http://www.proefschriftmaken.nl)

Cover designed by Fatemeh Azadi Chegeni

This research was financed by Leiden University, and a CW-VIDI grant of the Netherlands Organization of Scientific Research (NWO) under grant nr. 723.012.103 (granted to Anjali Pandit). The use of ultrahigh-field Nuclear Magnetic Resonance facility was sponsored by uNMR-NL, an NWO-funded National Roadmap Large-Scale Facility of the Netherlands (grant number: 184.032.207).

# **Towards *in-cell* structural study of light-harvesting complexes**

**An investigation with MAS-NMR**

**PROEFSCHRIFT**

Ter verkrijging van  
de graad van Doctor aan de Universiteit Leiden,  
op gezag van de Rector Magnificus Prof. mr. C. J. J. M. Stolker,  
volgens besluit van het College voor Promoties te  
verdedigen op dinsdag 12 maart 2019  
klokke 13:45 uur

door

**Fatemeh Azadi Chegeni**  
**Geboren te Khorram Abad, Iran**



## Promotiecommissie

---

Promotor: Prof. dr. H. J. M. de Groot  
Co-promotor: Dr. Anjali Pandit

Overige leden: Prof. dr. H. Overkleeft  
Prof. dr. H. Kirchhoff  
Prof. dr. M. Baldus  
Prof. dr. A. Matysik  
Prof. dr. M. van der Stelt

**FOR MY PARENTS**



## Table of contents

---

### Abbreviations

<b>Chapter 1</b>	Introduction & Methodological background	<b>1</b>
<b>Chapter 2</b>	Protein & lipid dynamics in photosynthetic thylakoid membranes investigated by in-situ NMR	<b>23</b>
<b>Chapter 3</b>	Conformational dynamics of photosynthetic light-harvesting complex II in native thylakoid membranes	<b>49</b>
<b>Chapter 4</b>	Conformational dynamics of zeaxanthin-binding LHCII in a lipid membrane	<b>77</b>
<b>Chapter 5</b>	In-vivo NMR as a tool for probing molecular structure and dynamics in intact <i>Chlamydomonas reinhardtii</i> cells	<b>95</b>
<b>Chapter 6</b>	General Discussion and future prospects	<b>115</b>
<b>Appendices</b>	Summary	<b>122</b>
	Samenvatting	<b>125</b>
	Curriculum vitae	<b>128</b>
	Publications	<b>129</b>
	Acknowledgement	<b>130</b>

## Abbreviations

---

Car	Carotenoid
Chl <i>a</i>	Chlorophyll <i>a</i>
Chl <i>b</i>	Chlorophyll <i>b</i>
CP	Cross polarization
<i>Cr.</i>	<i>Chlamydomonas reinhardtii</i>
CSA	Chemical Shielding Anisotropy
Cyt <i>b<sub>6</sub>f</i>	Cytochrome- <i>b<sub>6</sub>f</i> complex
DGDG	DiGalactosylDiacylGlycerol
DGTS	DiacylGlycerylTrimethylhomo-Ser
DP	Direct Polarization
FA	Fatty Acid
INEPT	Insensitive Nuclei Enhanced by Polarization Transfer
LH2	Light Harvesting 2
LHCI	Light Harvesting Complex I
LHCII	Light Harvesting Complex II
MAS	Magic Angle Spinning
MD	Molecular Dynamics
MGDG	MonoGalactosylDiacylGlycerol
Neo	Neoxanthin
NMR	Nuclear Magnetic Resonance
NPQ	Non-Photochemical Quenching
PARIS	Phase-Alternated Recoupling Irradiation Scheme
PE	PhosphatidylEthanolamine
PG	Phosphatidyl-Glycerol
Photo-CIDNP	Photo-Chemical Induced Nuclear Polarization
PQ	Plastoquinone
PQH <sub>2</sub>	Plastoquinol
PSI	Photosystem I
PSII	Photosystem II
SQDG	SulfoQuinovosylDiacylGlycerol
SSNMR	Solid State NMR
TAP	Tris-Acetate Phosphate
TOBSY	TOtal through Bond correlation Spectroscopy
Vio	Violaxanthin
ZE	Zeaxanthin Epoxidase
Zea	Zeaxanthin

# CHAPTER 1

---

**Introduction & Methodological background**

---

## General introduction

---

Current energy resources, fossil fuels, make that mankind faces a number of challenges including finite resources that will eventually dwindle, rising prices and environmental damages such as global warming and air pollution. In this light, development of renewable energy sources has drawn much attention in recent years.

As long as the sun is shining, solar energy reaching the earth is the cleanest source of renewable energy. Over the last decades a wide array of techniques such as photovoltaic cells have been developed to harvest the sunlight and convert it to power. However, nature has developed an efficient way of harnessing the solar energy for billions of years. Photosynthesis is the primary process that sustains the vast majority of life on earth. Photosynthetic organisms convert light energy through a complicated series of events into biochemical energy. For decades, researchers have been trying to improve this fundamental process and many biophysical and molecular biological techniques have been employed to characterize and manipulate different elements of photosynthetic organisms. Recent advances in photosynthesis research at the molecular level promise new routes for increasing biomass production <sup>1</sup>.

Harvesting light is the first step in the process of solar energy conversion that is carried out by antenna complexes of all photosynthetic organisms. Light harvesting antennas of plants and algae are flexible, which enable them to adapt to light fluctuations avoiding photodamages. Their antennas can switch into a photoprotective state that dissipates the incoming sunlight, which protects against light stress but reduces photosynthetic efficiency. To date, by combination of several spectroscopic methods and high resolution crystallography, our understanding of regulation of light harvesting has improved. However, due to the lack of an atomistic insight into the conformational dynamics of antenna complexes there are yet many questions concerning the molecular mechanisms of photo protection that have remained unanswered.

This thesis applies solid-state nuclear magnetic resonance (NMR) spectroscopy as an emerging technique for *in-situ* characterization of the conformational dynamics of photosynthetic light-harvesting complexes at atomistic level. Furthermore, this study paves the way for the use of solid state NMR for *in-situ* and *in-cell* detection of molecular dynamics of photosynthetic membrane constituents.

## *Chlamydomonas reinhardtii*

Microalgae are a group of eukaryotic photosynthetic organisms that recently attract a widespread attention for new generation of biofuels. *Chlamydomonas reinhardtii* (*Cr.*) is an ancient unicellular microalgae which has occupied the earth fresh water and soil over one billion years. High adaptability of *Cr.* to different conditions makes it a unique model system for research on many fundamental questions of photosynthesis. Manipulation of *Cr.* genes is relatively easy and the cells grow quickly in organic carbon sources under controlled environmental conditions while maintaining the function of the photosynthetic apparatus. *Cr.* cells are about 10 micrometers long and have two flagella's for mobility, several mitochondria, a single chloroplast that photosynthetic apparatus reside in, a cell wall made of glycoproteins and an eye spot to sense light direction and intensity <sup>2</sup>. A schematic picture of a *Chlamydomonas* cell is presented in figure 1.

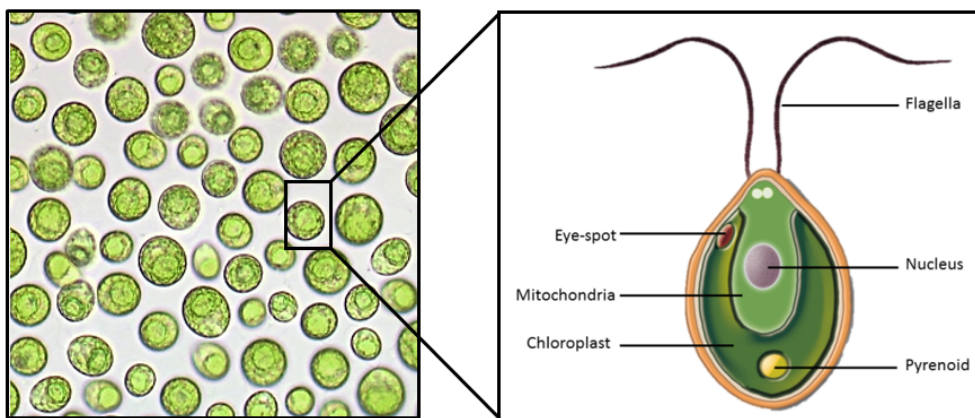
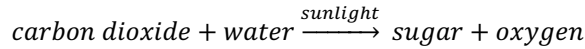


**Figure 1.** *Chlamydomonas reinhardtii* cell illustration (www.pt.pngtree.com).

## Thylakoid membrane architecture

Oxygenic photosynthesis is the process by which plants, algae and cyanobacteria use solar energy to synthesis biomass from carbon dioxide and produce oxygen as a waste product. The processes of oxygenic photosynthesis evolved approximately 2.5 billion years ago and produce all the oxygen on earth. The general reaction of oxygenic photosynthesis can be indicated by the following simplified equation:





All components of the photosynthetic apparatus that are necessary for the photosynthesis reside in the chloroplast of plant and algae, in cylindrical shaped sheets known as thylakoid membranes. Thylakoid membranes are differentiated into two membrane domains, the cylindrical stacked structures known as grana and the single-membrane regions called stroma lamellae (see figure 2).

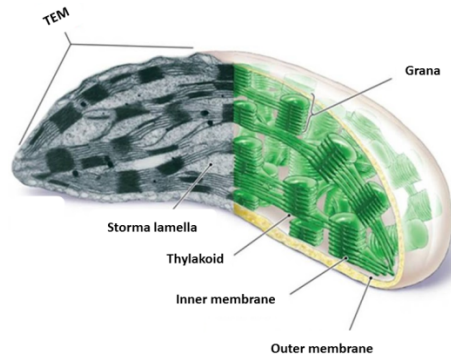


**Figure 2.** Schematic illustration of a chloroplast ([www.biologyexams4u.com](http://www.biologyexams4u.com)).

Photosynthesis takes place in two stages. In the light reactions, solar energy is harvested and stored in the form of ATP and NADPH and oxygen is released as a byproduct. In the dark reaction, ATP and NADPH drive sugar synthesis. There are four main membrane complexes that drive the light reaction in thylakoids: antenna-photosystem II (PSII-LHCII) and antenna-photosystem I (PSI-LHCI) protein-pigment super-complexes, cytochrome-*b<sub>6</sub>f* complex (Cyt *b<sub>6</sub>f*) and ATP-synthase complex. Figure 3 presents a schematic view of the electron transport through the thylakoid membrane. The process starts with light harvesting complexes of PSII, where light energy is absorbed by chlorophyll molecules and transferred via a series of carriers to the reaction center of PSII to induce the excitation of a special pair of chlorophylls (P680 to P680\*). This creates a charge-separated state and the electron is transferred on to the chain of electron carriers. The P680\* now is a potential electron acceptor and takes up an electron extracted from water, while protons are released to the thylakoid lumen. At this stage oxygen is produced as a byproduct. The electron is first transferred to a plastoquinone (PQ) in the PSII and after two turnovers, PQ is fully reduced to plastoquinol (PQH<sub>2</sub>). The plastoquinol then diffuses into the thylakoid membrane. Via the plastoquinol, electrons are transferred to Cyt *b<sub>6</sub>f* and then to plastocyanin via a cycle of reactions (Q-cycle) and finally to PSI. Similarly to PSII, harvested

solar energy is transferred to the reaction center of PSI and excites the special pair of chlorophylls, P700, to P700\*. A charge-separated state is created in P700 and the transferred electron reduces the protein ferredoxin in the stroma and from the ferredoxin, electrons are finally stabilized by reduction of NADP<sup>+</sup> to NADPH. The electrons from plastocyanin are used to reduce the P700<sup>+</sup>. During the electron transfer process, protons are also released into the thylakoid lumen. Finally, charge separation and electron transfer in thylakoid membranes lead to formation of a proton gradient which is used to drive ATP-synthase and produce ATP. The last stage of photosynthesis occurs in the dark via the Calvin-cycle in which the generated ATP and NADPH is used to convert CO<sub>2</sub> to carbohydrates <sup>3</sup>.

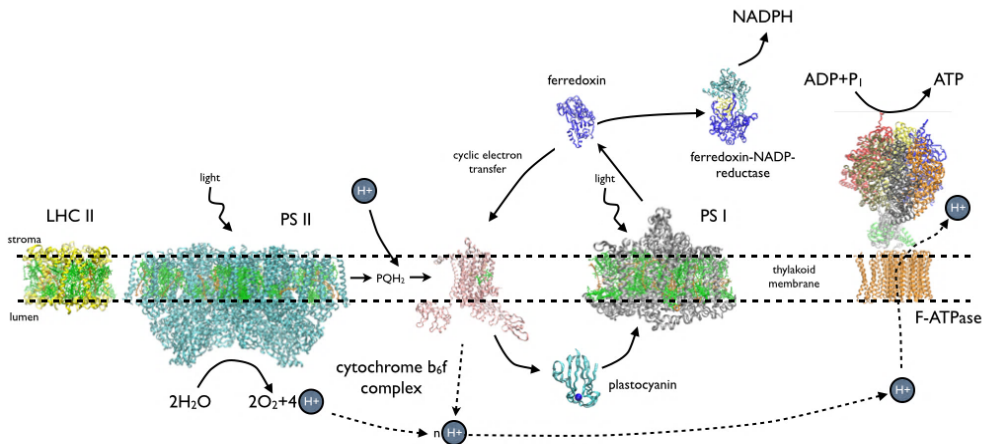


**Figure 3.** Process of photosynthesis in the thylakoid membrane and major protein complexes involved.

## Light-harvesting complexes

In higher plants and algae, PSI-LHCI and PSII-LHCII super complexes consist of two parts: a core complex that contains all the cofactors of the electron transport chain, and the outer antenna complexes (LHCs) to capture light energy and transfer excitation to the reaction center <sup>4-5</sup>. Considerable effort has been made to isolate PSI and PSII from a wide range of organisms in order to get more insight into their molecular structure and function.

The available X-ray structure of PSI from cyanobacteria at 2.5 Å provides the location of the individual subunits and cofactors together with information on protein-cofactor interactions. According to the X-ray structure, PSI forms as a trimer and the core complex of PSI is composed of 14 protein subunits binding 90 chlorophyll *a* (Chl *a*) and 22 carotenoids (Car) <sup>6</sup>. The outer antenna, known as light-harvesting complex I (LHCI), encoded by 4 genes (Lhc1-4) and also

coordinates cofactors <sup>4, 7</sup>. Although the core complex of PSI in cyanobacteria, higher plants and green algae is highly conserved <sup>8-12</sup>, the outer antenna (LHCI) of *Chlamydomonas reinhardtii* (*Cr.*) shows a significant difference in the number of genes that encode for the LHC polypeptides <sup>13-14</sup>. LHCI of *Cr.* is composed of nine Lhca proteins (Lhca1–9) with different spectroscopic properties, located on one side of the core in a double half ring arrangement <sup>15</sup>. However the light harvesting complex of PSI in higher plants consists of 4 (Lhca1-4) genes on one side of the core in the form of a single half ring <sup>16</sup>.

Several atomic structures of PSII are also available with resolutions ranging from 3.8 to 1.9 Å <sup>17-19</sup> and recently a high-resolution cryo-EM structure of a spinach PSII-LHCII supercomplex at 3.2 Å has become available <sup>20</sup> (see figure 4). According to the X-ray and cryo-EM structures, several major LHCII trimers and a few minor monomer antennas are associated with the two sides of dimeric PSII. Similar to PSI, the core complex of PSII is also conserved between different photosynthetic organisms <sup>5</sup>. In higher plants, the outer antenna of PSII is composed of three Lhcb (Lhcb1-3) genes which encode the major trimeric antenna complexes and three genes (Lhcb4-6) forming the minor antennas. Minor antennas of PSII form as monomers and depend on their molecular weight are differentiated as CP29, CP26 and CP24. In *Cr.* nine different genes (Lhcbm1-9) encode the protein polypeptides. CP24 minor antenna is lacking in the genome of *Cr.* algae while CP29 and CP26 are present. The LHCII trimers consist of isomers and the pigment binding sites are conserved among all sequences. However, different polypeptides have specialized roles in photoprotection, for example, among the most abundant polypeptides, Lhcbm1 is involved in excess energy dissipation <sup>21</sup>, whereas Lhcbm2 and Lhcbm7 are essential for state transitions where LHCII dislocate from PSII to PSI in order to reduce the light stress on PSII <sup>22</sup>.

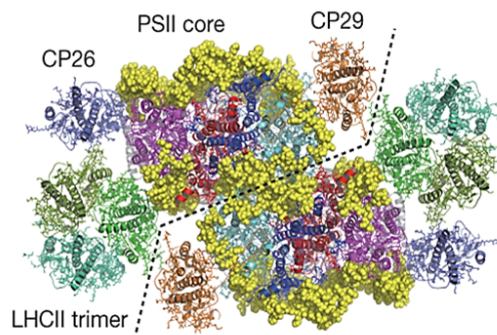


**Figure 4.** Top view of LHCII-PSII supercomplex resolved at 3.2 Å by cryo-electron microscopy <sup>20</sup>.

## Light harvesting complex II (LHCII)

Extensive efforts have been made to uncover the molecular structure of the major antenna complex LHCII. The first structure of LHCII from pea has been determined by electron crystallography at 3.4 Å resolution<sup>23</sup>. This model revealed three transmembrane  $\alpha$ -helices (helices A, B and C) and a short helix (helix D), 12 chlorophylls and two carotenoids. A more detailed structural picture of LHCII is essential to have a better understanding of the functional mechanism of LHCII. High-resolution X-ray crystallography provided a more detailed structure of protein and cofactors at 2.5 Å<sup>24</sup>. Each LHCII monomeric structure is characterized by three membrane-spanning helices (helix A-C) and two short helical fragments (helix D and E), an N-terminal stretch and C-tail, and segments containing large, water-exposed loops. Figure 5 (A-C) shows the (Lhcb1 based) monomeric protein structure of LHCII, the pigment-protein structure, and a top view of the trimeric structure of LHCII. Each monomer subunit binds many pigments including 8 Chl *a*, 6 Chl *b*, 2 lutein, neoxanthin and one xanthophyll-cycle carotenoid. Six Chls are close to the luminal side of the membrane, while the remaining chlorophylls are close to the stromal side. The binding of the Chls to the proteins involves amino acid side chains or backbones that coordinate the central Mg of the Chls. In addition, water molecules and lipids are involved in the binding of chlorophylls. The orientation of the pigments with respect to each other in the LHCII complex is presented in figure 6.

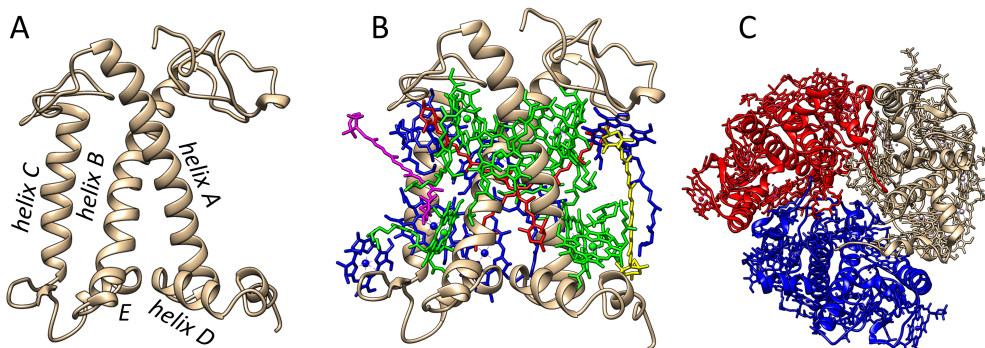


**Figure 5.** A: LHCII protein structure, B: LHCII structure including the pigments, C: top view of a trimeric LHCII complex.

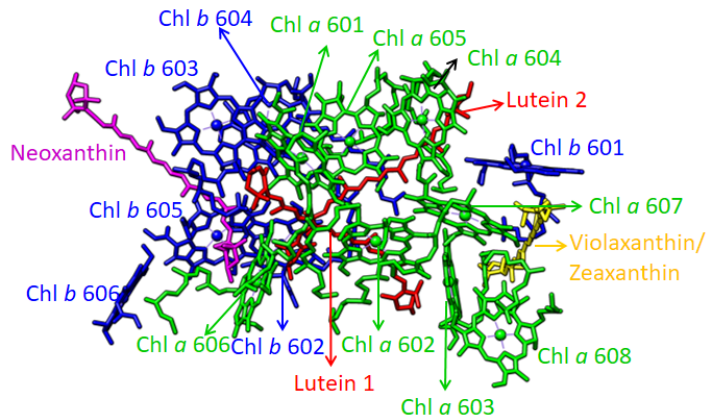


**Figure 6.** Orientation and numbering of pigments in each monomeric LHCII according to the crystal structure of LHCII spinach (*2bhw*). Chl *a* molecules are presented in green, Chl *b* in blue, lutein in red, neoxanthin in purple and violaxanthin/zeaxanthin in yellow.

## Photo-protection

Although light is essential for growth of photosynthetic organisms, fluctuation in light intensity could lead to over-excitation of the photosystems, resulting in photo oxidative damage. In excess light, plant and algae can regulate light harvesting using different photo protective mechanisms such as rearranging the light harvesting complexes, thermally dissipating excess light energy and altering electron transport <sup>25</sup>.

Photoprotective processes are highly regulated by thylakoid membrane responses, the conformational flexibility of proteins, as well as the interplay of the complexes within a dynamic thylakoid membrane environment <sup>26-27</sup>. In particular, light-harvesting antenna complexes (LHCs) can adapt to light harvesting, or form dissipative photo protective states as a mechanism to regulate photosynthesis under light stress. The photo-protective feedback response is activated by acidification of the thylakoid luminal environment as a result of over-excitation in a process called non-photochemical quenching (NPQ) <sup>28</sup>. Photo-protection and NPQ have a major influence for photosynthetic productivity and it was recently demonstrated that manipulation of the photo protective response could give a remarkable 15-20% increase of biomass yields in the field <sup>1</sup>.

So far numerous efforts have been made to understand the photo-protective mechanisms performed by photosynthetic organisms. Depending on the time scale of the induction and relaxation four types of NPQ processes can be

distinguished: energy dependent quenching (qE)<sup>29</sup>, state transition dependent quenching (qT)<sup>30</sup>, Zeaxanthin (Zea) dependent quenching (qZ)<sup>31</sup> and photo inhibitory quenching (qI)<sup>32</sup> see figure 7. Different NPQ processes are briefly explained as follows:

Due to the photo-induced damage of the reaction center in PSII, the energy conversion efficiency and photosynthesis capacity is reduced by photosynthetic organisms. This process is known as photoinhibition or qI. qI, the slowest NPQ process, is a reversible process and it is responsible for long, continuous thermal dissipation of excitations that might take hours<sup>33</sup>. qZ is induced on a time scale of minutes and it is related to the acidification of the thylakoid lumen under high light stress, which activates violaxanthin (Vio) de-epoxidase enzymes (VDE) that convert Vio to Zea via the reversible xanthophyll cycle<sup>3</sup>. The exact role of Zea is still under debate, However, it has been shown that zeaxanthin enhances the NPQ in the thylakoid membrane<sup>34</sup>. qT involves the phosphorylation of LHCII antenna complexes and reversible membrane state transitions where LHCII complexes detach from PSII and associate with PSI to balance the activity of PSII and PSI and reduce the light stress on PSII. This process is also induced within minutes<sup>30</sup>. The last NPQ component, qE, is the most rapid component of NPQ that is believed to dissipate the excess light energy by reducing the excited-state life times of the antenna chlorophylls, preventing the thylakoid membrane from over-excitation. qE is activated upon lumen acidification via a pH-sensing protein-pigment complex known as LHCSR in algae and PsbS in plants. qE also prevents the over reduction of electron carriers in the plastoquinone by decreasing the rate of singlet oxygen formation<sup>29</sup>.

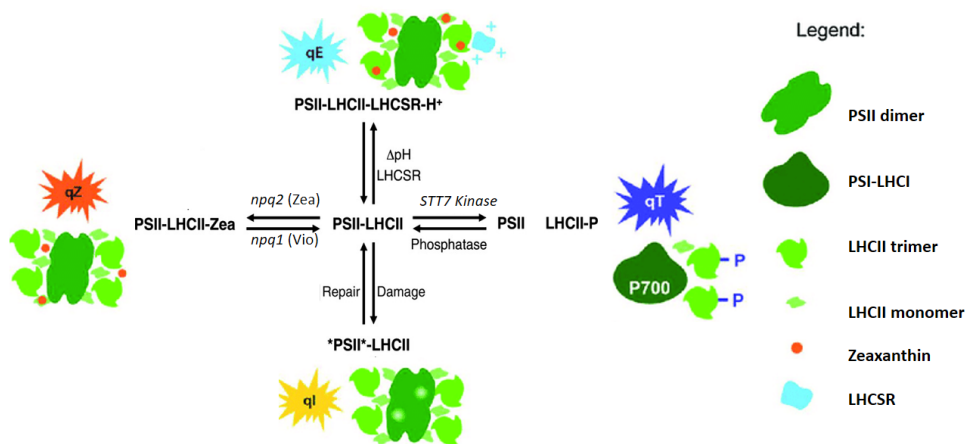


**Figure 7.** Schematic illustration of non-photochemical quenching in *Chlamydomonas reinhardtii* (Cr.) adapted from<sup>25, 35</sup> (Erikson 2015 and Malnoe 2018).

It is widely believed that the quenching mechanism is also active at the level of isolated light harvesting complexes and several quenching sites have been proposed <sup>25, 35</sup>. However the conformational changes associated with the quenching switch of the light harvesting complexes were not resolved.

pH-sensitive proteins like PsbS and LHCSR in plants and algae are suggested to play a role in inducing NPQ by protonation of their pH-sensing domains in membranes and isolated complexes <sup>36-38</sup>. Protonation of the pH-sensor proteins promotes a conformational switch of the antenna to a quenched state. The effect of Zea in quenching has been investigated extensively in plants and green algae and it has been proposed that Zea might be a direct quencher of excitations forming charge-transfer states <sup>39</sup>. Accumulation of Zea at the membrane level was also suggested to protect polyunsaturated lipids during light stress <sup>40</sup>. According to Horton & Ruban *et al*, Zea might have an allosteric effect owing to its hydrophobicity compared with Vio <sup>41</sup>. It might promote a conformational change in LHCs that stabilizes the quenched state in combination with low pH <sup>42</sup>. However Croce *et al*, showed that just the effect of Zea binding and low pH is not enough to create a quenched state and they propose that the important role of Zea lies in its location at the interfaces between complexes <sup>34</sup>. Moreover, based on the Chl-Car interactions, different quenching sites regarding the mechanism of quenching have been proposed <sup>43-47</sup>.

Up to date, various methods have been introduced to understand the molecular mechanisms that regulate photosynthesis. However until now, no structure-based methods have been presented that could provide a direct view of different photosynthetic molecular components inside the native membrane environments. Solid-state NMR spectroscopy has shown to be a powerful tool for atomistic detection of different molecular sites of membrane proteins even in native membranes or cellular environments <sup>48-58</sup>. Application of solid state NMR to photosynthetic systems and a methodological background of the method, which have been used in this thesis are discussed in the following sections.

## Application of solid-state NMR in photosynthesis research

---

During the past decades, X-ray crystallography has been the major technique to resolve the structure of photosynthetic membrane proteins <sup>59-60</sup>. However, detecting the atomistic details of structure-function interaction in flexible environments remains a daunting task <sup>61</sup>. Solid state NMR has become rapidly an emerging technique for atomistic detection of the structure and dynamics of photosynthetic membrane proteins.



Solid-state NMR spectroscopy has contributed to enhance the understanding of light harvesting, charge separation and photo protection in photosynthesis. A sequence specific assignment of protein sites has been obtained for light harvesting complex 2 of *Rhodospseudomonas acidophila* (LH2) providing the secondary structure to complement the crystallographic data. Later on, solid state NMR provided an accurate prediction of pigment electronic structures in the ground state of *Rhodospirillum Acidophila* LH1 and LH2 <sup>58</sup>. The structural and functional properties of heterogeneous chlorosome antenna of green bacteria were studied by solid state NMR and cryo-EM, introducing a model system for self-assembled artificial antenna <sup>62-63</sup>. Solid state NMR studies on LHCII demonstrated that the LHCII conformational switch involves rearrangements of the Arg residue in the stromal loop <sup>64</sup> and the LHCII switch into a photo-protective state is accompanied by changes in the Chl *a* ground-state electronic structures <sup>65</sup> which were explained by altered Chl-lutein interactions <sup>66</sup>.

Furthermore, the photo-chemical induced nuclear polarization (photo-CIDNP) effect has been observed for photosynthetic reaction centers of different bacterial and plant species, revealing the ground-state electronic structures of the special pair (B)Chls <sup>62</sup>. The strong enhancement of the special-pair NMR signals owing to the CIDNP effect even allowed their detection in intact photosynthetic cells <sup>67</sup>.

## Methodological background of solid-state NMR

---

### Introduction to solid-state NMR

The origin of NMR spectroscopy lies in studying the interactions between nuclear spins ( $I$ ) and an external magnetic field ( $B_0$ ). However, there are various external and intrinsic nuclear spin interactions either between nuclear spins and the external magnetic field, or among spins and the environment. A general Hamiltonian describing the NMR interaction is given by the following equation <sup>68</sup>.

$$H = H_0 + H_{cs} + H_D + H_J + \dots, \quad (1)$$

where  $H_0$  stands for the Zeeman interaction,  $H_{cs}$  is the chemical shielding,  $H_D$  presents the dipolar coupling and  $H_J$  describes the scalar coupling.

The Zeeman interaction (the interaction between nuclear spin and external magnetic field) is given by

$$H_0 = -\gamma\hbar I \cdot B_0, \quad (2)$$



where  $\gamma$  is the gyromagnetic ratio and  $B_0$  the strength of external magnetic field. The Zeeman interaction is in the order of  $10^7$ - $10^9$  Hz and it is the strongest interaction in NMR <sup>69</sup>. However the external magnetic field is not the same as the field that a nucleus locally feels. When atoms are placed in a strong external magnetic field, electrons start to circulate in their orbitals which results in the production of small local magnetic fields ( $B_{loc}$ ) in order of few parts per million (ppm). Therefore, each nucleus experiences an effective magnetic field known as  $B_{eff} = B_0 - B_{loc}$ , which results in a change of the resonance frequency. The interaction of spins with a local magnetic field is known as chemical shielding and can be described as

$$H_{CS} = -\gamma\hbar\sigma I_z B_0 , \quad (3)$$

where  $I_z$  is the z-component of the spin operator, and  $\sigma$  is the chemical shielding tensor and implies the anisotropic character of this interaction. Due to the fact that the charge distribution around a nucleus is rarely spherically symmetric a  $3 \times 3$  matrix is used to describe the orientation dependence of the chemical shift or chemical shielding anisotropy (CSA) (for detailed information see <sup>68</sup>). In solid and solid like materials CSA results in a line broadening compared to materials dissolved in liquid.

The magnetic moments of two spins can be described as two magnetic bars interacting with each other. These interactions are several orders of magnitude smaller than the Zeeman interaction ( $10^3$ - $10^5$  Hz) and could be either through space or through bond. Through space interactions depend on the distance between two spins and are known as dipolar interactions and described by the following equation

$$H_D = H_{homo} + H_{hetero} , \quad (4)$$

where  $H_{homo}$  is the dipolar interaction between the same type of nuclei and  $H_{hetero}$  stands for the interaction between the magnetic moments of two spins  $I$  and  $S$ . The corresponding quantum operator for homonuclear and heteronuclear dipolar interactions are given by

$$H_{hetero} = -\frac{\mu_0}{4\pi} \hbar \sum_i \sum_j \frac{\gamma^I \gamma^S}{r_{ij}^3} \frac{1}{2} (3 \cos^2 \theta_{ij} - 1) 2I_z^i S_z^j , \quad (5)$$

$$H_{homo} = -\frac{\mu_0}{4\pi} \hbar \sum_i \sum_j \frac{\gamma^2}{r_{ij}^3} \frac{1}{2} (3 \cos^2 \theta_{ij} - 1) (3I_z^i I_z^j - I^i \cdot I^j) , \quad (6)$$

where  $\gamma^i$  and  $\gamma^s$  are the gyromagnetic ratio of spin  $I$  and  $S$ ,  $r_{ij}$  represents the internuclear distance between the nuclei  $i$  and  $j$ ,  $\theta_{ij}$  stands for the orientation of

the vector connecting two spins with respect to the external magnetic field and  $I_z^i$  and  $S_z^j$  are the z components of the nuclear spin of  $I$  and  $S$  <sup>70</sup>.

Through bond interactions known as scalar or  $J$ -couplings are small field independent interactions in the order of 1-10<sup>3</sup> Hz. the  $J$ -coupling is very sensitive to the changes in molecular structure, providing detailed structural information of the materials. Since these interactions are usually much smaller than the other interactions, they are often negligible in NMR spectra of solids. However, in solid like materials like membrane proteins,  $J$ -interactions play an important role that enable detection of mobile sites. The Hamiltonian for  $J$ -couplings is often given by

$$H_j = 2\pi\hbar J_{jk} \left( I_j^{\vec{}} \cdot I_k^{\vec{}} \right), \quad (7)$$

where  $J_{jk}$  is the isotropic  $J$ -coupling.

### Magic angle spinning (MAS)

In soluble materials, rapid molecular tumbling results in averaging the anisotropy and dipolar interactions and consequently sharp resonances are observed <sup>68</sup>. However for large protein complexes or solid materials, the molecular tumbling is significantly reduced leading to line broadening. In order to reduce the line width and spectral overlap in solid state NMR, Magic Angle Spinning (MAS) technique is employed. MAS NMR consists of spinning the sample at an angle  $\theta_m$  with respect to the external magnetic field, by which anisotropic contributions to the dipolar and chemical anisotropy interactions that are scaled by the factor of  $3\cos^2\theta - 1$ , become time dependent and are averaged to zero. As a result, a sharp peak can be observed while the angular dependent anisotropic contributions are spun away. Equation 8 defines the magic angle,

$$3\cos^2\theta_m - 1 = 0, \quad (8)$$

where  $\theta_m = 54.74$  is the angle with respect to the external magnetic field  $B_0$ .

### The dynamic spectral-editing method

---

As mentioned in previous sections, the NMR sensitivity depends on the gyromagnetic ratio ( $\gamma$ ) of the nucleus. Therefore, in order to detect nuclei with small gyromagnetic ratio, specific polarization transfer methods should be considered. In large systems, such as proteins, proton NMR results in spectral

crowding and ambiguous assignments.  $^{13}\text{C}$  spectra with large spectral width of 200 ppm help to reduce spectral crowding, however due to the small  $\gamma_{\text{C}}$  which is  $\frac{1}{4}$  of  $\gamma_{\text{H}}$  and low natural abundance of  $^{13}\text{C}$ ,  $^{13}\text{C}$  NMR detection poses sensitivity problems.

The dynamic spectral-editing method consists of a combination of  $^{13}\text{C}$  polarization-transfer solid-state NMR experiments. In  $^1\text{H}$ - $^{13}\text{C}$  polarization-transfer NMR, polarization is transferred from abundant  $^1\text{H}$  nuclei with high gyromagnetic ratio ( $\gamma$ ) to low sensitivity  $^{13}\text{C}$  nuclei with low  $\gamma$  and the resulting  $^{13}\text{C}$  spectrum is intensity enhanced, depending on the polarization-transfer efficiencies. The polarization transfer occurs via heteronuclear couplings between  $^{13}\text{C}$  and  $^1\text{H}$  nuclei, which are dipolar and scalar ( $J$ -) couplings. In cross polarization (CP)-based experiments <sup>71</sup>, polarization is transferred via dipolar couplings. For mobile molecules, due to their fast random tumbling, dipolar couplings are averaged to zero within the contact time and consequently these components are filtered out from CP-based spectra. CP therefore acts as a dynamic filter that selectively probes rigid molecules. In INEPT-based experiments <sup>72</sup> polarization is transferred via  $J$ -couplings that are not affected by bond re-orientation. INEPT is effective if the transverse ( $T_2$ ) relaxation times of the protons and carbons are sufficiently slow compared to the polarization transfer times. This is not the case for rigid molecules and therefore INEPT selectively probes mobile molecules <sup>73</sup>. With direct polarization (DP) <sup>74</sup>,  $^{13}\text{C}$  are directly excited by applying a  $90^\circ$  pulse to the  $^{13}\text{C}$  carbons. DP provides a  $^{13}\text{C}$  NMR spectrum of all molecular constituents. Figure 8 illustrates the efficiency of DP, INEPT and CP in different dynamics regimes.

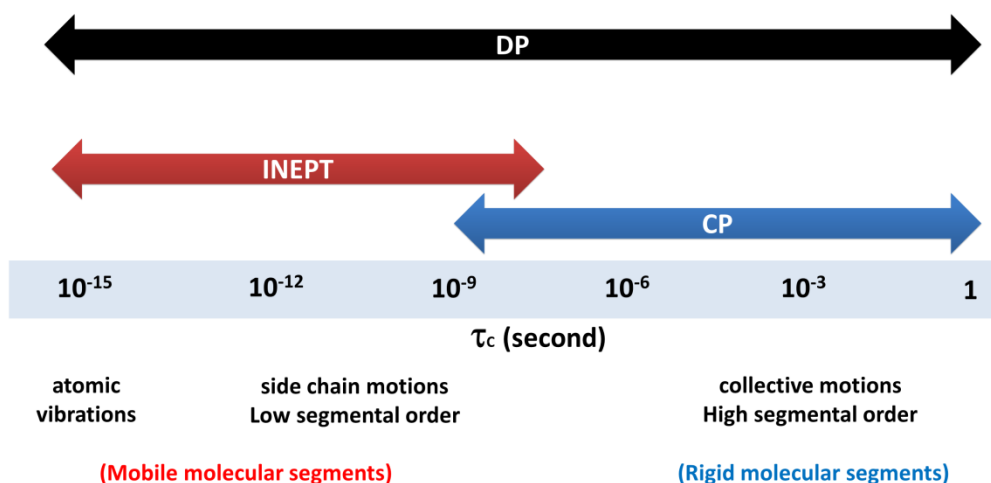


**Figure 8.** Schematic illustration of dynamic ranges where the DP, CP and INEPT pulse experiments are effective.

## Cross polarization

In solid-state NMR, cross polarization (CP) is the building block of many pulse sequences. It was introduced in 1962 by Hartmann and Hahn for the static conditions. When a rare spin is in proximity of abundant nuclei, during a contact time polarization can be transferred from abundant nuclei to rare nuclei through strong heteronuclear couplings (see equation 5). In this method, after a  $90^\circ$  pulse, radio frequency pulses  $B_{1I}$  and  $B_{1S}$  are applied to different frequency channels, for instance  $^1\text{H}$  and  $^{13}\text{C}$ . For polarization transfer to occur, the nutation frequencies of the spin  $I$  and  $S$  must be identical and fulfil the Hartman-Hahn condition <sup>75</sup>. Equation 8 presents the Hartman-Hahn condition at static conditions.

$$|\omega_{1I}| = |\omega_{1S}|, \quad (9)$$

where  $\omega_{1I} = -\gamma_{1I}B_{1I}$  and  $\omega_{1S} = -\gamma_{1S}B_{1S}$ .

The enhanced magnetization of the rare nuclei can hence be detected while the abundant nuclei are decoupled. The maximum enhancement of sensitivity is proportional to  $\gamma_{1I}/\gamma_{1S}$ . Figure 9 presents the schematics of the Hartman-Hahn condition and the basic pulse sequence of the CP experiment.

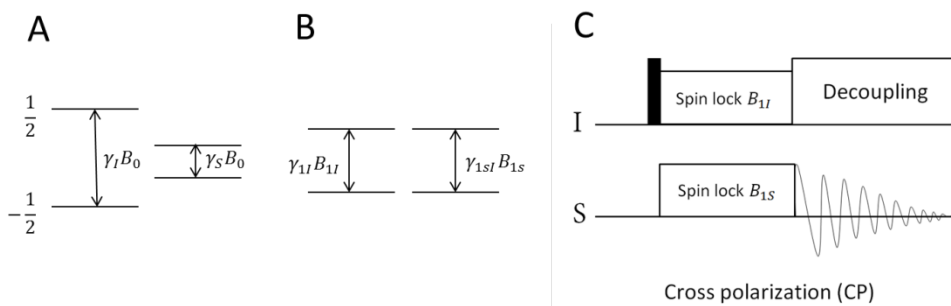


**Figure 9.** **A:** energy levels of spin  $I$  and  $S$  in the laboratory frame, **B:** energy levels of spin  $I$  and  $S$  in the rotating frame and **C:** basic pulse sequence of cross polarization between spin  $I$  and  $S$ .

Since the cross polarization (CP) occurs via dipolar couplings, it seems that under MAS conditions where dipolar couplings are averaged, CP must lose its efficiency. However, polarization transfer does occur as long as the coupling is not completely averaged, but becomes time dependent. In this condition CP is modified to the MAS version, where the  $B_1$  of one of the contact pulses linearly increases or decreases in order to fulfil the Hartman-Hahn condition. In the

Hartman-Hahn condition under MAS the difference between the frequencies of two spins has to be a multiple of the spinning frequency and it is given by

$$\gamma_{1I}B_{1I} - \gamma_{1S}B_{1S} = \pm n\omega_r, \quad (10)$$

where  $n$  is an integer number <sup>76-77</sup>.

## Insensitive Nuclei Enhanced by Polarization Transfer

Another polarization transfer method is based on  $J$ -couplings (see equation 7) and known as Insensitive Nuclei Enhanced by Polarization Transfer or INEPT. INEPT is widely used in liquid NMR where  $J$ -couplings are strong enough for polarization transfer between nuclei. Although  $J$ -couplings are smaller compared to other interactions in solid materials, in biosolids such as membrane proteins, the INEPT sequences open a route to detect mobile species and get insight into their structure and dynamics. Figure 10 presents the pulse sequence of an INEPT experiment. The INEPT pulse sequence consists of several  $90^\circ$  and spin-echo pulses which lead to sensitivity enhancement of dilute nuclei. Like other NMR sequences INEPT starts with applying a  $90^\circ$  pulse to spin  $I$  to create transverse magnetization, followed by a time period delay for evolution of heteronuclear  $J$ -couplings. Furthermore spin echo pulses are applied to both nuclei in the middle of the evolution delay. The chemical shift of a spin  $I$  is refocused by a spin echo or  $180^\circ$  pulse in the  $I$  channel, while the heteronuclear  $J$ -couplings are not affected and a second delay is involved by only  $I$ - $S$  couplings. As a result of spin echo pulses spin systems are in an antiphase state, this antiphase is converted to  $S$  nuclei and polarization is transferred from  $I$  to  $S$  by applying second  $90^\circ$  pulses on both channels. In order to create the in-phase x-magnetization, spin echo pulses are simultaneously applied to the  $I$  and  $S$  channels. Detailed steps of INEPT transfer by propagators are presented by equation 11 <sup>78</sup>.

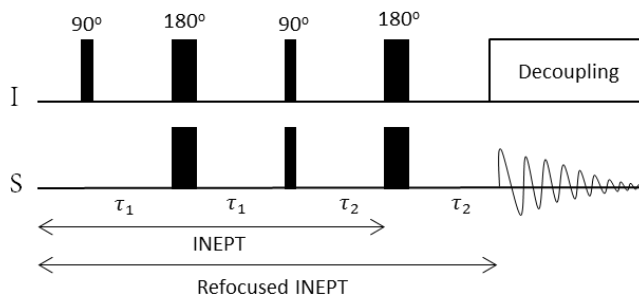


**Figure 10.** Pulse sequence of INEPT and refocused INEPT.

$$\begin{aligned}
I_x &\xrightarrow{2\pi J_{IS}\tau_1 I_z S_z} \cos(2\pi J_{IS}\tau_1) I_x + \sin(2\pi J_{IS}\tau_1) 2 I_y S_z & (11) \\
\sin(2\pi J_{IS}\tau_1) 2 I_y S_z &\xrightarrow{\left(\frac{\pi}{2}\right) I_x} \left(\frac{\pi}{2}\right) S_x \xrightarrow{\left(\frac{\pi}{2}\right) S_x} -\sin(2\pi J_{IS}\tau_1) 2 I_z S_y \\
&\xrightarrow{2\pi J_{IS}\tau_2 I_z S_z} \sin(2\pi J_{IS}\tau_2) \sin(2\pi J_{IS}\tau_1) S_x .
\end{aligned}$$

1

## Aim and scope of this thesis

---

This thesis aims to gain insight into the molecular mechanisms of light-harvesting regulation by addressing the conformational dynamics of light-harvesting complexes in native-like environments and the molecular dynamics of protein and lipid components in intact thylakoid membranes and whole cells.

The ability of MAS-NMR to study the *in-situ* conformational dynamics of light harvesting complexes at atomistic resolution in a native environment is demonstrated by employing polarization-transfer based dynamic filter experiments to isolated LHCII in lipid bilayers and intact thylakoid membranes.

**Chapter 2** explains the applicability of solid-state NMR spectroscopy for obtaining a microscopic picture of different molecular constituents inside native thylakoid membranes. Moreover, the effect of Zea accumulation on dynamic properties of protein, lipid and xanthophyll constituents at physiological temperatures are discussed by comparing the dynamic-filter NMR spectra of *Cr.* thylakoid membranes from wild-type (WT) cells and from the *npq2* mutant that accumulates Zea.

**Chapter 3** reveals that NMR signals of the most abundant light-harvesting complex, LHCII, can be detected in the spectra of native, heterogeneous thylakoid membranes. In order to investigate how the membrane environment influences on the dynamics and plasticity of LHCII, two-dimensional CP and INEPT based MAS-NMR experiments were performed on isolated *Cr.* LHCII reconstituted in lipid bilayers and on *Cr.* thylakoid membrane.

In **Chapter 4**, I describe the effect of Zea on the conformational dynamics of LHCII in a lipid bilayer. Hetero LHCII isolated from WT and *npq2 Cr.* cells were reconstituted in lipid bilayers and subjected to two-dimensional CP and INEPT based experiments.

**Chapter 5** demonstrates how the dynamic spectra-editing NMR method that is introduced in chapter 2 can be extended to the cell level to resolve and quantify molecular dynamics of different cellular components. To this end, NMR experiments were applied on fresh, intact *Cr.* cells and results were compared with simulated CP and INEPT intensities.

Finally, a general discussion and perspectives of the research presented in this thesis is provided in **Chapter 6**.

## References

---

1. Kromdijk, J.; Glowacka, K.; Leonelli, L.; Gabilly, S. T.; Iwai, M.; Niyogi, K. K.; Long, S. P., Improving photosynthesis and crop productivity by accelerating recovery from photoprotection. *Science (New York, N.Y.)* **2016**, *354* (6314), 857-861.
2. Harris, E., *Chlamydomonas* as a model system. *Annu. Rev. Plant Physiol. Plant Mol. Bio* **2001**, *52*, 363-406.
3. Blankenship, R. E., *Molecular mechanisms of photosynthesis*. Second edition ed.; Wiley/Blackwell: Chichester, West Sussex, 2014; p 296.
4. Croce, R.; van Amerongen, H., Light-harvesting in photosystem I. *Photosynth Res* **2013**, *116* (2-3), 153-66.
5. van Amerongen, H.; Croce, R., Light harvesting in photosystem II. *Photosynth Res* **2013**, *116* (2-3), 251-63.
6. Jordan, P.; Fromme, P.; Witt, H. T.; Klukas, O.; Saenger, W.; Krauss, N., Three-dimensional structure of cyanobacterial photosystem I at 2.5 Å resolution. *Nature* **2001**, *411*, 909-917.
7. Busch, A.; Hippler, M., The structure and function of eukaryotic photosystem I. *Biochim Biophys Acta* **2011**, *1807* (8), 864-77.
8. Ben-Shel, A.; Frolow, F.; Nelson, N., Crystal structure of plant photosystem I. *Nature* **2003**, *426*, 630-635.
9. Amunts, A.; Toporik, H.; Borovikova, A.; Nelson, N., Structure determination and improved model of plant photosystem I. *J Biol Chem* **2010**, *285* (5), 3478-86.
10. Scheller, H. V.; Jenson, P. E.; Haldrup, A.; Lunde, C.; Knoetzel, J., Role of subunits in eukaryotic Photosystem I. *Biochimica et Biophysica Acta* **2001**, *1507*, 41-60.
11. Allen, J. F.; de Paula, W. B.; Puthiyaveetil, S.; Nield, J., A structural phylogenetic map for chloroplast photosynthesis. *Trends Plant Sci* **2011**, *16* (12), 645-55.
12. Mazor, Y.; Nataf, D.; Toporik, H.; Nelson, N., Crystal structures of virus-like photosystem I complexes from the mesophilic cyanobacterium *Synechocystis* PCC 6803. *Elife* **2013**, *3*, e01496.
13. Ganeteg, U.; Klimmek, F.; Jansson, S., Lhca5 – an LHC-type protein associated with photosystem I. *Plant Molecular Biology* **2004**, *54*, 641-651.
14. Elrad, D.; Grossman, A. R., A genome's-eye view of the light-harvesting polypeptides of *Chlamydomonas reinhardtii*. *Curr Genet* **2004**, *45* (2), 61-75.
15. Drop, B.; Webber-Birungi, M.; Fusetti, F.; Kouril, R.; Redding, K. E.; Boekema, E. J.; Croce, R., Photosystem I of *Chlamydomonas reinhardtii* contains nine light-harvesting complexes (Lhca) located on one side of the core. *J Biol Chem* **2011**, *286* (52), 44878-87.

16. Boekema, E. J.; Jenson, P. E.; Schlodder, E.; van Breemen, J. F. L.; van Roon, H.; Scheller, H. V.; Dekker, J. P., Green Plant Photosystem I Binds Light-Harvesting Complex I on One Side of the Complex. *Biochemistry* **2001**, *40*, 1029-1036.
17. Zouni, A.; Witt, H. T.; Kern, J.; Fromme, P.; Krauss, N.; Saenger, W.; Orth, P., Crystal structure of photosystem II from *Synechococcus elongatus* at 3.8 Å resolution. *Nature* **2001**, *409*, 739-743.
18. Umena, Y.; Kawakami, K.; Shen, J. R.; Kamiya, N., Crystal structure of oxygen-evolving photosystem II at a resolution of 1.9 Å. *Nature* **2011**, *473* (7345), 55-60.
19. Guskov, A.; Kern, J.; Gabdulkhakov, A.; Broser, M.; Zouni, A.; Saenger, W., Cyanobacterial photosystem II at 2.9-Å resolution and the role of quinones, lipids, channels and chloride. *Nat Struct Mol Biol* **2009**, *16* (3), 334-42.
20. Wei, X.; Su, X.; Cao, P.; Liu, X.; Chang, W.; Li, M.; Zhang, X.; Liu, Z., Structure of spinach photosystem II-LHCII supercomplex at 3.2 Å resolution. *Nature* **2016**, *534* (7605), 69-74.
21. Pietrzykowska, M.; Pietrzykowska, M.; Suorsa, M.; Semchonok, D. A.; Tikkanen, M.; Boekema, E. J.; Jansson, S.; Jansson, S., The Light-Harvesting Chlorophyll a/b Binding Proteins Lhcb1 and Lhcb2 Play Complementary Roles during State Transitions in *Arabidopsis*. *Plant Cell* **2014**, *26* (9), 3646-3660.
22. Ferrante, P.; Ferrante, P.; Ballottari, M.; Bonente, G.; Giuliano, G.; Bassi, R., LHCBM1 and LHCBM2/7 Polypeptides, Components of Major LHCII Complex, Have Distinct Functional Roles in Photosynthetic Antenna System of *Chlamydomonas reinhardtii*. *Journal of biological chemistry* **2012**, *287* (20), 16276-16288.
23. Kulbrandt, W.; Wang, d. N.; Fojiyoshi, Y., Atomic model of plant light-harvesting complex by electron crystallography. *Nature* **1994**, *367*, 614-621.
24. Liu, Z.; Yan, H.; Wang, K.; Kuang, T.; Zhang, J.; Gui, L.; An, X.; Chang, W., Crystal structure of spinach major light-harvesting complex at 2.72 Å resolution. *Nature* **2004**, *428*, 287-292.
25. Erickson, E.; Wakao, S.; Niyogi, K. K., Light stress and photoprotection in *Chlamydomonas reinhardtii*. *Plant J* **2015**, *82* (3), 449-65.
26. Kirchoff, H., Structural changes of the thylakoid membrane network induced by high light stress in plant chloroplasts. *Philosophical Transactions of the Royal Society B: Biological Sciences* **2014**, *369* (1640), 20130225.
27. Horton, P.; Ruban, A., Molecular design of the photosystem II light-harvesting antenna: photosynthesis and photoprotection. *Journal of Experimental Botany* **2005**, *56* (411), 365-373.
28. Ruban, A.; Ruban, M.; Duffy, The photoprotective molecular switch in the photosystem II antenna. *Biochimica et biophysica acta. Bioenergetics* **2012**, *1817* (1), 167-181.
29. Müller, P.; L, X-P.; Niyogi, K. K., Non-Photochemical Quenching. A Response to Excess Light Energy1. *Plant Physiol* **125**, 1558-1566.
30. Minagawa, J., State transitions--the molecular remodeling of photosynthetic supercomplexes that controls energy flow in the chloroplast. *Biochim Biophys Acta* **2011**, *1807* (8), 897-905.
31. Nilkens, M.; Kress, E.; Lambrev, P.; Miloslavina, Y.; Muller, M.; Holzwarth, A. R.; Jahns, P., Identification of a slowly inducible zeaxanthin-dependent component of non-photochemical quenching of chlorophyll fluorescence generated under steady-state conditions in *Arabidopsis*. *Biochim Biophys Acta* **2010**, *1797* (4), 466-75.
32. Krause, G. H., Photoinhibition of photosynthesis. An evaluation of damaging and protective mechanisms. *PHYSIOLOGIA PLANTARUM* **1988**, *74*, 566-574.
33. Lambrev, P. H.; Nilkens, M.; Miloslavina, Y.; Jahns, P.; Holzwarth, A. R., Kinetic and spectral resolution of multiple nonphotochemical quenching components in *Arabidopsis* leaves. *Plant Physiol* **2010**, *152* (3), 1611-24.
34. Xu, P.; Tian, L.; Kloz, M.; Croce, R., Molecular insights into Zeaxanthin-dependent quenching in higher plants. *Scientific Reports* **2015**, *5*, 13679.



35. Malnoë, A., Photoinhibition or photoprotection of photosynthesis? Update on the (newly termed) sustained quenching component qH. *Environmental and Experimental Botany* **2018**.
36. Li, X.-P.; Muller-Mulle, P.; Gilmore, A. M.; Niyogi, K. K., PsbS-dependent enhancement of feedback de-excitation protects photosystem II from photoinhibition. *PNAS* **2016**, *113* (27).
37. Dinc, E.; Tian, L.; Roy, L. M.; Roth, R.; Goodenough, U.; Croce, R., LHCSR1 induces a fast and reversible pH-dependent fluorescence quenching in LHCII in *Chlamydomonas reinhardtii* cells. *Proc Natl Acad Sci U S A* **2016**, *113* (27), 7673-8.
38. Peers, G.; Truong, T. B.; Ostendorf, E.; Busch, A.; Elrad, D.; Grossman, A. R.; Hippler, M.; Niyogi, K. K., An ancient light-harvesting protein is critical for the regulation of algal photosynthesis. *Nature* **2009**, *462* (7272), 518-21.
39. Ballottari, M.; Alcocer, M. J.; D'Andrea, C.; Viola, D.; Ahn, T. K.; Petrozza, A.; Polli, D.; Fleming, G. R.; Cerullo, G.; Bassi, R., Regulation of photosystem I light harvesting by zeaxanthin. *Proc Natl Acad Sci U S A* **2014**, *111* (23), E2431-8.
40. Dall'Osto, L.; Cazzaniga, S.; Havaux, M.; Bassi, R., Enhanced photoprotection by protein-bound vs free xanthophyll pools: a comparative analysis of chlorophyll b and xanthophyll biosynthesis mutants. *Mol Plant* **2010**, *3* (3), 576-93.
41. Horton, P.; Ruban, A. V.; Wentworth, M., Allosteric regulation of the light-harvesting system of photosystem II. *Philos Trans R Soc Lond B Biol Sci* **2000**, *355* (1402), 1361-70.
42. Gruber, J. M.; Malý, P.; Krüger, T. P. J.; Grondelle, R. v., From isolated light-harvesting complexes to the thylakoid membrane: a single-molecule perspective. *Nanophotonics* **2018**, *7* (1), 81-92.
43. Park, S.; Fischer, A. L.; Steen, C. J.; Iwai, M.; Morris, J. M.; Walla, P. J.; Niyogi, K. K.; Fleming, G. R., Chlorophyll-Carotenoid Excitation Energy Transfer in High-Light-Exposed Thylakoid Membranes Investigated by Snapshot Transient Absorption Spectroscopy. *J Am Chem Soc* **2018**, *140* (38), 11965-11973.
44. Bode, S.; Quentmeier, C. C.; Liao, P.-N.; Hafi, N.; Barros, T.; Wilk, W.; Bittner, F.; Walla, P. J., On the regulation of photosynthesis by excitonic interactions between carotenoids and chlorophylls. *PNAS* **2009**, *106*, 12311-12316.
45. Ruban, A. V.; Berera, R.; Ilioaia, C.; van Stokkum, I. H.; Kennis, J. T.; Pascal, A. A.; van Amerongen, H.; Robert, B.; Horton, P.; van Grondelle, R., Identification of a mechanism of photoprotective energy dissipation in higher plants. *Nature* **2007**, *450* (7169), 575-8.
46. Holt, N. E.; Zigmantas, D.; Valkunas, L.; Li, X.; Niyogi, K.; Fleming, G. R., Carotenoid Cation Formation and the Regulation of Photosynthetic Light Harvesting. *Science* **2005**, *307*, 433-436.
47. Barros, T.; Royant, A.; Standfuss, J.; Dreuw, A.; Kuhlbrandt, W., Crystal structure of plant light-harvesting complex shows the active, energy-transmitting state. *EMBO J* **2009**, *28* (3), 298-306.
48. Higman, V. A.; Varga, K.; Aslimovska, L.; Judge, P. J.; Sperling, L. J.; Rienstra, C. M.; Watts, A., The Conformation of Bacteriorhodopsin Loops in Purple Membranes Resolved by Solid-State MAS NMR Spectroscopy. *Angewandte Chemie International Edition* **2011**, *50* (36), 8432-8435.
49. Kulminskaya, N. V.; Pedersen, M. Ø.; Bjerring, M.; Underhaug, J.; Miller, M.; Frigaard, N.-U.; Nielsen, J. T.; Nielsen, N. C., In Situ Solid-State NMR Spectroscopy of Protein in Heterogeneous Membranes: The Baseplate Antenna Complex of *Chlorobaculum tepidum*. *Angewandte Chemie International Edition* **2012**, *51* (28), 6891-6895.
50. Kaplan, M.; Cukkemane, A.; van Zundert, G. C.; Narasimhan, S.; Daniels, M.; Mance, D.; Waksman, G.; Bonvin, A. M.; Fronzes, R.; Folkers, G. E.; Baldus, M., Probing a cell-embedded megadalton protein complex by DNP-supported solid-state NMR. *Nature methods* **2015**, *12* (7), 649-52.

51. Kaplan, M.; Narasimhan, S.; de Heus, C.; Mance, D.; van Doorn, S.; Houben, K.; Popov-Celeketic, D.; Damman, R.; Katrukha, E. A.; Jain, P.; Geerts, W. J. C.; Heck, A. J. R.; Folkers, G. E.; Kapitein, L. C.; Lemeer, S.; van Bergen En Henegouwen, P. M. P.; Baldus, M., EGFR Dynamics Change during Activation in Native Membranes as Revealed by NMR. *Cell* **2016**, *167* (5), 1241-1251 e11.
52. Pinto, C.; Mance, D.; Julien, M.; Daniels, M.; Weingarth, M.; Baldus, M., Studying assembly of the BAM complex in native membranes by cellular solid-state NMR spectroscopy. *Journal of structural biology* **2017**.
53. Baker, L. A.; Sinnige, T.; Schellenberger, P.; de Keyzer, J.; Siebert, C. A.; Driessen, A. J. M.; Baldus, M.; Grunewald, K., Combined (1)H-Detected Solid-State NMR Spectroscopy and Electron Cryotomography to Study Membrane Proteins across Resolutions in Native Environments. *Structure (London, England : 1993)* **2017**.
54. Ward, M. E.; Wang, S.; Munro, R.; Ritz, E.; Hung, I.; Gor'kov, Peter L.; Jiang, Y.; Liang, H.; Brown, Leonid S.; Ladizhansky, V., In Situ Structural Studies of Anabaena Sensory Rhodopsin in the E. coli Membrane. *Biophysical Journal* **2015**, *108* (7), 1683-1696.
55. Fu, R.; Wang, X.; Li, C.; Santiago-Miranda, A. N.; Pielak, G. J.; Tian, F., In situ structural characterization of a recombinant protein in native Escherichia coli membranes with solid-state magic-angle-spinning NMR. *Journal of the American Chemical Society* **2011**, *133* (32), 12370-3.
56. Miao, Y.; Qin, H.; Fu, R.; Sharma, M.; Can, T.; Hung, I.; Luca, S.; Gor'kov, P. L.; Brey, W. W.; Cross, T. A., M2 Proton Channel Structural Validation from Full Length Protein Samples in Synthetic Bilayers and E. coli Membranes. *Angewandte Chemie (International ed. in English)* **2012**, *51* (33), 8383-8386.
57. Renault, M.; Pawsey, S.; Bos, M. P.; Koers, E. J.; Nand, D.; Tommassen-van Boxtel, R.; Rosay, M.; Tommassen, J.; Maas, W. E.; Baldus, M., Solid-state NMR spectroscopy on cellular preparations enhanced by dynamic nuclear polarization. *Angew Chem Int Ed Engl* **2012**, *51* (12), 2998-3001.
58. Jacso, T.; Franks, W. T.; Rose, H.; Fink, U.; Broecker, J.; Keller, S.; Oschkinat, H.; Reif, B., Characterization of membrane proteins in isolated native cellular membranes by dynamic nuclear polarization solid-state NMR spectroscopy without purification and reconstitution. *Angew Chem Int Ed Engl* **2012**, *51* (2), 432-5.
59. Bill, R. M.; Henderson, P. J.; Iwata, S.; Kunji, E. R.; Michel, H.; Neutze, R.; Newstead, S.; Poolman, B.; Tate, C. G.; Vogel, H., Overcoming barriers to membrane protein structure determination. *Nat Biotechnol* **2011**, *29* (4), 335-40.
60. Stroud, R. M., New tools in membrane protein determination. *F1000 Biol. Rep* **2011**, *3* (8).
61. Wang, S.; Munro, R. A.; Shi, L.; Kawamura, I.; Okitsu, T.; Wada, A.; Kim, S. Y.; Jung, K. H.; Brown, L. S.; Ladizhansky, V., Solid-state NMR spectroscopy structure determination of a lipid-embedded heptahelical membrane protein. *Nat Methods* **2013**, *10* (10), 1007-12.
62. Alia, A.; Buda, F.; de Groot, H. J.; Matysik, J., Solid-state NMR of nanomachines involved in photosynthetic energy conversion. *Annu Rev Biophys* **2013**, *42*, 675-99.
63. Pandit, A.; de Groot, H. J., Solid-state NMR applied to photosynthetic light-harvesting complexes. *Photosynth Res* **2012**, *111* (1-2), 219-26.
64. Sunku, K.; de Groot, H. J.; Pandit, A., Insights into the photoprotective switch of the major light-harvesting complex II (LHCII): a preserved core of arginine-glutamate interlocked helices complemented by adjustable loops. *J Biol Chem* **2013**, *288* (27), 19796-804.
65. Pandit, A.; Reus, M.; Morosinotto, T.; Bassi, R.; Holzwarth, A.; Holzwarth, A. R., An NMR comparison of the light-harvesting complex II (LHCII) in active and photoprotective states reveals subtle changes in the chlorophyll a ground-state electronic structures. *Biochimica et biophysica acta. Bioenergetics* **2013**, *1827* (6), 738-744.

66. Duffy, C. D.; Pandit, A.; Ruban, A. V., Modeling the NMR signatures associated with the functional conformational switch in the major light-harvesting antenna of photosystem II in higher plants. *Phys Chem Chem Phys* **2014**, *16* (12), 5571-80.
67. Prakash, A. S.; Gast, P.; de Groot, H. J.; Matysik, J.; Jeschke, G., Photo-CIDNP MAS NMR in Intact Cells of Rhodospirillum rubrum: Molecular and Atomic Resolution at Nanomolar Concentration. *Journal of the American Chemical Society* **2008**, *128*, 68.
68. Duer, M. J., *Solid-State NMR Spectroscopy Principles and Applications*. 2002.
69. Smith, M. E.; Mackenzie, E., *Multinuclear Solid-State Nuclear Magnetic Resonance of Inorganic Materials*. 1th ed.; 2002.
70. Schmidt-Rohr, K.; Spiess, W., *Multidimensional Solid-State NMR and Polymers*. Academic Press Ltd., London **1994**.
71. Pines, A.; Waugh, J. S.; Gibby, M. G., Proton-Enhanced Nuclear Induction Spectroscopy - Method for High-Resolution NMR of Dilute Spins in Solids. *The Journal of Chemical Physics* **1972**, *56* (4), 1776.
72. Morris, G. A.; Freeman, R., Enhancement of nuclear magnetic resonance signals by polarization transfer. *J. Am. Chem. Soc* **1979**, *101* (3), 760-762.
73. Nowacka, A.; Mohr, P. C.; Norrman, J.; Martin, R. W.; Topgaard, D., Polarization transfer solid-state NMR for studying surfactant phase behavior. *Langmuir* **2010**, *26* (22), 16848-56.
74. Purusottam, R. N.; Bodenhausen, G.; Tekely, P., Quantitative one- and two-dimensional <sup>13</sup>C spectra of microcrystalline proteins with enhanced intensity. *J Biomol NMR* **2013**, *57* (1), 11-9.
75. Hartmann, S. R.; Hahn, E. L., Nuclear Double Resonance in the Rotating Frame. *Physical Review* **1962**, *128* (5), 2042-2053.
76. Stejskal, E.; Schaefer, J.; Waugh, J., Magic-angle spinning and polarization transfer in proton-enhanced NMR. *J. Magn. Reson* **1977**, *28*, 105-112.
77. Pines, A.; Gibby, M. G.; Waugh, J. S., Proton-enhanced NMR of dilute spins in solids. *The Journal of Chemical Physics* **1973**, *69* (2), 569-590.
78. Morris, G. A.; Freeman, R., Enhancement of nuclear magnetic resonance signals by polarization transfer. *J. Am. Chem. Soc* **1979**, *101* (3), 760-762.

# CHAPTER 2

---

---

## Protein & lipid dynamics in photosynthetic thylakoid membranes investigated by *in-situ* NMR

---

---

This work is published as: Azadi Chegeni F., Perin G., Sai Sankar Gupta K.B., Simionato D., Morosinotto T., Pandit A. BBA-Bioenergetics, 1857 (12): 1849-1859 (2016)

## Abstract

---

Photosynthetic thylakoid membranes contain the protein machinery to convert sunlight into chemical energy and regulate this process in changing environmental conditions via interplay between lipid, protein and xanthophyll molecular constituents. This work addresses the molecular effects of zeaxanthin accumulation in thylakoid membranes, which occurs in native systems under high light conditions through the conversion of the xanthophyll violaxanthin into zeaxanthin via the so called xanthophyll cycle. We applied biosynthetic isotope labeling and  $^{13}\text{C}$  solid-state NMR spectroscopy to simultaneously probe the conformational dynamics of protein, lipid and xanthophyll constituents of thylakoid membranes isolated from wild type (CW15) and *npq2* mutant of the green alga *Chlamydomonas reinhardtii*, that accumulates zeaxanthin constitutively. Results show differential dynamics of wild type and *npq2* thylakoid membranes. Ordered-phase lipids have reduced dynamics and mobile-phase lipids have enlarged dynamics in *npq2* membranes, together spanning a broader dynamical range than for WT. The total fraction of ordered lipids is much larger than the fraction of mobile lipids in thylakoid membrane, which explains why zeaxanthin accumulation causes overall reduction of thylakoid membrane fluidity. In addition to the ordered lipids, also the xanthophylls and a subset of protein sites in *npq2* thylakoid membranes have reduced conformational dynamics. Our work demonstrates the application of solid-state NMR spectroscopy for obtaining a microscopic picture of different membrane constituents simultaneously, inside native, heterogeneous membranes.

## Introduction

---

Conversion of sunlight into chemical energy takes place inside photosynthetic membranes, where pigment-protein nano-machines carry out a cascade of reactions that evolve in time and space <sup>1</sup>. In order to safely perform the photosynthesis reactions and ensure organism fitness under fluctuating light conditions, constant membrane remodeling takes place. In excess light, feedback deregulation mechanisms induce quenching of sunlight excitations, dissipating the excess light energy as heat and creating a safety valve for the photosynthetic apparatus <sup>2-3</sup>. In plant and algae thylakoid membranes, photosynthesis is regulated through complex interplay between molecular conformational changes, reversible supramolecular interactions and membrane phase transitions <sup>4</sup>. Thylakoid membranes are densely packed with proteins that occupy ~70% of the membrane space and control the membrane phases <sup>5</sup>. Short-

and long-term acclimation of thylakoid membranes to light and cold stress involves reorganization of antenna-supercomplexes<sup>4, 6-9</sup>, conversion of the xanthophyll violaxanthin (Vio) into zeaxanthin (Zea) via the xanthophyll cycle<sup>10</sup> and increase of lipid unsaturation by changing lipid composition<sup>11</sup>. Modulated by low pH, phosphorylation and the xanthophyll cycle, a part of the light-harvesting complex II (LHCII) antenna population disconnects from the Photosystem II (PSII) complexes and self-aggregates to form Chl-quenched states, which dissipate excess light<sup>12</sup>. The effects of xanthophyll composition on regulation and photoprotection in thylakoid membranes have been investigated in various studies. Zea is known to play a central role in photoprotection, through its participation in Non-Photochemical Quenching (NPQ)<sup>13</sup> but also by preventing lipid oxidative damage in the membrane<sup>14</sup>. The antioxidant activity of xanthophyll pigments present in membranes was indeed found to be related to their physical-chemical interaction with lipids<sup>15</sup> and their presence was shown to increase the penetration barrier to molecular oxygen<sup>16</sup>. Moreover, several *in vivo* and *in-vitro* studies have reported increased rigidity of Zea-containing membranes<sup>14, 17</sup>, contributing to their stabilization. The precise role of Zea in NPQ is still under debate. *Chlamydomonas reinhardtii* (*Cr.*) *npq2* mutants, that have an impaired xanthophyll cycle and accumulate Zea constitutively in their thylakoid membranes, show faster fluorescence quenching upon actinic-light exposure<sup>18-19</sup>. Zea has been suggested to quench of excess energy by multiple mechanisms, by activating a quenched state in LHC protein complexes upon binding<sup>20-22</sup> but also at the membrane level, mediating the complexes interactions<sup>23</sup>.

In this work, we explored the use of *in-situ* <sup>13</sup>C solid-state Nuclear Magnetic Resonance (NMR) on whole thylakoid membranes to gain insight in protein and lipid conformational dynamics and the effect of Zea accumulation. <sup>13</sup>C-NMR spectroscopy in conjunction with biosynthetic uniformly <sup>13</sup>C isotope labeling provides us with a unique method to simultaneously detect protein, lipid and xanthophyll molecular constituents and measure their molecular dynamics directly. We analyzed *Cr.* thylakoid membranes from wild type (WT) and from *npq2* mutant that, as already mentioned accumulates Zea in the thylakoid membranes. <sup>13</sup>C Magic Angle Spinning (MAS) NMR spectra were obtained by direct and cross polarization to separate and quantify rigid and dynamic membrane molecular components. To measure the temperature-dependent dynamical properties, spectra were collected over a temperature range from 0 to 25°C. In addition,  $T_{1\rho}$  relaxation experiments were performed to further analyze protein backbone molecular dynamics. Results show differential dynamics of proteins, lipids and xanthophylls in WT and *npq2* membranes. The *npq2* membranes contain more xanthophylls and ordered-phase lipids with reduced dynamics, as well as mobile-phase lipids with enlarged dynamics, spanning a

broader dynamic range. Our study validates the application of  $^{13}\text{C}$  solid-state NMR spectroscopy for functional screening of molecular membrane characteristics and demonstrates how Zea accumulation influences the conformational dynamics of protein and lipid constituents, affecting the functionality of biological thylakoid membranes.

## Material & Methods

---

### Chlamydomonas reinhardtii strains and growth conditions

In this work we employed *Cr.* strains CW15 and *npq2*. The first is a cell wall-less mutant <sup>24</sup> used as WT, while the second is affected in zeaxanthin epoxidase (ZE) activity <sup>25</sup>. Both strains were cultivated in Erlenmeyer flasks with liquid Tris-Acetate Phosphate (TAP) medium, at 100 rpm agitation and 21°C in a growth chamber. Continuous illumination was provided from cool-white fluorescent lamps under low (<25  $\mu\text{moles photons m}^{-2} \text{ s}^{-1}$ ) photosynthetically active radiation (400-700 nm). The TAP medium <sup>26</sup> used to grow labeled cells, was prepared using  $^{13}\text{C}$  labeled sodium acetate (Sigma-Aldrich) and  $^{15}\text{N}$  labeled ammonium chloride (Sigma-Aldrich). Cultures in labeled medium were set up starting from an optical density at 750 nm ( $\text{OD}_{750}$ ) equal to 0.1 and cells were grown until  $\text{OD}_{750} = 1$ . Three rounds of cultivation in labeled medium were performed to ensure > 95 % labelling of the cells with  $^{13}\text{C}$  and  $^{15}\text{N}$  atoms.

### Thylakoid isolation

Cells were harvested by 10 minutes of centrifugation at 4°C, at 3500×g and then washed twice in isolation medium A (IMA, 10mM MES pH 6.5, 2mM KCl, 5mM EDTA pH 8, 1M sorbitol). After centrifugation, cells were resuspended in cold IMA buffer with 0.5 % milk powder and 1 mM PMSF, 1 mM DNP- $\epsilon$ -amino-n-caproic acid and 1 mM benzamidine, and then disrupted at 4°C using an ultrasonic homogenizer (Sonic Rupter 400 – OMNI International - PBI) for 5 s, with the maximum power. Immediately after rupture, the samples were centrifuged for 15 minutes at 2500×g at 4°C to collect unbroken cells on the bottom of the tube. The latter were again resuspended in IMA buffer containing inhibitors and milk powder and treated again with the homogenizer. This step was repeated 3 times to be sure to break all the harvested cells, always collecting the supernatant containing the thylakoids. The latter was centrifuged for 15 minutes at 2500×g at 4°C, to eliminate cells debris. The supernatant was then centrifuged for 30 minutes at 40000×g at 4°C to collect the thylakoids. The

pellet, containing the thylakoids, was washed twice with isolation medium B (IMB, 10mM MES pH 6.5, 2mM KCl, 5mM EDTA pH 8) and resuspended in T3 buffer (50 mM Hepes-KOH pH 7.5, 5 mM MgCl<sub>2</sub>, 50% glycerol). Immediately, thylakoids were frozen in liquid nitrogen and stored at -80°C until use. All steps were performed at 4°C and in dim light. Thylakoids total pigments were extracted with 80% acetone, and the chlorophyll concentration of the samples was determined spectrophotometrically using specific extinction coefficients<sup>27</sup> and the acetone spectra fitting, previously described in<sup>28</sup>.

## Gel electrophoresis

Coomassie-stained SDS-page was performed using 12.5% Tris-glycine gels as in<sup>29</sup>. Samples were solubilized with a solubilization buffer (4X) containing 30% glycerol, 125 mM Tris pH 6.8, 0.1 M dithiothreitol, 9% SDS and were loaded according to the same amount of membranes.

## NMR sample preparation

The thylakoids suspension containing 1.5 mg of Chl (approx. 10 times more in protein content) were pelleted by ultra-centrifugation at 223000×g for 40 minutes and transferred into NMR rotor inserts.

## NMR experimental setup

All the NMR spectra were collected with a Bruker Advance-III 750 (17.4T) solid state NMR spectrometer equipped with a 4 mm CP/ MAS trip-probe. Presented 2D <sup>13</sup>C-<sup>13</sup>C proton driven spin diffusion NMR experiments (PDSO) were collected with 256 scans and mixing time of 25 ms at -29°C. Two-pulse phase modulation (TPPM) decoupling (2 dB) was applied during the t<sub>1</sub> and t<sub>2</sub> periods. Each Polarization Transfer ssNMR experiment was performed with 256 scans under SPINAL-64 decoupling (1.8 dB) and the frequency of the magic-angle spinning (MAS) was set to 11.6 kHz. All the <sup>13</sup>C spectra were referenced to the carbonyl signal of solid <sup>13</sup>C-tyrosine at 172.2 ppm. CP experiments were performed with the contact time of 2 ms, a recycle delay of 2 s and acquisition time (AQ) of 20 ms, ω<sub>1</sub><sup>C</sup>/2π of 40.3 kHz and <sup>1</sup>H nutation frequency linearly ramped from 80 to 100 kHz. Two delays of 1.25ms and AQ time of 80ms were used in INEPT. For Direct Polarization (DP) experiments, delay time was 2s and acquisition time was set to 43 ms. Presented temperature curves are the averaged results of two independent sets of experiments. As a control, CP and DP experiments were also performed on a tri-amino acid (<sup>13</sup>C/<sup>15</sup>N N- formyl-Met-Leu-Ple-OH (f-MLF)) using the same pulse sequences. In this case, CP signal



intensities were about four times the DP signal intensities, in line with expected enhancement from the  $^1\text{H}$  and  $^{13}\text{C}$  gyromagnetic ratio.

### $T_{1\rho}$ setting

$^{13}\text{C}$   $T_{1\rho}$  experiments were performed at 7 and 25°C. We applied SPINAL-64 heteronuclear decoupling with 1.5 dB power during the relaxation delay. To acquire the spectra after the CP MAS pulse, variable spin-lock pulses from 10  $\mu\text{s}$  to 200 ms were applied. The acquisition time was 11 ms and  $\tau_{\text{CP}}$  was set to 256  $\mu\text{s}$  for all the experiments, except if stated otherwise. Relaxation curves were obtained by integrating the appropriate regions as a function of the relaxation delay in each experiment. The reported rates were determined by fitting the data to stretched- or double-exponentials.

### Temperature calibration

Temperatures were calibrated by analyzing the  $^{207}\text{Pb}$  NMR chemical shift of lead nitrate ( $\text{Pb}(\text{NO}_3)_2$ ) which is the standard sample for temperature calibration in magic-angle spinning (MAS) probes. The readout temperature was regulated from -2.0 to 20.0°C within  $\pm 0.1$  °C. Effective sample temperature as a function of read out temperature and spinning speed can be obtained as described in <sup>30</sup>.

## Results

---

### $^{13}\text{C}$ labeling of *Cr.* cells

*Cr.* strains CW15 (further referred to as WT) and *npq2* were chosen for this work and cultivated according to the following considerations. In order to be detectable through the solid-state NMR technique, cells needed to be labeled with carbon ( $^{13}\text{C}$ ) and nitrogen ( $^{15}\text{N}$ ) isotopes. While  $^{15}\text{N}$  labeled ammonium chloride was the only nitrogen source in the medium, *Cr.* is a photosynthetic organism that is also able to fix  $\text{CO}_2$  from the atmosphere to support its photoautotrophic metabolism. However, in mixotrophic conditions in presence of acetate, the latter becomes the prominent carbon source <sup>31</sup>. We exploited this metabolic feature for incorporating  $^{13}\text{C}$  providing the carbon source in form of labeled sodium acetate. Cells were nevertheless exposed to a low light intensity, close to the compensation point, to maintain photosynthetic metabolism active. Also cells were cultivated in flasks, where  $\text{CO}_2$  diffusion from the atmosphere is limited in order to further stimulate acetate assimilation from the medium <sup>32</sup>.

Three rounds of cultivation in labeled medium were performed in these conditions with a tenfold dilution at every step. This assured the labeling of a very large majority of the molecules at the end of the cultivation.

## Characterization by SDS-page analysis and by $^{13}\text{C}$ - $^{13}\text{C}$ NMR

NMR spectra contain a wealth of structural information because the NMR isotropic chemical shifts are unique fingerprints for each type of atom. However, going from isolated protein or lipid systems to heterogeneous biological membranes, spectra become very crowded and individual molecular components are no longer resolved. Thylakoid membranes have the advantage that one type of proteins, the photosynthetic light-harvesting complexes, are abundant, reminiscent of recombinant-expressed proteins in host cell membranes. This is illustrated in figure 1, presenting a Coomassie-stained SDS-page analysis of the *Cr.* thylakoid membrane preparations of both WT and *npq2*, loaded with equal volume amounts of membrane material. The LHCII (indicated with the arrows) appears as the most abundant polypeptides in both strains. The *Cr.* LHCII trimeric complexes are isomers built from polypeptides encoded by 9 genes<sup>33-34</sup> with molecular masses between 22 and 26 kDa.

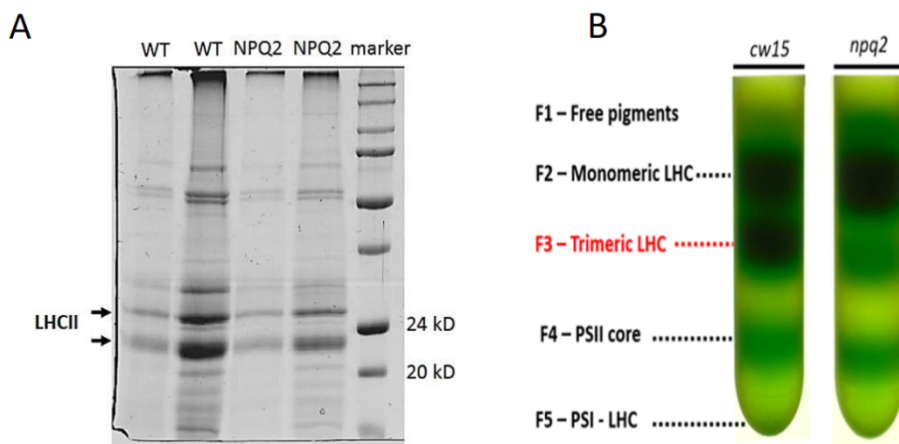


**Figure 1.** **A:** Coomassie-stained SDS-page of WT and *npq2* *Cr.* thylakoid membranes, with 2 μl (lane 1 and 3) or 10 μl (lane 2 and 4) loading of membrane material. **B:** Monomeric and trimeric distribution of LHCII in WT and *npq2* thylakoid membranes.

Figure 2 shows a spin-diffusion  $^{13}\text{C}$ - $^{13}\text{C}$  NMR spectrum (PDSF, mixing time 25 ms) of the WT and *npq2* thylakoid membranes compared with the one of isolated *Cr.* LHCII. The NMR spectrum of WT thylakoid membranes strongly overlaps

with the spectrum of isolated LHCII, indicating that the LHC signals dominate the NMR spectra of thylakoid membranes, consistent with the fact that this is the most abundant protein according to the SDS-page analysis in figure 1. Nevertheless, the membrane spectra are very congested due to the fact that cells were uniformly isotope-labeled and resonances of protein, lipid and pigment constituents are detected simultaneously.

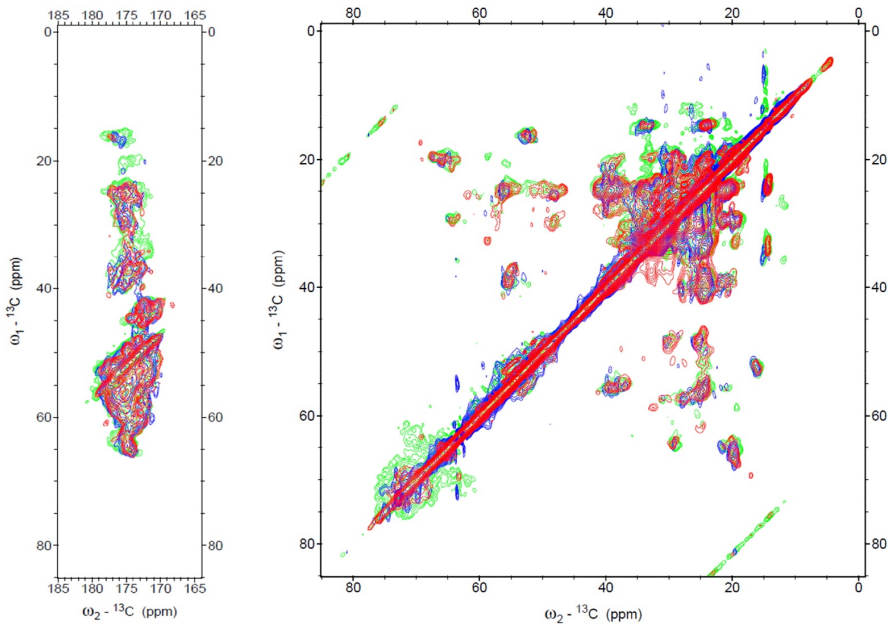


**Figure 2.**  $^{13}\text{C}$ - $^{13}\text{C}$  spectrum of isolated LHCII overlaid on the spectrum of WT and *npq2* thylakoid membranes. Green; *npq2* thylakoid membrane, red; LHCII, blue; WT thylakoid membrane.

## Polarization transfer NMR

An elegant way to reduce spectral crowding and improve resolution is by use of NMR  $^1\text{H}$ - $^{13}\text{C}$  polarization-transfer spectral editing. NMR polarization-transfer experiments are selective for molecules with dynamics within a certain frequency window and filter out the NMR signals of all other components. By combining polarization-transfer experiments with different frequency filters, rigid and mobile molecular components are differentiated by their selective enhancement. In addition, the transfer of the magnetization from protons to  $^{13}\text{C}$  gives rise to signal enhancement owing to the  $\sim 4$  times enlarged gyromagnetic ratio of  $^1\text{H}$  compared to  $^{13}\text{C}$ . A comparison of polarization-transfer obtained spectra with spectra obtained through direct  $^{13}\text{C}$  excitation, which

detects signals within a large frequency window, provides an estimation of the rigid and mobile fractions out of the total number of molecular constituents.

To gain insight in protein and lipid molecular dynamics inside thylakoid membranes, a set of one-dimensional solid-state  $^{13}\text{C}$  NMR experiments were employed applying  $^1\text{H}$ - $^{13}\text{C}$  polarization-transfer sequences that used cross polarization (CP)<sup>35</sup> or insensitive nuclei enhancement (INEPT)<sup>36</sup>, and applying direct  $^{13}\text{C}$  polarization (DP)<sup>37</sup>. In DP experiments, the  $^{13}\text{C}$  nuclei are directly polarized during the spin-lattice relaxation process and DP detects all type of molecular constituents. CP and INEPT experiments can be applied as frequency filters<sup>38</sup> that are selective for slow, resp. fast molecular dynamics. CP experiments provide NMR spectra of  $^{13}\text{C}$  in solids or insoluble proteins by polarization transfer from  $^1\text{H}$  nuclei via dipolar couplings. CP signal intensity enhancement depends on the relative gyromagnetic ratios of  $^1\text{H}$  and  $^{13}\text{C}$ , which are  $\gamma_{\text{H}} = 267.5$  ( $10^6 \text{ rad S}^{-1} \text{ T}^{-1}$ ) and  $\gamma_{\text{C}} = 67.2$  ( $10^6 \text{ rad S}^{-1} \text{ T}^{-1}$ ). The enhancement factor of the CP signal intensity compared to DP is maximal  $\gamma_{\text{H}}/\gamma_{\text{C}}$ , which is almost a factor of 4. However, the actual enhancement factor depends on molecular motions since the CP technique is based on dipolar  $^1\text{H}$ - $^{13}\text{C}$  couplings, which for dynamic molecules will average to zero, marking loss of CP signal intensity and lower CP/DP intensity ratios. Mobile constituents, on the other hand, are signal enhanced when the polarization is transferred via scalar couplings ( $J$ -couplings), which occur in INEPT. The process of polarization via  $J$ -couplings is in itself not affected by motions, but scalar coupling occurs in the transverse plane where polarization relaxation ( $T_2$ ) depends on motion. Consequently, rigid segments that have fast relaxation times in the transverse plane are not detectable in INEPT<sup>39</sup>.

In solid-state NMR spectra of bio-membranes, CP-enhanced signals typically include lipid molecules with high segmental order in the crystalline phase. Because of their restricted motions, the  $^1\text{H}$ - $^{13}\text{C}$  dipolar couplings are not averaged to zero, making CP efficient, while fast  $T_2$  relaxation excludes their visibility in INEPT spectra. In addition,  $^{13}\text{C}$  carbonyl resonances of membrane-embedded proteins, which have restricted conformational dynamics, are visible in CP-based spectra. INEPT is sensitive for molecules with fast (sub-nanosecond) dynamics. For bio membranes, these typically include mobile lipids with low segmental order in the fluid gel phase, which have long  $T_2$  relaxation times that makes INEPT efficient, while averaging of the  $^1\text{H}$ - $^{13}\text{C}$  dipolar couplings by bond re-orientation excludes them from CP spectra.

We analyzed thylakoid membrane preparations of WT and *npq2* by  $^{13}\text{C}$  MAS NMR using DP, CP and INEPT for mobile spectral editing. In addition, as a comparison the set of experiments was performed on samples of isolated LHCII

in  $\beta$ -dodecyl maltoside ( $\beta$ -DM) detergent micelles and of LHCII aggregates, obtained by detergent removal, of which preparations have been described in detail in <sup>40</sup>. As presented in <sup>40</sup> the detergent-solubilized LHCII proteins are in a fluorescent state, mimicking the proteins under active light-harvesting conditions. The LHCII aggregates are in strongly fluorescence-quenched states, mimicking the photoprotective states of the proteins. Figure 3 illustrates which thylakoid membrane components are signal-enhanced and distinguished in the CP and INEPT experiments, as described in detail below. In the additional DP experiments, in the figure 3 depicted membrane components are detected.

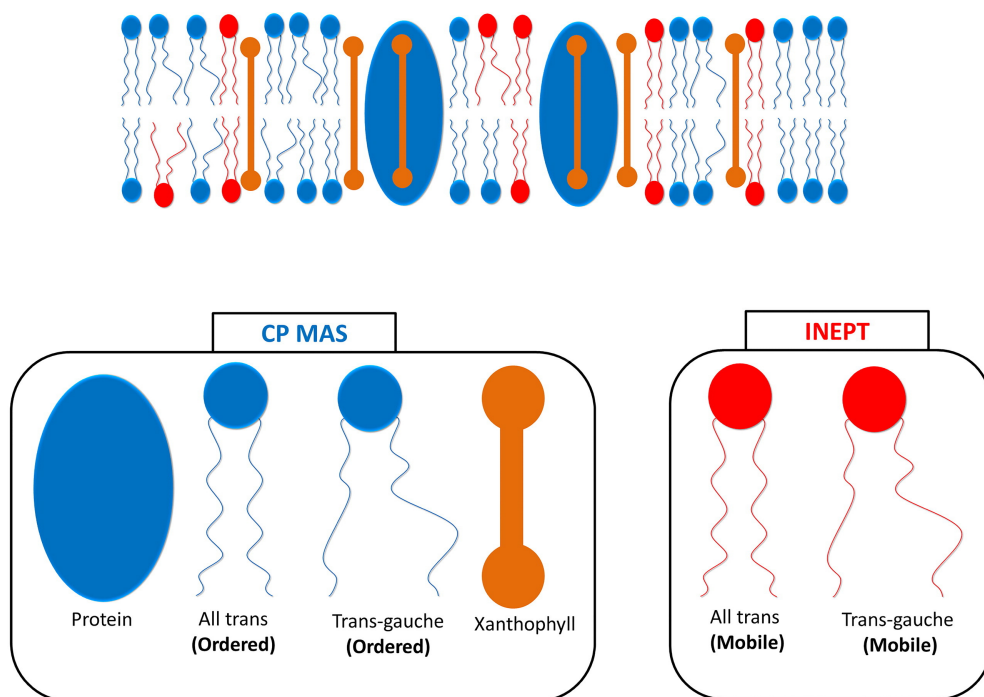


**Figure 3.** Illustration of thylakoid membrane constituents that are selectively probed with CP and INEPT experiments, showing the lipids in blue and red, proteins in blue and xanthophylls in orange.

Figure 4 presents the CP (blue), DP (black) and INEPT (red)  $^{13}\text{C}$  MAS-NMR spectral intensities for WT (A) and *npq2* (B) thylakoid membranes and for WT isolated LHCII in detergent micelles (C) and LHCII aggregates (D). The INEPT spectra in figure 4 contain NMR signals characteristic for lipids, while CP spectra contain bands typical of protein backbone and side-chain carbon atoms, as well as peaks typical of fatty-acyl chains. In figure 4A and B the lipid galactosyl head-group resonances are obscured by the natural-abundance  $^{13}\text{C}$

resonances of glycerol that was present in the buffer. The large intensities of the lipid signals in CP (blue spectra) compared to INEPT (red spectra) indicate that the majority of the lipid molecules are in the ordered phase with restrained dynamics, while there is only a small fraction of mobile lipids. The two resonance peaks around 40 ppm are identified as Chl phytol chain signals that are visible both in CP and INEPT, and a small band between 135-140 ppm is identified as the unresolved accumulated resonances of the xanthophyll fatty-acyl chains. NMR resonances of the chlorophyll (Chl) macrocycles are not observed at ambient temperatures, but could be observed in 2D  $^{13}\text{C}$ - $^{13}\text{C}$  spectra at cryogenic temperatures <sup>40</sup>.

For both the WT and *npq2* membrane preparations, protein signals from the backbone C' and C $_{\alpha}$  atoms are more pronounced in DP than in CP, indicating that the proteins have considerable conformational dynamics on micro to millisecond time scales where cross polarization becomes inefficient. As a control, CP and DP experiments were performed on a tri-peptide powder sample using the same pulse sequences (data not shown). In this case,  $^{13}\text{C}$  CP signal intensities were roughly four times larger than the directly polarized  $^{13}\text{C}$  signal intensities, in line with the maximal expected enhancement of CP based on the  $^1\text{H}$  and  $^{13}\text{C}$  gyromagnetic ratios for a rigid solid. For the WT, the xanthophyll band between 135-140 ppm is only observed in DP while for the *npq2* mutant the band appears in CP, indicating that *npq2* mutant contains xanthophylls with reduced fatty-acyl chain dynamics. No CP signal was detected for LHCII in  $\beta$ -DM micelles (figure 4C, blue curve) that undergo fast tumbling in solution, which confirms that all LHCII protein complexes were solubilized, representing a fully liquid state without protein aggregation. On the contrary, for LHCII aggregates (figure 4D), strong CP signals are detected. However, also here the DP intensities dominate over the CP, as is the case for the membrane preparations, indicating that despite their strong aggregation, the LHCII complexes possess significant dynamics on sub-millisecond time scales. The  $^{13}\text{C}$  NMR spectra of isolated LHCII (figure 4C and D) also contain resonance signals of lipids that are co-purified with the proteins. LHCII-associated lipids are also observed in the LHCII crystal structures of *pea* and *spinach* <sup>41-42</sup>. In two-dimensional  $^{13}\text{C}$ - $^{13}\text{C}$  spin-diffusion spectra of isolated LHCII, resonances of the mono-galactosylglycerol (MGDG) and di-galactosylglycerol (DGDG) lipid sugar head groups could be resolved <sup>40</sup>. The 2D-resolved resonances confirm that these signals are not natural-abundance  $^{13}\text{C}$  resonances of traces of detergent. Although galactosyl head groups of  $\beta$ -dodecyl maltoside detergent molecules have  $^{13}\text{C}$  chemical shifts that overlap with those of galactolipids, the probability of detecting natural abundance  $^{13}\text{C}$  carbons in two-dimensional  $^{13}\text{C}$ - $^{13}\text{C}$  spectra ( $\sim 0.01\%$ ) can be neglected.

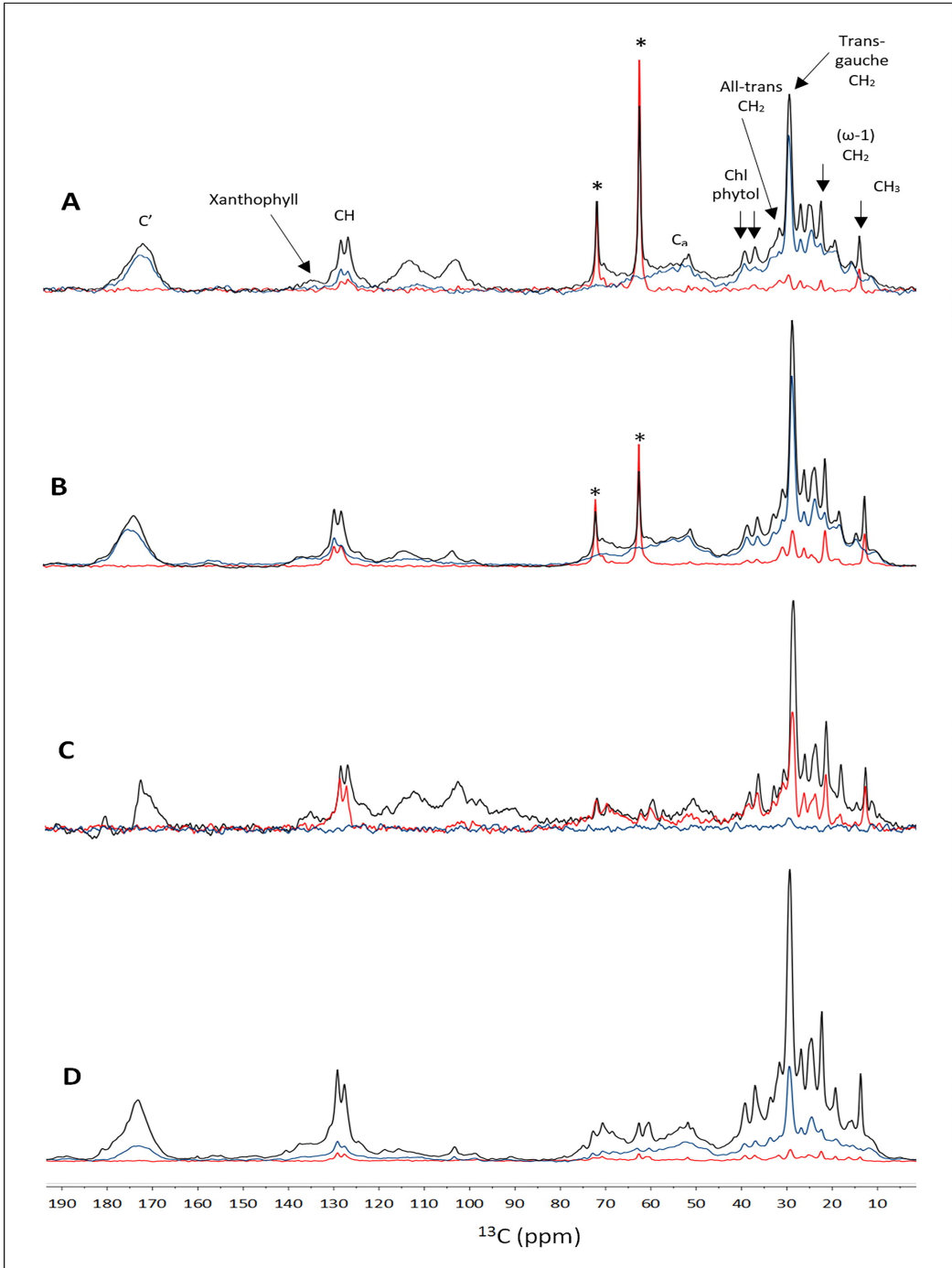


**Figure 4.** Overlaid  $^{13}\text{C}$  DP (black),  $^{13}\text{C}$  CP (blue) and  $^{13}\text{C}$  INEPT (red) spectra recorded at 25 °C. **A:** WT thylakoid membranes; **B:** *npq2* thylakoid membranes; **C:** LHCII in detergent micelles; **D:** LHCII aggregates. \*Natural-abundance  $^{13}\text{C}$  signals of glycerol.

## Temperature-dependent dynamics of protein and lipid constituents

To detect molecular dynamics over a physiological temperature range, CP and INEPT spectra were collected between 0 and 25°C. At high temperatures, a small gradual decrease of the CP intensities is observed, consistent with loss of CP efficiency due to increased molecular dynamics. This is shown in figure 5, where the carbonyl and  $C_\alpha$  integrated peak intensities are plotted against temperature. Simultaneously, INEPT intensities, which detect the dynamic behavior of the mobile lipids, gradually increase with temperature, indicating enlargement of the fraction of mobile lipids. This is shown in the data in figure 6 that reflect the temperature-dependent dynamics of the mobile-phase lipids along their fatty-acyl chains. The end-tails of the mobile lipids are probed via the methyl ( $\text{CH}_3$ ) and ( $\omega-1$ )  $\text{CH}_2$  resonances at 21 ppm (figure 6B), and their fatty-acyl chains are probed via their  $n\text{CH}_2$  resonances at 30 ppm (figure 6C) and via the CH resonances between 128-132 ppm (figure 6D). The assignment of discussed resonances is presented in figure 4A and 6A. The fatty-acyl chain INEPT intensities of the *npq2* mutant increase more steeply with temperature, indicating enlarged dynamics of the mobile lipids in *npq2* membranes at elevated temperatures, compared to the WT.

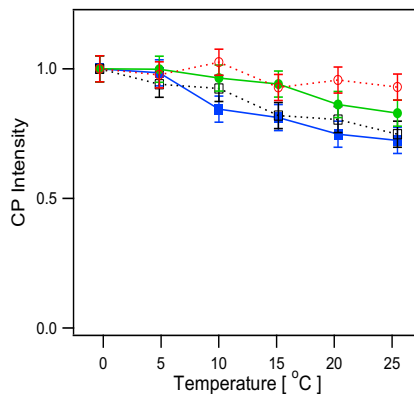


**Figure 5.**  $^{13}\text{C}$  CP-MAS integrated  $C'$  and  $C_\alpha$  intensities of WT and *npq2* as function of temperature. Filled blue squares:  $C'$  region WT; open black squares:  $C'$  region *npq2*; filled green circles:  $C_\alpha$  region WT; open red circles:  $C_\alpha$  region *npq2*.

The dynamics of the ordered lipids with temperature was followed in CP spectra. The lipid peaks here are not fully resolved because they overlap with the broad bands of protein side chains. Figure 7 shows the CP intensities of the main lipid peak at 30 ppm containing the unresolved  $n\text{CH}_2$  resonances, and of the small



lipid peak at 32 ppm at different temperatures. Lipids can adapt an *all-trans* or *trans-gauche* conformation with different  $^{13}\text{C}$  chemical shifts for the acyl chain carbons.

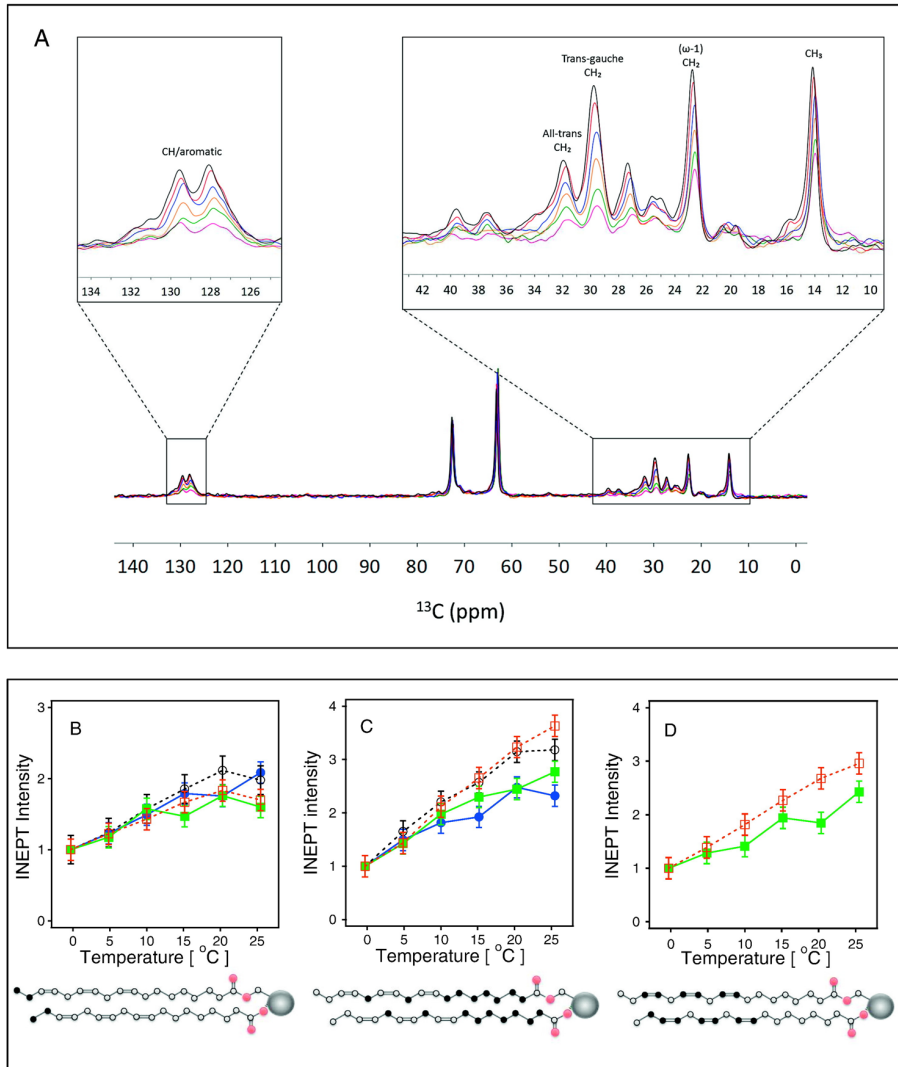


**Figure 6.**  $^{13}\text{C}$  INEPT intensities of WT and *npq2* membranes at different temperatures. **A:** INEPT spectra of *npq2* recorded at temperatures between 0 and 25 °C. **B-D:** integrated INEPT spectral regions at different temperatures. The regions correspond to the lipid carbon atoms colored in black in the lipid molecules schematically drawn in the pictures below. **B:** Filled green squares:  $\text{CH}_3$  region WT; open red squares:  $\text{CH}_3$  region *npq2*; filled blue circles:  $(\omega-1)$   $\text{CH}_2$  region WT; open black circles:  $(\omega-1)$   $\text{CH}_2$  region *npq2*. **C:** Filled green squares: *trans-gauche*  $\text{CH}_2$  region WT; open red squares: *trans-gauche*  $\text{CH}_2$  region *npq2*; filled blue circles: *all-trans*  $\text{CH}_2$  region WT; open black circles: *all-trans*  $\text{CH}_2$  region *npq2*. **D:** Filled green squares: CH/aromatic region WT; open red squares: CH/aromatic region *npq2*.

The small peak at 32 ppm originates from CH<sub>2</sub> carbons of lipids in the *all-trans* conformation, while the main peak at 30 ppm represents the CH<sub>2</sub> carbons of lipids in *trans-gauche* conformation<sup>43</sup> (see also figures 4 and 6). The latter lipid conformation is abundant because thylakoid membranes have a high degree of unsaturated lipids. In contrast to other CP signal intensities that decrease at elevated temperatures due to enlarged molecular dynamics, the intensity of the *trans-gauche* lipid peak at 30 ppm increases with temperature. The observed increase is indicative of *all-trans* => *trans-gauche* isomerization at elevated temperatures. The gain of CP signal due to accumulation of *trans-gauche* lipids is partly compensated by loss of CP efficiency caused by increased lipid mobility. To disentangle the counteracting effects of dynamics and isomerization on the main lipid peak, we compared the 30/32 peak ratios in DP experiments that are not sensitive to dynamics changes. The WT and *npq2* membranes have similar 30/32 ratios at 7 and 25°C (0.32, resp. 0.42 for WT and 0.32, resp. 0.48 for *npq2*), from which we conclude that the fractions of *trans-gauche* and *all-trans* lipids in the two samples are similar. The differential slopes of the WT (solid lines) and *npq2* (dashed lines) temperature curves in figure 7 we therefore ascribe to differential dynamics of the ordered lipids in WT and *npq2*. The ordered lipids in *npq2* apparently are less responsive to temperature changes, with smaller losses of CP efficiencies, having reduced dynamics compared to the WT.

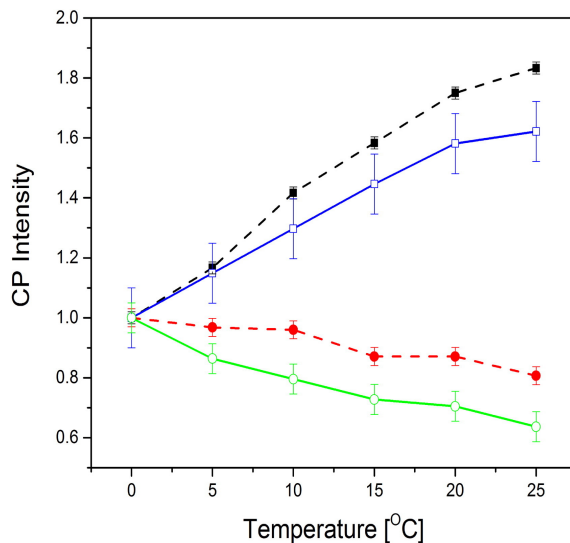


**Figure 7.** <sup>13</sup>C CP-MAS intensities of WT and *npq2*, illustrating lipid isomerization as a function of temperature. Filled black squares: *trans-gauche* CH<sub>2</sub> region *npq2*; open blue squares: *trans-gauche* CH<sub>2</sub> region WT; Filled red circles: *all-trans* CH<sub>2</sub> region *npq2*; Filled green circles: *all-trans* CH<sub>2</sub> region WT.

## $T_{1\rho}$ relaxation experiments

In addition to the polarization-transfer experiments, we measured  $^{13}\text{C}$   $T_{1\rho}$  relaxation of the WT and *npq2* membranes at 7 and 25 °C. Measurements of spin-lattice longitudinal relaxation in the rotating frame ( $T_{1\rho}$ ) offer investigations of molecular dynamics from microsecond to millisecond and are sensitive to protein slow conformational dynamics.  $T_{1\rho}$  describes the decay of magnetization along the RF field  $B_1$ , by applying a spin-lock pulse in the rotating frame of reference. Molecular fluctuations with frequencies close to  $\gamma B_1$ , i.e. in the range of 10-100 kHz, will induce relaxation of the magnetization along  $B_1$ . The  $^{13}\text{C}$   $T_{1\rho}$  relaxation rates also depend on the rate of  $^1\text{H}$ - $^{13}\text{C}$  magnetization exchange ( $K_{\text{HC}}$ ) and on the  $^1\text{H}$  spin-lattice relaxation rate ( $K_{\text{H}}$ ), as illustrated in the kinetic scheme in figure 8. The mixing time during which magnetization is exchanged is set experimentally by the CP contact time,  $\tau_{\text{CP}}$ .

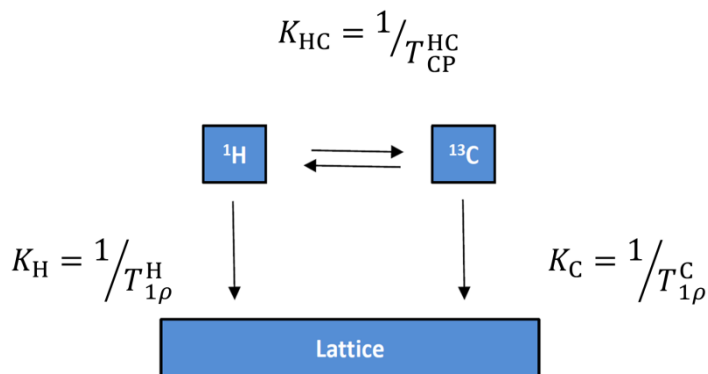


**Figure 8.** Kinetic scheme of  $^1\text{H}$  to  $^{13}\text{C}$  polarization transfer and  $T_{1\rho}$  spin relaxation.

We performed  $^{13}\text{C}$   $T_{1\rho}$  experiments with  $\tau_{\text{CP}}=256 \mu\text{s}$  in order to limit proton-driven spin diffusion and inter-carbon magnetization transfer, which lead to averaging of relaxation lifetimes of neighboring carbons. Figure 9 shows the backbone  $T_{1\rho}$  relaxation curves, obtained by integrating intensities over the backbone carbonyl peak. Instead of a single lifetime, we expect a distribution of lifetimes since the membranes contain a distribution of proteins and each protein contains multiple amino-acid residues with varying structures and dynamics. Therefore backbone  $T_{1\rho}$  relaxation curves were fit with stretched exponentials  $(e^{-t/T_{1\rho}})^\beta$  using a fixed parameter ( $\beta=0.7$ ). The  $\text{C}'$   $T_{1\rho}$  lifetimes for WT and *npq2* are similar at 7 °C, but at 25 °C the  $\text{C}'$   $T_{1\rho}$  lifetime is much more shortened for the WT, suggesting enlarged protein dynamics for the WT, but not

for *npq2* membranes, at high temperature. WT  $T_{1\rho}$  relaxation curves at 7 °C were also recorded with a  $\tau_{CP}$  of 2 ms. As shown in Table 1, the longer  $\tau_{CP}$  shortens the observed average C'  $T_{1\rho}$  from 9.4 to 6.8 ms.  $C_\alpha$   $T_{1\rho}$  lifetimes were analyzed by taking the integrated intensities of the  $C_\alpha$  band (see also Table 1). For some of the  $C_\alpha$  data sets, the fit significantly improved if instead of a stretched exponential a double-exponential fit function was used, which suggests that despite the short  $\tau_{CP}$  applied, the observed  $C_\alpha$  relaxation kinetics are partly averaged over the side chains, giving rise to multi-exponential kinetics. Overall, the observed  $C_\alpha$  lifetimes do not change much at the two temperature conditions and are quite similar for the *npq2* and WT membranes. The  $C_\alpha$   $T_{1\rho}$  lifetimes differ significantly from the C'  $T_{1\rho}$  lifetimes, confirming that the C' relaxation rates are not averaged over all the carbons, but contain the characteristics of the specific atom type.

Sample/atom	$T_{1\rho}$ (ms, 7 °C)		$T_{1\rho}$ (ms, 25 °C)	
<b>WT</b>				
C'	9.4 ± 1.5		1.5 ± 0.5	
$C_\alpha$	± 0.3	[2.7 ± 0.9]*	± 0.4	[3.1 ± 2.0]*
C' ( $\tau_{CP}$ = 2 ms)	6.8 ± 1.1		--	
<b><i>npq2</i></b>				
C'	10.4 ± 3.1		7.2 ± 2.2	
$C_\alpha$	0.7 ± 0.5	[5.0 ± 2.0]*	0.9 ± 0.3	[4.4 ± 1.8]*
<b>LHCII<sub>agg</sub></b>				
C'	9.5 ± 4.0		1.8 ± 1.3	
$C_\alpha$	0.9 ± 0.8	[3.6 ± 1.6]*	0.5	[7.9 ± 3.7]*

**Table 1.**  $T_{1\rho}$  lifetimes of the carbonyl and  $C_\alpha$  atoms, for WT and *npq2* *Cr.* thylakoid membranes and for LHCII aggregates (LHCII<sub>agg</sub>). \*Fitting with a double-exponential fit instead of a stretched exponential; value presents the lifetimes of the slow components.

The difference between the WT and the *npq2* C'  $T_{1\rho}$  lifetimes seems in apparent contradiction with the observed CP/DP ratios of the carbonyl peaks in the spectra in figure 4, that are very similar for WT and *npq2*. The reason lies in the short  $\tau_{CP}$  that was used for the  $T_{1\rho}$  experiments. Figure 10 shows the buildup curves for C' and  $C_\alpha$  polarization as function of CP contact times for isolated LHCII. The rise and decay reflect the rates for resp.  $^1\text{H}$ - $^{13}\text{C}$  transfer, building up

the carbon magnetization, and for  $T_{1\rho}$  spin-lattice relaxation as illustrated in the scheme in figure 8.

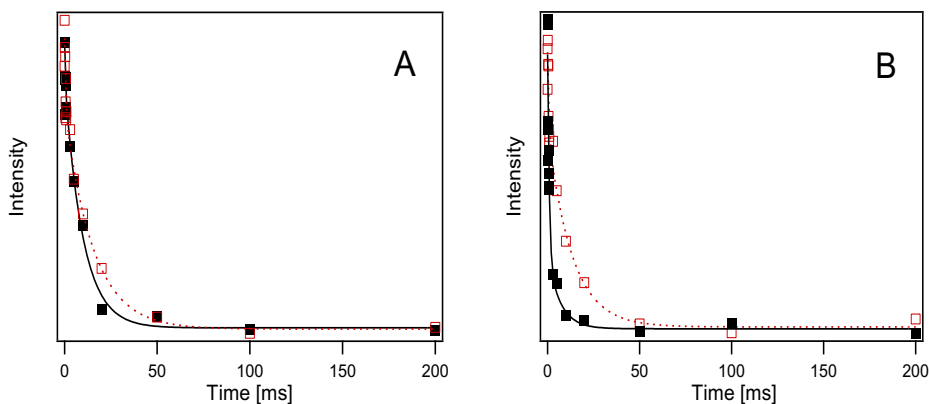


**Figure 9.**  $^{13}\text{C}'$   $T_{1\rho}$  relaxation curves of WT and *npq2*.  $T_{1\rho}$  relaxation at 7 °C. **A:** and 25 °C. **B:** of WT (black filled squares) and *npq2* (red open squares) and stretched-exponential fits (WT, solid black lines; *npq2*, red dashed lines). The fit relaxation lifetimes are 9.4 ms (WT, 7 °C), 10.4 ms (*npq2*, 7 °C), 1.4 ms (WT, 25 °C) and 7.8 ms (*npq2*, 25 °C).

The carbonyl carbons have slow buildup of the polarization because they lack directly attached protons. With  $\tau_{\text{CP}}=256 \mu\text{s}$ , only a fraction of the  $\text{C}'$  carbons are polarized, while with  $\tau_{\text{CP}}=2 \text{ ms}$  (used for the experiments presented in figure 4) the signal is maximal and all  $\text{C}'$  carbons are polarized. As shown in Table 1, the  $\text{C}'$   $T_{1\rho}$  lifetime substantially increases with  $\tau_{\text{CP}}=256 \mu\text{s}$  compared to  $\tau_{\text{CP}}=2 \text{ ms}$ . We conclude from this that with  $\tau_{\text{CP}} = 256 \mu\text{s}$  a fraction of  $\text{C}'$  carbons is detected that has reduced conformational dynamics compared to the average carbonyls. This is consistent with the fact that dynamical molecules will have smaller  $^1\text{H}$ - $^{13}\text{C}$  coupling compare to rigid molecules, requiring longer contact times for efficient cross polarization. In contrast, the  $\text{C}_\alpha$  carbons have a fast buildup of the polarization that is already maximal at  $256 \mu\text{s}$  and have fast spin-lattice relaxation, causing loss of signal with longer  $\tau_{\text{CP}}$ . The  $\text{C}_\alpha$   $T_{1\rho}$  lifetimes thus represent the mean value of all the  $\text{C}_\alpha$  carbons. The  $T_{1\rho}$  data enables us to identify a fraction of rigid protein carbonyls that only for the WT gain significant dynamics between 7 and 25 °C.

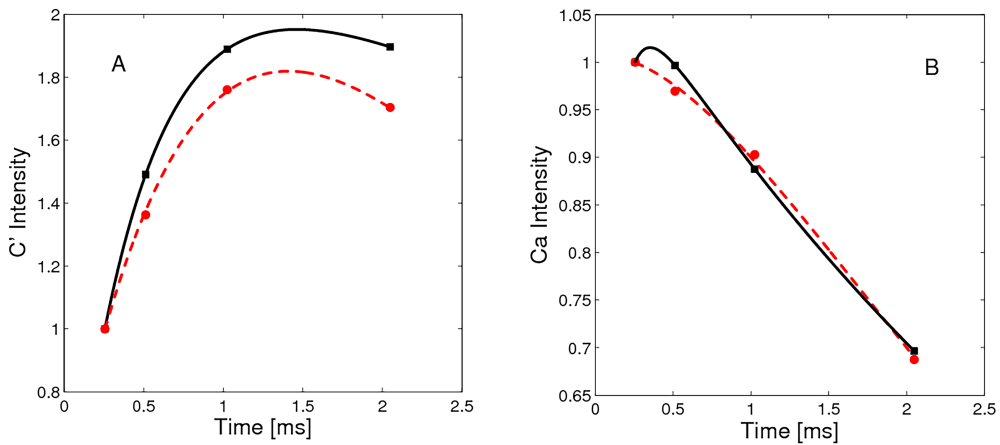


**Figure 10.** A:  $C'$  buildup curve of LHCII aggregates at 7 °C (black squares) and 25 °C (red circles) and double-exponential fits (7 °C, solid black lines; 25 °C, red dashed lines). B:  $C_\alpha$  buildup curve of LHCII aggregates at 7 °C (black squares) and 25 °C: (red circles) and double-exponential fits (7 °C, solid black lines; 25 °C, red dashed lines).

## Discussion

### Molecular dynamics of LHCII *in-vivo* and of pigment-protein complexes *in-vitro*

*Cr.* thylakoid membranes are heterogeneous and contain the full photosynthetic apparatus with different protein constituents. Based on the  $^{13}\text{C}$ - $^{13}\text{C}$  NMR spectra that are dominated by LHCII we can conclude that the observed *in-situ* protein dynamics to large extent represent the properties of LHC proteins. Compared to the lyophilized tri-peptide model used as a control, the proteins inside thylakoid membranes contain considerable dynamics on a microsecond to millisecond time scale, reflected by the relatively low CP/DP intensity ratios. For the LHCII aggregate sample the CP/DP ratios were even lower, implying that in the aggregates the LHCII complexes retain significant mobility that is more comparable with the dynamics of polymers or hydrogels than that of protein crystals. The INEPT background signal, typical of protein  $C_\alpha$  and side-chain atoms, could represent a small fraction of non-aggregated LHCII with high mobility. This would indicate that equilibrium exists between aggregated and free proteins, which is strongly shifted towards the aggregated forms. The lipid signals in the LHCII aggregate spectra are much more pronounced in CP than in INEPT, demonstrating that the contained lipids have restrained dynamics and likely are protein associated, and not co-purified from the bulk. No

significant CP signal could be detected for LHCII in detergent micelles at ambient temperatures, confirming that highly concentrated samples, as required for solid-state NMR, can be prepared without aggregation. Previous data have shown that CP-based spectra can be obtained of frozen protein-micelle solutions at cryogenic temperatures <sup>40, 44-45</sup>.

The LHCII Chl macrocycle signals are neither detected by CP nor by INEPT-based <sup>13</sup>C-<sup>13</sup>C spectra at ambient temperatures. Their molecular motions apparently occur on intermediate time scales where both type of experiments are inefficient. The Chl macrocycle NMR resonances of the membrane preparations emerge in NMR spectra at cryogenic temperatures and are weakly visible at 244K (data not shown). In our previous work, a dynamic transition was revealed between 223K and 244K for the Chls in detergent-solubilized LHCII <sup>40</sup> and their macrocycle chemical shifts started to disappear from CP-based <sup>13</sup>C-<sup>13</sup>C spectra above 223K. In line with these NMR observations, quasi-elastic neutron scattering experiments showed a dynamical transition at 244K for LHCII in detergent micelles <sup>46</sup>. The transition was accompanied with a shift of the Chl *a* absorption maximum that was ascribed to a variety of conformational sub-states of Chl612, based on altered results for a Chl612 mutant. Our previous NMR study also showed that for LHCII aggregates the Chl macrocycle chemical shifts are still visible at 244K, demonstrating that LHCII aggregation reduces the Chl conformational dynamics. According to our low-temperature data of the thylakoid membrane samples, the conformational dynamics of protein-bound Chls in the membranes is intermediate between the values for LHCII aggregates and for LHCII detergent micelles. The difference in dynamics suggests that the detergent micelle forms an artificial microenvironment where the LHC pigment-protein complexes are more flexible than in their native states. Liposomal membranes or lipid nano-discs may provide a microenvironment that is closer to their *in-vivo* states <sup>44, 47</sup> and it will be of interest to address the dynamics and conformational sub-states of Chls in membrane-reconstituted LHCII.

## Differential dynamics in *npq2* and WT membranes: the effects of Zea accumulation

No abrupt changes were detected following CP and INEPT intensities over the range 0-25 °C that would clearly mark a phase transition. Instead, the temperature curves show gradual increase in dynamics of the 'fast' and 'slow' membrane components and of lipid isomerization, consistent with an overall rise of membrane molecular dynamics at elevated temperatures on both fast (ps-ns) and slow (>ms) time scales. In *npq2* membranes, the ordered lipids are less sensitive to temperature changes, whereas the mobile lipids have enlarged

dynamics compared to the WT. This effect is the opposite of the reported influence of polar xanthophylls that were shown to act as membrane modulators, increasing membrane fluidity in the ordered phase, while decreasing the fluidity in the liquid crystalline phase, thereby broadening gel-to-fluid phase transitions<sup>48</sup>. The reverse effect might show for *Zea*-accumulating membranes, compared to WT membranes that mainly constitute Vio, because *Zea* is a less-polar xanthophyll<sup>20</sup>. Our lipid dynamics analysis predicts that *Zea*-accumulating membranes will have narrower gel-to-fluid phase transitions than for WT, which might be an advantage under stress conditions since this allows faster switching between the phases.

In both WT and *npq2* thylakoid membranes the fraction of mobile lipids is small compared to the fraction of ordered lipids. The overall membrane fluidity will therefore be dominated by the behavior of the ordered-phase lipids and consequently, is reduced for *Zea*-containing membranes. The fraction of ordered lipids could represent lipids that are associated with proteins or stabilized in between super complexes, while the mobile lipids represent the bulk lipids that are not in direct protein contact. The restricted dynamics of the majority of the lipids despite their large number of unsaturation suggests that in the tightly packed thylakoid membranes, where greater part of the surface area is protein occupied, most of the lipids are immobilized between the protein complexes.

The slow-dynamics membrane components that are observable via CP can be further separated in rigid and dynamic subsets based on  $T_{1\rho}$  relaxation kinetics using short contact times. The  $T_{1\rho}$  lifetimes indicate that the *npq2* membranes contain a subset of protein sites with limited conformational dynamics that only modestly respond to temperature changes between 7 and 25 °C. *Npq2* mutation was shown to not affect photosynthetic apparatus composition, nor photosystems antenna size, even in different light conditions<sup>49</sup>. In the *npq2* membranes, however, LHCII proteins are more prone to monomerization as shown in previous studies in *A. thaliana*<sup>50-53</sup> and confirmed in Figure 1. Upon monomerization though rather an increase of flexibility is expected than enlarged rigidity. In the *npq2* membranes however, protein aggregates may have formed that do not disassemble at high temperature and in which proteins have restricted conformational dynamics. On the other hand,  $T_{1\rho}$  measurements on WT LHCII *in-vitro* aggregates do not show a reduced conformational dynamics compared to proteins in the WT membranes. Alternatively to aggregation, binding of *Zea* could alter the intrinsic dynamics of pigment-protein complexes at local sites. Such sites would form a subset of carbonyls that are rigidified compared to protein carbonyls in the WT membranes explaining the increased  $C'$   $T_{1\rho}$  of *npq2* membranes at room temperature. In that respect it is interesting that we also observe reduced conformational dynamics of the



xanthophylls in *npq2*. The molecular structure of *Zea* only differs from *Vio*, its epoxidized form, at the head group. Due to the de-epoxidized head groups, *Zea* xanthophylls are more hydrophobic <sup>20</sup>, which could change their interactions with both the lipid and protein direct environments.

## Conclusion

---

Summarizing the results from spectral editing and relaxation experiments, we can conclude that *Zea* accumulating membranes have (1) more rigid xanthophylls, (2) contain a subset of rigid protein sites that are less sensitive to temperature changes, and (3) contain thylakoid lipids that span a broader dynamical range with reduced fluidity of the large pool of ordered-phase lipids, and enlarged acyl-chain dynamics of the small pool of mobile lipids. Our observation that *Zea*-rich *npq2* membranes contain xanthophylls, protein and ordered-phase lipid constituents with lower backbone and fatty-acyl chain dynamics is consistent with the detected overall increase in membrane rigidity in *Zea*-containing membranes as discussed in literature, at least for what concerns *A. thaliana* <sup>50, 54</sup>. The co-existence of ordered and mobile lipids suggests that the thylakoid membranes of both WT and *npq2 Cr.* cells contain segregated membrane domains, which may differ in size and composition. Additional electron or atomic-force microscopy would have to be performed to address the effect of *Zea* accumulation on the supramolecular membrane organization, while additional NMR experiments on *Zea*-containing LHCII could address the effect of xanthophyll exchange on protein internal molecular dynamics.

## References

---

1. Blankenship, R. E., *Molecular mechanisms of photosynthesis*. Second edition ed.; Wiley/Blackwell: Chichester, West Sussex, 2014; p 296.
2. Kruger, T. P.; Ilioaia, C.; Johnson, M. P.; Ruban, A. V.; Papagiannakis, E.; Horton, P.; van Grondelle, R., Controlled disorder in plant light-harvesting complex II explains its photoprotective role. *Biophys J* **2012**, *102* (11), 2669-76.
3. Cruz, J.; Avenson, T.; Kanazawa, A.; Takizawa, K.; Edwards, G.; Kramer, D., Plasticity in light reactions of photosynthesis for energy production and photoprotection. *Journal of experimental botany* **2005**, *56* (411), 395-406.
4. Kirchhoff, H., Structural changes of the thylakoid membrane network induced by high light stress in plant chloroplasts. *Philos Trans R Soc Lond B Biol Sci* **2014**, *369* (1640), 20130225.
5. Kirchhoff, H.; Mukherjee, U.; Galla, H. J., Molecular Architecture of the Thylakoid Membrane: Lipid Diffusion Space for Plastoquinone. *Biochemistry* **2002**, *41* (15), 4872-4882.

6. Kirchhoff, H.; Haase, W.; Wegner, S.; Danielsson, R.; Ackermann, R.; Albertsson, P. A., Low-light-induced formation of semicrystalline photosystem II arrays in higher plant chloroplasts. *Biochemistry* **2007**, *46* (39), 11169-76.
7. Kouřil, R.; Wientjes, E.; Bultema, J. B.; Croce, R.; Boekema, E. J., High-light vs. low-light: Effect of light acclimation on photosystem II composition and organization in *Arabidopsis thaliana*. *Biochimica et biophysica acta. Bioenergetics* **2013**, *1827* (3), 411-419.
8. Schneider, A. R.; Geissler, P. L., Coexistence of fluid and crystalline phases of proteins in photosynthetic membranes. *Biophys J* **2013**, *105* (5), 1161-70.
9. Betterle, N.; Ballottari, M.; Zorzan, S.; de Bianchi, S.; Cazzaniga, S.; Dall'osto, L.; Morosinotto, T.; Bassi, R., Light-induced Dissociation of an Antenna Hetero-oligomer Is Needed for Non-photochemical Quenching Induction. *Journal of biological chemistry* **2009**, *284* (22), 15255-15266.
10. Blankenship, R. E., *Molecular Mechanisms of Photosynthesis*, 2nd Edition. 2014.
11. Mullineaux, C. W.; Kirchhoff, H., Role of Lipids in the Dynamics of Thylakoid Membranes. **2009**, *30*, 283-294.
12. Ruban, A. V.; Johnson, M. P.; Duffy, C. D. P., The photoprotective molecular switch in the photosystem II antenna. *Biochimica et biophysica acta. Bioenergetics* **2012**, *1817* (1), 167-181.
13. Erickson, E.; Wakao, S.; Niyogi, K. K., Light stress and photoprotection in *Chlamydomonas reinhardtii*. *Plant J* **2015**, *82* (3), 449-65.
14. Havaux, M.; Dall'osto, L.; Bassi, R., Zeaxanthin has enhanced antioxidant capacity with respect to all other xanthophylls in *Arabidopsis* leaves and functions independent of binding to PSII antennae. *Plant Physiol* **2007**, *145* (4), 1506-20.
15. McNulty, H. P.; Byun, J.; Lockwood, S. F.; Jacob, R. F.; Mason, R. P., Differential effects of carotenoids on lipid peroxidation due to membrane interactions: X-ray diffraction analysis. *Biochim Biophys Acta* **2007**, *1768* (1), 167-74.
16. Subczynski, W. K.; Markowska, E.; Sieiewiesiuk, J., Effect of polar carotenoids on the oxygen diffusion-concentration product in lipid bilayers. An EPR spin label study *Biochimica et Biophysica Acta*, **1991**, *1068*, 68-72.
17. Jahns, P.; Latowski, D.; Strzalka, K., Mechanism and regulation of the violaxanthin cycle: The role of antenna proteins and membrane lipids. *Biochimica et Biophysica Acta (BBA) - Bioenergetics* **2009**, *1787* (1), 3-14.
18. Holub, O.; Seufferheld, M. J.; Gohlke, C.; Govindjee, G.; Heiss, J.; Clegg, R. M., Fluorescence lifetime imaging microscopy of *Chlamydomonas reinhardtii*: non-photochemical quenching mutants and the effect of photosynthetic inhibitors on the slow chlorophyll fluorescence transient. *Journal of Microscopy*, **2006**, *226*, 90-120.
19. Niyogi, K. K.; Grossman, A. R.; Björkman, O., *Arabidopsis* mutants define a central role for the xanthophyll cycle in the regulation of photosynthetic energy conversion. *Plant Cell* **1998**, *10* (7), 1121-34.
20. Ruban, A. V.; Johnson, M. P., Xanthophylls as modulators of membrane protein function. *Archives of Biochemistry and Biophysics* **2010**, *504* (1), 78-85.
21. Holt, N. E.; Zigmantas, D.; Valkunas, L.; Li, X.-P.; Niyogi, K. K.; Fleming, G. R., Carotenoid Cation Formation and the Regulation of Photosynthetic Light Harvesting. *Science* **2005**, *307* (5708), 433-436.
22. Wilk, L.; Grunwald, M.; Liao, P.-N.; Walla, P. J.; Kühlbrandt, W., Direct interaction of the major light-harvesting complex II and PsbS in nonphotochemical quenching. *Proceedings of the National Academy of Sciences* **2013**, *110* (14), 5452-5456.
23. Xu, P.; Tian, L.; Kloz, M.; Croce, R., Molecular insights into Zeaxanthin-dependent quenching in higher plants. *Scientific Reports* **2015**, *5*, 13679.
24. CLARKE, A.; COULSON, G.; MORRIS, G. J., Relationship between Phospholipid Breakdown and Freezing Injury in a Cell Wall-Less Mutant of *Chlamydomonas reinhardtii*. *Plant Physiol* **1982**, *70*, 97-103.

25. Niyogi, K. K.; Bjorkman, O.; Grossman, A. R., Chlamydomonas Xanthophyll Cycle Mutants Identified by Video Imaging of Chlorophyll Fluorescence Quenching *The Plant Cell* **1997**, *9*, 1369-1380.
26. Harris, E. H., The Chlamydomonas Sourcebook. A Comprehensive Guide to Biology and Laboratory Use. *Science* **1989**, *246*, 4936-1504.
27. Porra, R. J.; Thompson, W. A.; Kriedemann, W. A., Determination of accurate extinction coefficients and simultaneous equations for assaying chlorophylls a and b extracted with four different solvents: verification of the concentration of chlorophyll standards by atomic absorption spectroscopy *Biochimica et biophysica acta* **1989**, *975*, 384-394.
28. Croce, R.; Canino, G.; Ros, F.; Bassi, R., Chromophore Organization in the Higher-Plant Photosystem II Antenna Protein CP26. *Biochemistry* **20025**, *41* (7334-7343).
29. Laemmli, U. K., Cleavage of Structural Proteins during the Assembly of the Head of Bacteriophage T4. *Nature* **1970**, *227* (5259), 680-685.
30. Guan, X.; Stark, R. E., A general protocol for temperature calibration of MAS NMR probes at arbitrary spinning speeds. *Solid State Nucl Magn Reson* **2010**, *38* (2-3), 74-6.
31. Dent, R. M.; Sharifi, M. N.; Malnoe, A.; Haglund, C.; Calderon, R. H.; Wakao, S.; Niyogi, K. K., Large-scale insertional mutagenesis of Chlamydomonas supports phylogenomic functional prediction of photosynthetic genes and analysis of classical acetate-requiring mutants. *Plant J* **2015**, *82* (2), 337-51.
32. Singh, H.; Shukla, M. R.; Chary, K. V.; Rao, B. J., Acetate and bicarbonate assimilation and metabolite formation in Chlamydomonas reinhardtii: a <sup>13</sup>C-NMR study. *PLoS One* **2014**, *9* (9), e106457.
33. Minagawa, J.; Takahashi, Y., Structure, function and assembly of Photosystem II and its light-harvesting proteins. *Photosynthesis Research* **2004**, *82*, 241-263.
34. Natali, A.; Croce, R., Characterization of the major light-harvesting complexes (LHCBM) of the green alga Chlamydomonas reinhardtii. *PLoS One* **2015**, *10* (2), e0119211.
35. Pines, A.; Waugh, J. S.; Gibby, M. G., Proton-Enhanced Nuclear Induction Spectroscopy - Method for High-Resolution Nmr of Dilute Spins in Solids. *Journal of Chemical Physics* **1972**, *56* (4), 1776.
36. Morris, G. A.; Freeman, R., Enhancement of nuclear magnetic resonance signals by polarization transfer. *J. Am. Chem. Soc* **1979**, *101* (3), 760-762.
37. Purusottam, R. N.; Bodenhausen, G.; Tekely, P., Quantitative one- and two-dimensional <sup>13</sup>C spectra of microcrystalline proteins with enhanced intensity. *J Biomol NMR* **2013**, *57* (1), 11-9.
38. Arnold, A. A.; Genard, B.; Zito, F.; Tremblay, R.; Warschawski, D. E.; Marcotte, I., Identification of lipid and saccharide constituents of whole microalgal cells by (1)(3)C solid-state NMR. *Biochim Biophys Acta* **2015**, *1848* (1 Pt B), 369-77.
39. Diehl, P.; Fluck, E.; Kosfeld, R., *NMR Basic Principles and Progress / NMR Grundlagen und Fortschritte*. Springer-Verlag Berlin Heidelberg: 1971; p VIII, 144.
40. Pandit, A.; Reus, M.; Morosinotto, T.; Bassi, R.; Holzwarth, A. R.; de Groot, H. J. M., An NMR comparison of the light-harvesting complex II (LHCII) in active and photoprotective states reveals subtle changes in the chlorophyll a ground-state electronic structures. *Biochimica et biophysica acta. Bioenergetics* **2013**, *1827* (6), 738-744.
41. Liu, Z.; Yan, H.; Wang, K.; Kuang, T.; Zhang, J.; Gui, L.; An, X.; Chang, W., Crystal structure of spinach major light-harvesting complex at 2.72[thinsp]Å resolution. *Nature* **2004**, *428* (6980), 287-292.
42. Standfuss, J.; Terwisscha van Scheltinga, A. C.; Lamborghini, M.; Kühlbrandt, W., Mechanisms of photoprotection and nonphotochemical quenching in pea light-harvesting complex at 2.5 Å resolution. *The EMBO Journal* **2005**, *24* (5), 919-928.
43. Purusottam, R. N.; Senicourt, L.; Lacapère, J. J.; Tekely, P., Probing the gel to liquid-crystalline phase transition and relevant conformation changes in liposomes by

- 13C magic-angle spinning NMR spectroscopy. *Biochimica et Biophysica Acta (BBA) - Biomembranes* **2015**, *1848* (12), 3134-3139.
44. Pandit, A.; Morosinotto, T.; Reus, M.; Holzwarth, A. R.; Bassi, R.; de Groot, H. J. M., First solid-state NMR analysis of uniformly <sup>13</sup>C-enriched major light-harvesting complexes from *Chlamydomonas reinhardtii* and identification of protein and cofactor spin clusters. *Biochimica et Biophysica Acta (BBA) - Bioenergetics* **2011**, *1807* (4), 437-443.
45. Pandit, A.; Buda, F.; van Gammeren, A. J.; Ganapathy, S.; de Groot, H. J. M., Selective Chemical Shift Assignment of Bacteriochlorophyll a in Uniformly [<sup>13</sup>C-<sup>15</sup>N]-Labeled Light-Harvesting 1 Complexes by Solid-State NMR in Ultrahigh Magnetic Field. *The Journal of Physical Chemistry B* **2010**, *114* (18), 6207-6215.
46. Vrandečić, K.; Rätsep, M.; Wilk, L.; Rusevich, L.; Golub, M.; Reppert, M.; Irrgang, K.-D.; Kühlbrandt, W.; Pieper, J., Protein Dynamics Tunes Excited State Positions in Light-Harvesting Complex II. *The Journal of Physical Chemistry B* **2015**, *119* (10), 3920-3930.
47. Akhtar, P.; Pawlak, K.; Kovacs, L.; Bota, A.; Dorogi, M.; Kovács, L.; Bóta, A.; Kiss, T.; Garab, G.; Lambrev, P., Pigment Interactions in Light-harvesting Complex II in Different Molecular Environments. *Journal of biological chemistry* **2015**, *290* (8), 4877-4886.
48. Gruszecki, W. I.; Strzałka, K., Carotenoids as modulators of lipid membrane physical properties. *Biochimica et Biophysica Acta (BBA) - Molecular Basis of Disease* **2005**, *1740* (2), 108-115.
49. Kalituho, L.; Rech, J.; Jahns, P., The roles of specific xanthophylls in light utilization. *Planta* **2007**, *225* (2), 423-39.
50. Tardy, F.; Havaux, M., Thylakoid membrane fluidity and thermostability during the operation of the xanthophyll cycle in higher-plant chloroplasts. *Biochimica et biophysica acta* **1997**, *1330* (2), 179-93.
51. Lokstein, H.; Tian, L.; Polle, J. E. W.; Penna, D. D., Xanthophyll biosynthetic mutants of *Arabidopsis thaliana*: altered nonphotochemical quenching of chlorophyll fluorescence is due to changes in Photosystem II antenna size and stability. *Biochimica et Biophysica Acta* **2002**, *1553*, 309-319.
52. Havaux, M.; Dall'Osto, L.; Cuine, S.; Giuliano, G.; Bassi, R., The effect of zeaxanthin as the only xanthophyll on the structure and function of the photosynthetic apparatus in *Arabidopsis thaliana*. *J Biol Chem* **2004**, *279* (14), 13878-88.
53. Dall'Osto, L.; Caffarri, S.; Bassi, R., A mechanism of nonphotochemical energy dissipation, independent from PsbS, revealed by a conformational change in the antenna protein CP26. *Plant Cell* **2005**, *17* (4), 1217-32.
54. Havaux, M., Carotenoids as membrane stabilizers in chloroplasts. *Trends in Plant Science* **1998**, *3* (4), 147-151.



# CHAPTER 3

---

---

## Conformational dynamics of photosynthetic light- harvesting complex II in native thylakoid membrane

---

---

This work is available as preprint: Azadi Chegeni F., Ward. E. M., Perin G.,  
Simionato D., Morosinotto T., Baldus, M., Pandit A. bioRxiv.  
Doi: <https://doi.org/10.1101/288860>

## Abstract

---

Photosynthetic light-harvesting antenna complexes (LHCs) of plants, moss and green algae form dynamic switches between light harvesting and excitation-quenched, dissipative states. This mechanism protects the photosynthetic apparatus under light stress via a photo protective membrane response. Herein, we demonstrate the application of solid-state NMR spectroscopy to wild type, heterogeneous thylakoid membranes of *Chlamydomonas reinhardtii* (*Cr.*) and purified *Cr.* Light harvesting Complex II (LHCII) reconstituted in thylakoid lipid membranes, to investigate the structure and dynamics of LHCII in native conditions. We find that membrane-reconstituted LHCII contains sites that undergo fast, large-amplitude motions, including the phytol tails of two chlorophylls. In intact thylakoids, the dynamics of these protein and pigment sites is significantly reduced. Furthermore, plasticity is observed in the N-terminal stretch and in the trans-membrane helical edges facing the thylakoid lumen. We conclude that LHCII contains flexible sites but that their conformational dynamics is constrained *in vivo*, implying that changes in the physicochemical environment are required to enable switching between different conformational states. *In situ* NMR spectroscopy opens a new route to investigate the plasticity of light-harvesting complexes and their seminal role in biological regulation mechanisms such as membrane state transitions, non-photochemical quenching or post-translational modifications.

## Introduction

---

Multi-pigment protein complexes in plants, moss, and photosynthetic algae perform delicate photo-physical and chemical tasks. These processes are highly regulated by the conformational flexibility of the proteins and their interplay within a dynamic thylakoid membrane environment<sup>1-2</sup>. Obtaining atomic-level structures of these complexes under physiological conditions is an essential step towards understanding the molecular mechanisms that regulate the excitation energy flow. To understand the molecular mechanisms that regulate photosynthesis, the most abundant, peripheral antenna complex, Light Harvesting Complex II (LHCII), has been studied extensively and the conformational switch of LHCII has been the topic of much debate<sup>2-12</sup>. Single-molecule fluorescence studies have demonstrated that individual LHCII complexes can fluctuate between light harvesting and dissipative states<sup>4, 7</sup> and MD (Molecular Dynamics) simulations on LHCII in a lipid bilayer<sup>9</sup> suggest that the N-terminal region is highly disordered and could modulate excitation quenching. Results from single-molecule data have been combined with

structure-based data on photosystem II supercomplexes to propose fluctuating antenna models for excitation energy transfer, in which individual LHCs continuously alternate between fluorescent and quenched states. Furthermore, protein solvation, vibration-induced coherences and structural disorder have been put forward as functional design principles by which antenna pigment-protein assemblies can direct and optimize the excitation energy transfer flow. The conformational states and dynamics of LHCII however have only been investigated in crystals or detergent solutions<sup>4, 10, 13-14</sup>. These conditions are very different from more native conditions where complexes are stabilized in a lipid bilayer and can interact with other proteins, which has been shown to affect their fluorescent states<sup>15-16</sup>. Moreover, in native thylakoid membranes the antenna proteins are held in specific arrangements within LHCII-Photosystem II super complexes<sup>17</sup>. The presence of zeaxanthin, phase transitions, specific lipids and membrane stacking further controls the conformational dynamics of the individual LHCs<sup>18</sup>.

To understand the molecular switch functions of LHCs, and the role of the thylakoid environment in controlling their light-harvesting function, it is essential to study their dynamic behavior in their native setting. Until now, no structure-based methods have been presented that could detect the molecular structure and dynamics of LHCs inside a membrane environment. Herein, we applied solid-state NMR (Nuclear Magnetic Resonance) spectroscopy to study the conformational dynamics of LHCII in lipid bilayers and in native thylakoid membranes. Solid-state NMR spectroscopy has shown to be a powerful tool for atomistic detection of membrane proteins in native membrane or cellular environments. Several *in-situ* and *in-cell* solid-state NMR studies have investigated membrane proteins that were overexpressed in prokaryotic and eukaryotic host-expression systems<sup>19-25</sup>. We take advantage of the fact that our target protein is present at a high natural abundance in thylakoid membranes under native conditions, and demonstrate that LHCII NMR signals can be detected in thylakoids isolated from wild-type eukaryotic *Chlamydomonas reinhardtii* (Cr.) green algae cells. Isolated U-<sup>13</sup>C, <sup>15</sup>N Cr. LHCII were analyzed that were reconstituted in thylakoid-lipid membranes, to obtain a view on the conformational dynamics of LHCII in a lipid environment. By comparing these data to the spectra of native thylakoid membranes, we uncover marked differences in the conformational dynamics of LHCII, with implications for the role of the thylakoid environment for LHCII function.



## Material and Methods

---

### Biosynthetic isotope labeling of *Cr.* cells, thylakoid extraction and LHCII isolation

For the experiments on isolated WT LHCII trimers, *Cr.* cells from strain CW 15 were cultivated and thylakoid membranes were isolated as described in chapter 2. Thylakoid membranes corresponding to 3mg/ml of total chlorophylls, according to the optical density at 680 nm, were unstacked with 50 mM Ethylenediaminetetraacetic acid (EDTA) and solubilized for 20 minutes on ice in 3 ml of final 1.2% *n*-Dodecyl  $\alpha$ -D-maltoside ( $\alpha$ -DM) in 10 mM Hepes (pH 7.5), after vortexing for 1 minute. The solubilized samples were centrifuged at  $15000 \times g$  for 30 minutes to eliminate any unsolubilized material and the supernatant with the photosynthetic complexes was then fractionated by ultracentrifugation in a 0–1 M continuous sucrose gradient containing 0.06%  $\alpha$ -DM and 10 mM Hepes (pH 7.5), at  $141000 \times g$  for 40 hours at 4 °C. The green fraction corresponding to LHCII proteins was harvested with a syringe and Chl concentration adjusted to 2mg/ml with buffer (50 mM Hepes, 5 mM  $MgCl_2$ , pH 7.5). LHCII proteins solubilized in  $\alpha$ -DM were reconstituted in lipid membranes whose composition mimics the native thylakoid membrane (47% monogalactosyldiacylglycerol (MGDG), 12% sulfoquinovosyldiacylglycerol (SQDG), 14% phosphatidylglycerol (PG) and 27% digalactosyldiacylglycerol (DGDG)) with a protein-to-lipid molar ratio of 1:55, according to the method described by Crisafi and Pandit<sup>15</sup>. The chosen protein to lipid ratio is in the range of native protein packing densities in thylakoid membranes, where 70-80% of the membrane surface area is occupied by proteins<sup>26</sup>.

For experiments on whole fresh thylakoids, *Cr.* cells were cultivated in TAP medium using <sup>13</sup>C labeled sodium acetate in a home-built photo chamber, under continuous illumination with cool white LEDs ( $\sim 50 \mu\text{mol m}^{-2} \text{s}^{-1}$ ). Cells were harvested in the exponential growth phase, centrifuged, and re-suspended in 0.2 volumes of  $MgCl_2$  buffer (1 mM  $MgCl_2$ , 0.1 M Hepes, pH 7.5/KOH, 10% sucrose), and were ruptured by sonication on a 2500 Watt sonicator set at 10 %. The isolation of fresh thylakoids was performed according to Chua and Bennoun<sup>27</sup> with some modifications. This procedure differed from the steps described above for LHCII isolation, by using sucrose gradient layers for purification of the thylakoids in order to obtain more pure fractions. In the procedure, disrupted cells were overlaid with layers of sucrose (3 ml of 1.8 M, 1 ml of 1.3 M, 1 ml of 0.5 M and 5 ml of 0 M) containing 0.1 M Hepes (pH=7.5) and 0.5 M EDTA. The gradients were ultracentrifuged for one hour at 4 °C in a SW41 swing-bucket rotor (Beckmann) at 24000 rpm ( $100000 \times g$ ). The thylakoid fraction was isolated from the dark-green sucrose band (see figure 1A).

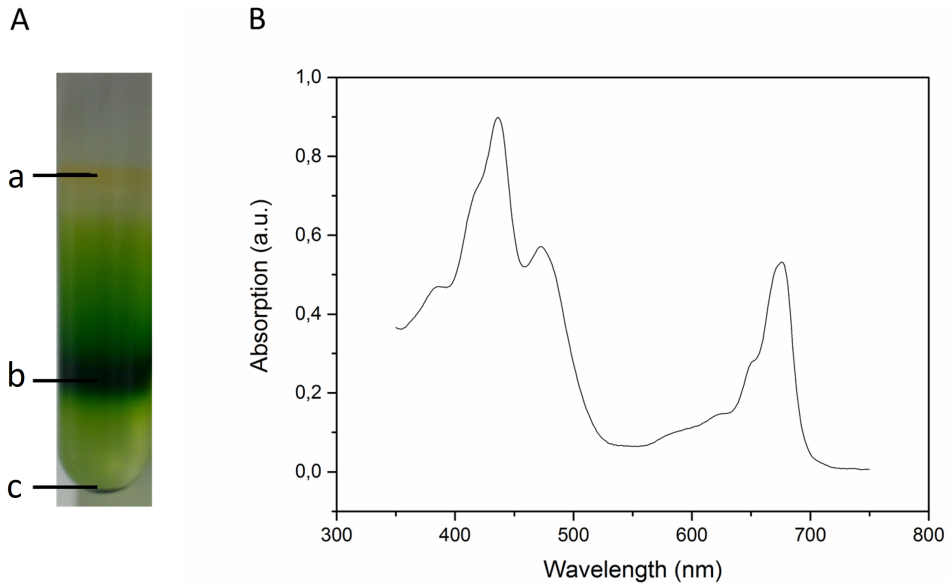


**Figure 1. A:** Example of thylakoid extraction using a layered sucrose gradient. a. eye spot containing  $\beta$ carotenes; b. thylakoid membranes; c. cell walls and unbroken cell material. Band b was extracted with a syringe and contained the purified thylakoid fraction. **B:** Absorption spectra of  $^{13}\text{C}$  Cr. thylakoid membranes. The  $Q_y$  absorbance bands of Chl *a* and *b* are distinguished at 672 and 650 nm respectively, and carotenoids and Chl higher-energy states contribute to the spectrum in the region between 400 and 500 nm.

3

## Gel electrophoresis

Coomassie-stained SDS-page was performed using 15% Tris-glycine gels <sup>28</sup>. Samples were solubilized with a solubilization buffer (4 $\times$ ) containing 30% glycerol, 125 mM Tris pH 6.8, 0.1 M dithiothreitol, 9% SDS.

## Pigment analysis

The content of individual carotenoids of *npq2* LHCII was determined using HPLC (Beckman System Gold), as described in <sup>29</sup>. The peaks of each sample were identified through the retention time and absorption spectrum <sup>30</sup>.

## UV/Visible spectroscopy

Absorption spectra were recorded on a Cary 60 UV–visible spectrophotometer (Agilent Technologies) with the wavelength range from 350 to 750 nm.

## Preparation of thylakoid-lipid liposomes

LHCII proteins solubilized in  $\alpha$ -DM were reconstituted in lipid membranes of which the composition mimics the native thylakoid membrane. 47% MGDG, 12% SQDG, 14% PG and 27% DGDG with a protein-to-lipid ratio of 1:55<sup>15</sup>. The chosen protein to lipid ratio is in the range of native protein packing densities in thylakoid membranes, where 70-80% of the membrane surface area is occupied by proteins<sup>26</sup>. Thylakoid lipids were dissolved in chloroform and dried into a thin film using a rotary evaporator at 40 °C. The thylakoid lipids film was hydrated by reconstitution buffer (50mM HEPES, 5mM MgCl<sub>2</sub>, pH=7.5 and 0.03%  $\beta$ -DM) and were exposed to 10 freeze-thaw cycles. After that, LHCII was inserted into liposomes and detergent was removed by 3 days incubation with bio beads (SM-2, Bio Rad).

## Time-resolved fluorescence spectroscopy (TRF) and 77K fluorescence

TRF measurements on LHCII in detergent and in liposomes were performed using a FluoTime 200 (PicoQuant) time-correlated photon counter spectrometer. Samples were held in a 1×1 cm quartz cuvette that was thermostated at 20 °C and excited at 440 nm using a diode laser (PicoQuant). Fluorescence decay traces were fitted with multi-exponentials using a  $\chi^2$  least-square fitting procedure. 77K fluorescence measurements were performed using a Fluoromax 3, Horiba, Jobin-Yvon. The samples were diluted in 50 mM HEPES, 5mM MgCl<sub>2</sub> buffer and cooled in a nitrogen-bath cryostat to 77K. The samples were excited at 440 nm and a bandwidth of 2 nm was used for excitation and emission.

## NMR sample preparation

For the LHCII sample, 18 ml of LHCII in liposomes, containing approximately 10 mg LHCII and 1.5 mg Chl (as determined by OD<sub>680</sub> of the Chls), was pelleted by ultra-centrifugation (223000×g, 4 °C, 90 min) and transferred to a 3.2 mm solid-state NMR MAS (Magic Angle Spinning) rotor through centrifugation. For the thylakoid sample, 12 ml of fresh thylakoid membrane containing 2 mg Chl and approximately 10 times more in protein content was pelleted by ultra-centrifugation (100000×g, 4 °C, 45 min) and transferred to a thin-wall 3.2 mm MAS rotor.

## Solid-state NMR experiments

Solid-state NMR spectra of U-<sup>13</sup>C-<sup>15</sup>N LHCII in proteoliposomes and of <sup>13</sup>C-enriched thylakoid membranes were recorded with an ultra-high field 950-MHz <sup>1</sup>H Larmor frequency spectrometer (Bruker, Biospin, Billerica) equipped with a triple-channel

$^1\text{H}$ ,  $^{13}\text{C}$ ,  $^{15}\text{N}$  3.2 mm MAS probe. Typical  $\pi/2$  pulses were 3  $\mu\text{s}$  for  $^1\text{H}$ , 5  $\mu\text{s}$  for  $^{13}\text{C}$ , and 8  $\mu\text{s}$  for  $^{15}\text{N}$ . The  $^1\text{H}/^{15}\text{N}$  and  $^1\text{H}/^{13}\text{C}$  cross-polarization (CP) <sup>31</sup> contact times were 800  $\mu\text{s}$  and 1 ms, respectively, with a constant radio frequency (rf) field of 35 and 50 kHz on nitrogen and carbon, respectively, while the proton lock field was ramped linearly around the  $n=1$  Hartmann/Hahn condition <sup>32</sup>. The  $^{15}\text{N}/^{13}\text{C}$  SPECIFIC-CP transfer<sup>33</sup> was implemented with an optimized contact time of 4.2 ms with a constant lock field of  $2.5 \times \nu_r$  applied on  $^{15}\text{N}$ , while the  $^{13}\text{C}$  field was ramped linearly (10% ramp) around  $1.5 \times \nu_r$ .  $^1\text{H}$  decoupling during direct and indirect acquisition was performed using SPINAL64 <sup>34</sup> with  $\sim 83$  kHz irradiation. The presented 2D  $^{13}\text{C}$ - $^{13}\text{C}$  PARIS <sup>35</sup> spectra were collected with a mixing time of 30 ms at 17 kHz MAS at a set temperature of  $-18$  °C. The 2D NCA and NCACX experiments <sup>36</sup> were performed on the LHCII sample at 14 kHz MAS frequency and a readout temperature of  $-18$  °C. For the NCACX experiment a PARIS mixing time of 50 ms was used. The  $J$ -coupling based 2D  $^{13}\text{C}$ - $^{13}\text{C}$  INEPT-TOBSY <sup>37-38</sup> experiments were recorded at  $-3$  °C with TOBSY mixing of 6 ms at 14 kHz MAS. Spectra were processed with Bruker TopSpin 3.2 (Bruker, Germany) with LPfr linear prediction and fqc mode for Fourier transformation. Spectra were analyzed by Sparky version 3.114 <sup>39</sup> and MestReNova 11.0 (Mestrelab Research SL, Santiago de Compostela, Spain).

## NMR chemical shift prediction using a plant-LHCII homology model

Homology models of *Cr.* LHCII were built using the SWISS model web server <sup>40</sup> based on the LHCII crystal structure of spinach and using the Lhcmb1 or Lhcmb2 sequence of *Cr.* LHCII <sup>41</sup>. The Lhcmb sequences and respective PDB models were used as input for SHIFTX2 <sup>42</sup> in order to predict the  $^{13}\text{C}$  and  $^{15}\text{N}$  chemical shifts.  $^{13}\text{C}$ - $^{13}\text{C}$  predicted correlation spectra for use in Sparky <sup>39</sup> were generated by FANDAS <sup>43</sup>.

## Results and Discussion

---

### Biochemical analysis of *Cr.* thylakoid membranes and of isolated *Cr.* LHCII trimers

To investigate the occurrence of LHCII in the thylakoid sample, we used the procedure described for the isolation of the LHCII trimers (*i.e.* re-suspending the thylakoids in Hepes buffer with EDTA and  $\alpha$ -DM, see material and methods) and ran a sucrose gradient. Figure 2A shows that the most dense sucrose band contains LHCII trimers, indicating that these are the most abundant pigment-containing complexes in the thylakoids. In addition, SDS-page analysis of the purified *Cr.*

thylakoids was compared to the SDS-page analysis of the isolated *Cr.* LHCII sample (figure 2B). Different molecular-weight bands are distinguished for LHCII in the SDS page analysis due to the fact that the LHCII trimers are isomers consisting of different polypeptides with different molecular weights.

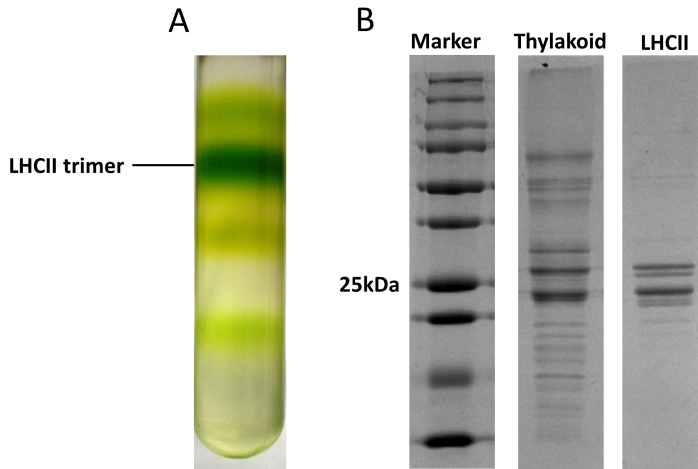


**Figure 2. A:** Sucrose gradient of *Cr.* thylakoids after solubilizing with 0.6%  $\alpha$ -DM, showing the fraction of trimeric LHCII. **B:** SDS page gel analysis of the *Cr.* thylakoid preparation and of isolated LHCII.

The most abundant polypeptides are Lhcbm1, Lhcbm2/7 (Lhcbm2 and Lhcbm7 have identical mature peptide sequences) and Lhcbm3<sup>44</sup>. In the SDS page gel of the thylakoid sample, two strong bands are observed for LHCII. Based on the relative molecular weights of the polypeptides and other reported analyses, we conclude that the upper band contains Lhcbm3 and the thicker lower band contains Lhcbm1 and Lhcbm2/7<sup>44-45</sup>. In the SDS-page gel of LHCII two additional smaller bands are observed, which could originate from other Lhcbm polypeptides. The absorbance spectrum of the thylakoid preparation (figure 1B) confirms the presence of protein-associated carotenoids and Chl *a* and *b* pigments. High Performance Liquid Chromatography (HPLC) was performed to determine the pigment composition of LHCII as described previously<sup>46</sup>. The HPLC data show that *Cr.* LHCII proteins bind Chl *a* and *b*, lutein, neoxanthin or loroxanthin and violaxanthin, together with small traces of betacarotene and antheraxanthin (figure 3).

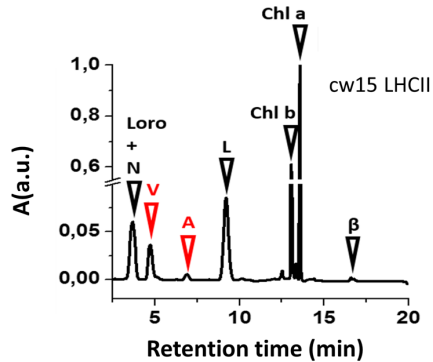


**Figure 3.** HPLC analysis of trimeric LHCII indicating the presence of violaxanthin.

LHCII were reconstituted into liposomes to mimic the native lipid environment close to those in thylakoid membranes as described in Material and Methods. Under these conditions LHCII form aggregates as reflecting in the 77K fluorescence spectra (figure 4A). Time resolved fluorescence spectra of LHCII before and after insertion into liposomes were measured (figure 4B). Results indicate that the LHCII that are reconstituted in the liposomes are strongly fluorescence quenched. The LHCII in detergent has an average life time of 3.5 ns which reduces to 670 ps after insertion into liposomes.

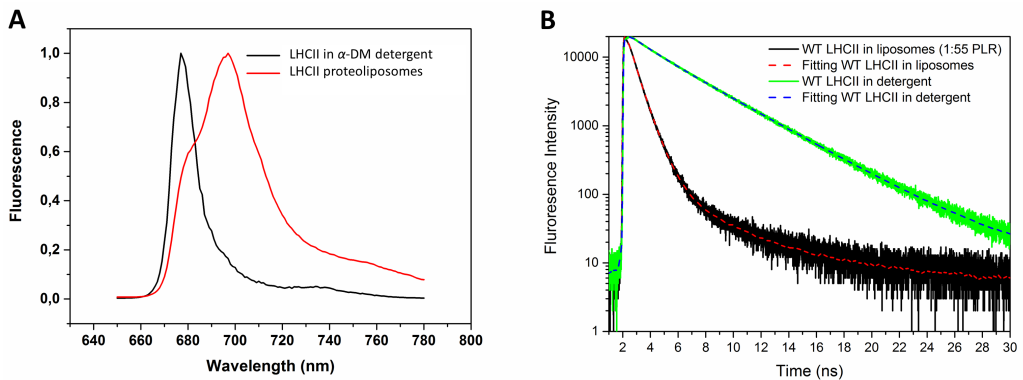


**Figure 4.** **A:** 77K fluorescence spectra of LHCII in  $\alpha$ -DM detergent (black) and after inserting into liposomes (red). **B:** time resolved fluorescence traces of LHCII in  $\alpha$ -DM detergent (green) and of LHCII in liposomes (black).

## NMR analysis of LHCII in lipid membranes: detection of resonance from protein, pigment and lipids

Two complementary types of solid-state NMR experiments were employed in this study that are selective for rigid, respectively highly dynamic, molecules. In cross-Polarization (CP) based experiments,  $^1\text{H}$ - $^{13}\text{C}$  or  $^{13}\text{C}$ - $^{15}\text{N}$  magnetization is transferred via dipolar interaction, which is dependent on the angle between an internuclear vector and the magnetic field. Dipolar-based transfer experiments become inefficient for dynamic molecules, where the dipolar couplings are averaged to zero due to fast tumbling in solution. In INEPT based experiments, magnetization is transferred via  $J$ -couplings. In the presence of strong motions, where orientation dependent interactions are sufficiently averaged out by magic-angle spinning and fast molecular tumbling, the combination of  $J$ -based pulse sequences can be employed for screening very flexible parts of large biomolecules <sup>47</sup>. Membrane proteins typically contain large transmembrane stretches with low flexibility, of which the majority of signals are detected in dipolar-based experiments. We first analyzed the membrane-reconstituted LHCII complex in dipolar-based  $^{13}\text{C}$ - $^{13}\text{C}$  (CC) and  $^{15}\text{N}$ - $^{13}\text{C}$  (NC) experiments, to verify the incorporation of isotope labels and to identify resonance signals of selective amino-acid and pigment types. Figure 5 presents the CC and NC spectra, showing that several amino-acid types can be identified based on their unique chemical-shift patterns. Helix and coil distributions can be distinguished for alanine, serine, threonine and glycine, as indicated <sup>48</sup>, that are in agreement with the known crystallographic structure of plant LHCII which contains both helical stretches and large, coiled loops and tails. In addition to signals originating from the protein content, Chl and carotenoid signals can be identified in regions of the CC spectrum where no protein signals are expected, verifying that these components are also isotopically labeled. Remarkably, in the CC spectrum also a single set of lipid glycerol carbon resonances is observed. It is well-known that each monomer unit of LHCII contains one phosphatidyl-glycerol (PG) lipid, which forms the ligand for Chl611 (nomenclature Liu et al. <sup>13</sup>) and based on their chemical shifts, we attribute the detected lipid resonances in the CC spectrum to the head carbons of LHCII-bound intrinsic PG lipid molecules that were isotope labeled and isolated together with the complex.

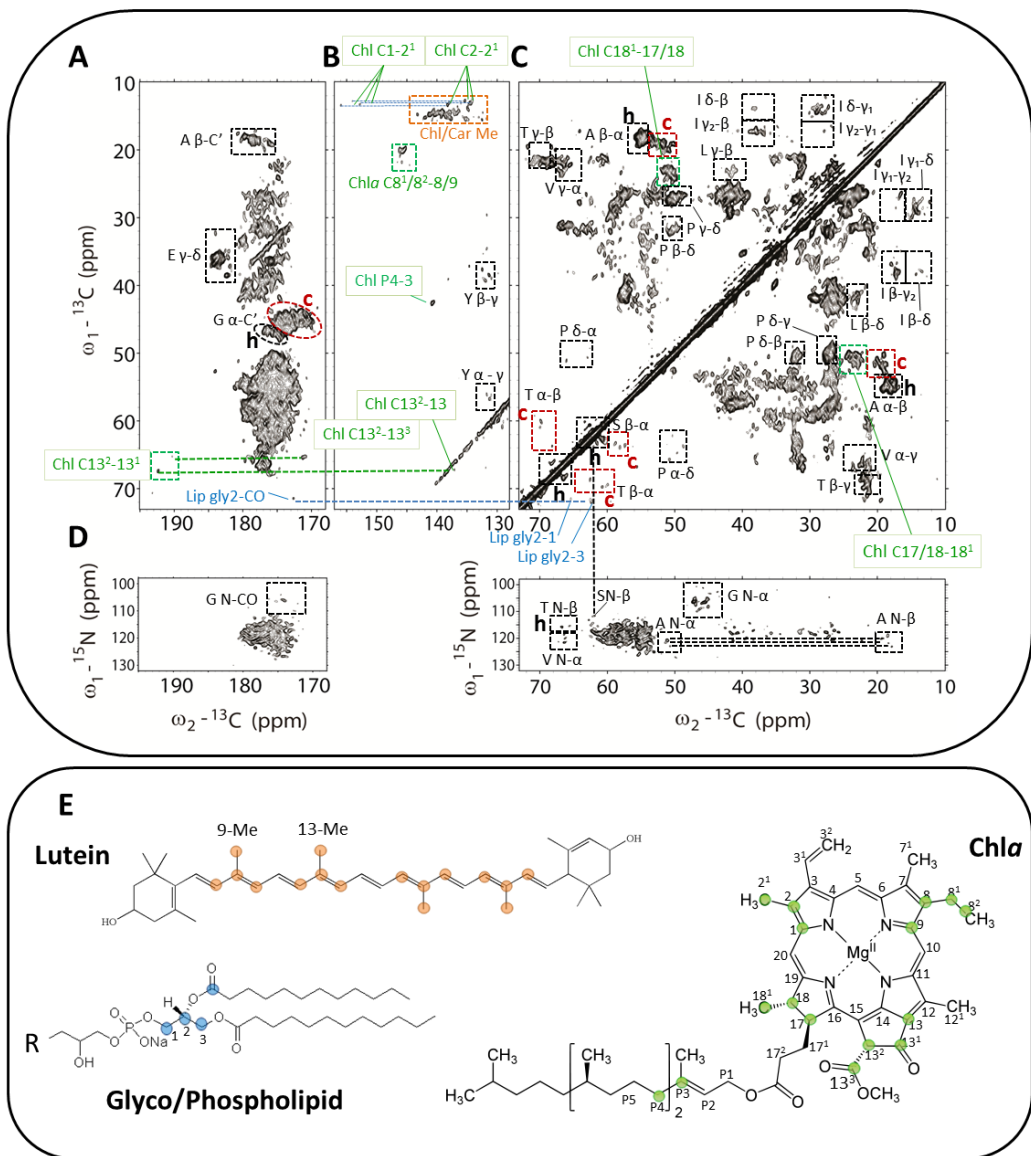


**Figure 5.** A-C: CP-PARIS  $^{13}\text{C}$ - $^{13}\text{C}$  spectrum of membrane-reconstituted LHCII. Helix (h) and coil (c)  $C_{\alpha}$ - $C_{\beta}$  correlations of Thr, Ser and Ala and  $C_{\alpha}$ -C correlations of Gly are indicated. In addition, protein correlations of Pro, Glu, Ile, and Val are indicated with black contour boxes. Chl, carotenoid and lipid correlations are indicated in respectively green, orange and blue. Their attributed carbon atom types are color-coded in the chemical structures in panel E. **D:** NCACX spectrum of membrane-reconstituted LHCII. N- $C_{\alpha}$  correlations of Gly, Ser, Ala and Thr are indicated. **E:** Chemical structures of lutein, Chl *a* and of a glyco- or phospholipid molecule with the NMR detected atom types indicated.



## Comparison of LHCII structure and dynamics in reconstituted and in native thylakoid membranes: results from dipolar-based experiments

Dipolar-based CC spectra of native thylakoid membranes were collected using parameters that were identical to those used for the isolated LHCII. Figure 6A shows the CC spectrum of LHCII (black) overlaid with the thylakoid spectrum (red). The strong overlap of the two spectra demonstrates, in agreement with the biochemical analysis of our samples, that the most abundant signals in the thylakoid spectra arise from LHCII. Many of the additional peaks that are detected in the thylakoid spectrum can be attributed to lipid signals, confirming that isotope labels are also incorporated into the thylakoid lipids. In particular, multiple resonance signals are detected between 70 and 80 ppm (indicated in figure 5A) that are outside the region of the protein signals and that are attributed to lipid galactosyl heads.

To have a closer view on the LHCII protein secondary structure in reconstituted and in native membranes, we used correlation signals of Ala, Thr and Ser amino-acid types as reporters for the protein fold. These residue types were chosen because of the clear spectral separation of Ala, Thr and Ser  $C_{\alpha}$ - $C_{\beta}$  correlation signals. The distribution of those amino acids along the LHCII polypeptide sequences involves both helical and coil regions, and their resonance signals thus are informative of the fold at several protein sites. The insets of panel 6B, C and D show the Ala, Thr and Ser selective regions. The helical and coil signals fall into separate regions as indicated. To compare the experimental shift correlations with the LHCII structure, three steps were undertaken: (i) models were built for Lhcbm1 and Lhcbm2, the two most abundant polypeptides that form the LHCII trimers in *Cr.*, based on the spinach and pea crystal structures; (ii)  $C_{\alpha}$  and  $C_{\beta}$  chemical shifts predictions were generated from the Lhcbm1 and Lhcbm2 homology models using the program SHIFTX2<sup>42</sup> and (iii) simulated CC correlations were generated from the predicted chemical shifts using FANDAS<sup>43</sup>. The resulting chemical shift predictions are overlaid in the inset spectra and shown as cyan and black crosses. Figure 7 presents the spectra of LHCII and thylakoids in the full aliphatic region, with the Lhcbm1 and Lhcbm2 chemical-shift predictions overlaid. The sequences of Lhcbm1 and Lhcbm2, presented in the lower panel in figure 4 show that most of the residues are conserved among Lhcbm1 and Lhcbm2. In the Thr and Ser insets, those residues are labeled together.

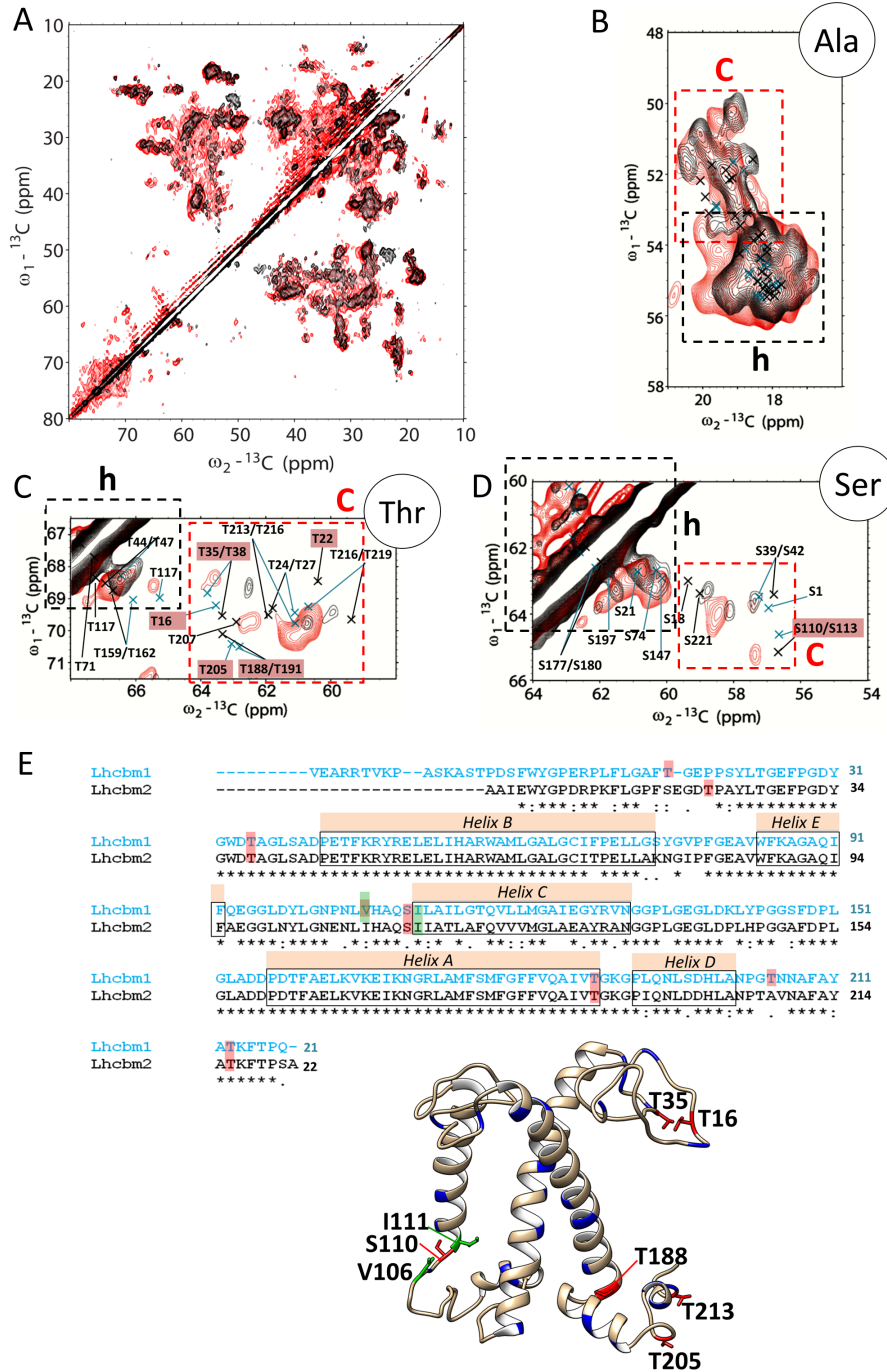


**Figure 6. A:** CP-PARIS spectrum of thylakoid membranes (red) with the LHCII spectrum (black) overlaid. The insets show the Ala (**B**), Thr (**C**) and Ser (**D**) spectral regions. **E:** chemical-shift predictions of Lhcbm1 (cyan crosses) and Lhcbm2 (orange crosses) are overlaid. Predicted shifts that significantly deviate from experimental correlations in the LHCII spectrum are highlighted in red.

We first focus on the spectrum of isolated LHCII. In panel 6B, C and D the experimental resonances of Ala, Thr and Ser for isolated LHCII are shown in black. If we compare the experimental resonances with the structure-based predictions (cyan and orange), we see that some of the LHCII correlations match closely with predicted correlations, also for non-conserved residues. For instance, experimental peaks are detected close to the predictions for S18 and S221, Ser residues that are found in Lhcbm2 but not in Lhcbm1, which points out that signals of specific polypeptides can be distinguished. However, other predicted signals are not matched by any experimental peak in the LHCII spectrum. For those residues, experimental cross-correlation signals either are not identified because they appear outside their predicted region, or cross resonance signals are not detected because of inefficient cross polarization caused by residue dynamics. Both cases are indicators of protein flexibility. We considered deviations between predicted ( $\omega$  pred) and experimentally observed ( $\omega$  exp) correlations significant if  $\sqrt{(\omega_1 \text{ exp} - \omega_1 \text{ pred})^2 + (\omega_2 \text{ exp} - \omega_2 \text{ pred})^2} \geq 1.2$  ppm and used this as error margin for the chemical-shift predictions. Using this error margin, we find that no experimental signals are observed in the LHCII spectrum within the predicted range for residues T16, T35, S110, T205 and T188 in Lhcbm1 and for T22, T38, S113 and T191 in Lhcbm2. In the LHCII NC spectrum, we observe additional anomalies for V106, I111 and T213 for Lhbm1, and for G20, I114, T191 and T216 for Lhcbm2 (Figure 8). According to the LHCII crystal structures, none of these residues is in direct Van der Waals contact with pigment ligands, excluding that protein-pigment interactions are the cause of the chemical-shift anomalies. The lower panel in Figure 6 shows the Lhcbm1 structure in which residues with deviating shifts are highlighted in red and purple, revealing that the N-terminal stretch at the stromal site and in the CE loop, the edge of helix A, and the C terminus facing the lumen contains flexible protein sites.

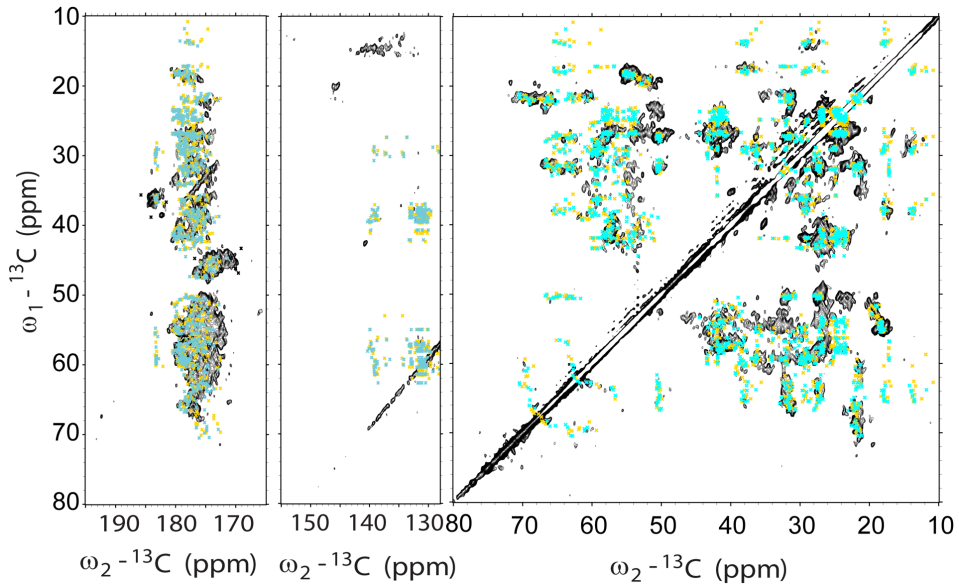


**Figure 7.** CP-PARIS  $^{13}\text{C}$ - $^{13}\text{C}$  spectrum of LHCII (black) overlaid with SHIFTX2-generated correlations prediction of Lhcbm1 (cyan) and Lhcbm2 (orange). The spectrum was collected with a mixing time of 30 ms at 17 kHz MAS at a set temperature of  $-18^\circ\text{C}$ .

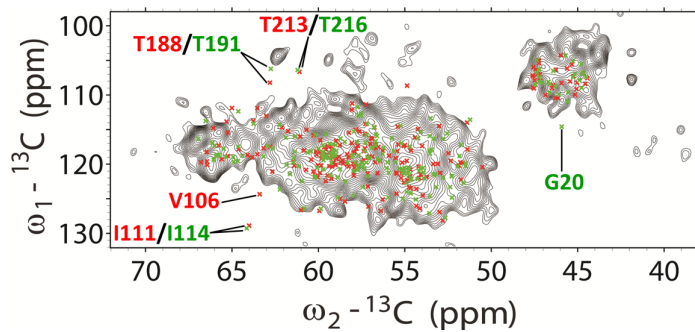


**Figure 8.** NCA  $^{15}\text{N}$ - $^{13}\text{C}$  spectrum of LHCII (black) overlaid with predicted correlations of Lhcbm1 (red dots) and Lhcbm2 (green dots). The NCA spectrum was collected at 14 kHz MAS frequency at  $-18^\circ\text{C}$ , using a mixing time of  $800\ \mu\text{s}$   $^1\text{H}$ - $^{15}\text{N}$  CP step, 4.2 ms for  $^{15}\text{N}$ - $^{13}\text{C}$  and the number of scans was set to 704. Significant deviations between predicted and experimentally observed cross peaks are observed for Val106, Ile111, Thr188 and Thr213 in Lhcbm1, and in Gly20, Ile114 and Thr216 in Lhcbm2.

Now we compare the above results on LHCII in proteo liposomes with those on LHCII in native thylakoid membranes. In the thylakoid CC spectrum, several signals are shifted compared to the LHCII spectrum. Furthermore, in the Thr and

Ser coil regions stronger signal intensities are observed and additional peaks appear compared to the LHCII spectrum. Comparing the LHCII signals in the thylakoid spectrum (red) to the predicted Thr and Ser chemical-shift predictions, a better overlap is observed. The enhanced signal intensities are indicative of improved cross-polarization efficiencies, signifying that the thylakoid membrane is more rigid than the reconstituted membrane and causes reduced dynamics in LHCII. To test this hypothesis, we proceeded with *J*-based (INEPT-TOBSY) experiments that are selective for molecules with strong dynamics and large-amplitude motions, such as disordered segments.

A comparison of the LHCII and the thylakoid spectrum in other spectral regions is presented in in figure 9 and shows several changes as well. In the CO region, membrane-reconstituted LHCII has an upfield shifted Glu carboxyl peak, indicating a change in the structure or local environment of a Glu residue. In the aromatic region where the chromophore signals are distinguished, chemical shift changes are observed for Chl *a* 8-8<sup>1</sup> resonances, and the LHCII spectrum has three downshifted Me resonance signals (indicated with arrows in the spectrum) that could be attributed to either Chl or carotenoid Me groups, and indicate a change in the local environment of Chl, or possibly of a carotenoid acyl chain.

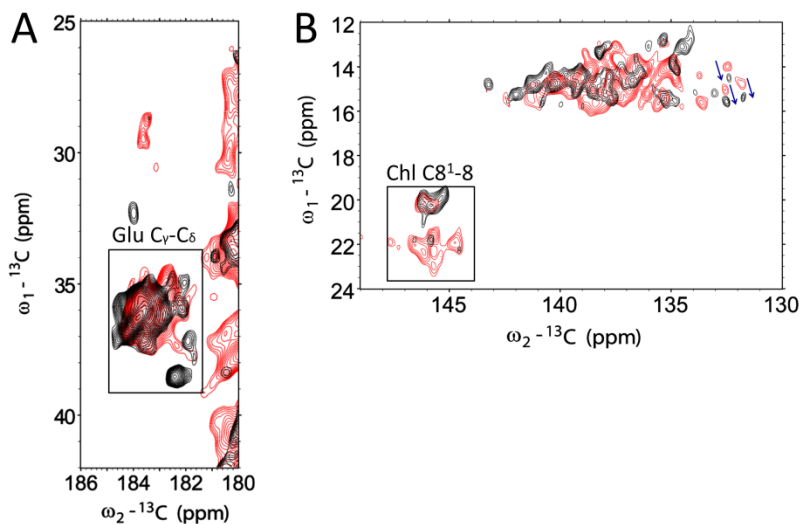


**Figure 9.** CP-PARIS  $^{13}\text{C}$ - $^{13}\text{C}$  spectrum of thylakoid membranes (red) with the spectrum of *Cr.* LHCII (black) overlaid. **A:** Carboxyl region showing the Glu C $\gamma$ -C $\delta$  correlations. A downfield shift of one Glu in the spectrum of thylakoid membranes is indicated with the arrow. **B:** Carotenoid and Chl region. Downfield shifts of three Me carbons in the spectrum of LHCII are indicated with blue arrows.

## J-based experiments reveal reduced LHCII dynamics in native membranes

INEPT based experiments are sensitive for molecules that undergo fast, large-amplitude motions. For biomolecules, these are typically disordered, protein segments with random-coil structures, flexible ligands or mobile lipids with a low degree of segmental order. Figure 10 presents the 2D INEPT-TOBSY spectrum of LHCII (black) overlaid on the INEPT-TOBSY spectrum of thylakoid membranes (red). As expected by the fact that the majority of the protein signals are detected in the dipolar-based spectra, only limited sets of protein signals are detected in the *J*-based spectra that we refer to as “*J*” amino acids. The overlaid spectra clearly show that several *J* amino-acid residues are detected in the INEPT-TOBSY spectrum of LHCII (black), whereas only few residues are detected in the INEPT-TOBSY spectrum of thylakoid membranes (red).

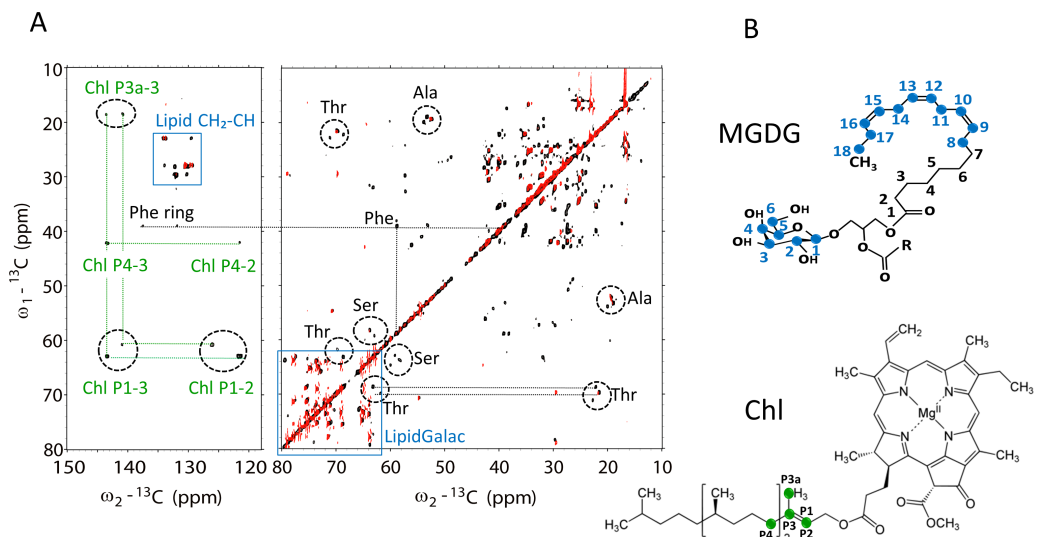


**Figure 10. A:** Overlay of the INEPT-TOBSY spectrum of *Cr.* LHCII (black) and of *Cr.* thylakoids (red). Resonance signals of the two Chls, the lipids and Ala, Thr, Ser, and Phe are indicated. **B:** Chemical structure of MGDG lipid and Chl, highlighting the lipid (blue) and Chl (green) atom types that are detected in the spectra.

We analyzed the chemical-shift correlations in the spectrum of isolated LHCII. We could assign the *J* residues in the LHCII spectrum to Ala, Thr, Ser, Phe, Pro, Val, Lys, Ile, Glu, Asn and Leu amino acid types (3×A,T,S and 1×F,P,V,K,I,E,N,L plus 1 L or D, see table 1 and figure 11). Because these represent residues that display fast and large-amplitude motions, we predict that they are located in the non-

helical loop stretches and in the terminal tails. Interestingly, three distinct peaks are observed for Ala, Thr and Ser, whereas their  $J$ -based correlations usually tend to strongly overlap. The N terminus of Lhcbm2/7 (AAI, first three amino acids) and the C-terminal stretch of Lhcbm1 starting from A212 (ATKFTPQ) or the equivalent stretch in Lhcbm2/7 and Lhcbm3 (ATKFTPSA) contain many of the observed  $J$  amino-acid types and we predict that the observed  $J$  residue signals are from those protein sites. In addition, a Val  $J$  residue is observed in the LHCII spectrum. The only Val residues outside the helical regions are V106 and V83 that occur in the luminal loop connecting helix E, and we attribute the Val signal to either one of those two residues. Taking the results together, the  $J$  analysis of membrane-reconstituted LHCII predicts that fast-amplitude motions could occur for residues in the N- and C-terminus and/or for residues in the lumen loops connecting helix E.

Remarkably, the  $J$ -based spectrum of LHCII also contains two sets of Chl signals that are assigned to P1, P2, P3, P3a and P4 phytol tail resonances (table 2 and figure 11), indicating the presence of two Chl tails that exhibit strong dynamics. Resonance signals of the Chl phytol chains further towards the tail fall into the aliphatic region (10-30 ppm) and overlap with lipid CH<sub>2</sub> signals. In the LHCII crystal structures, the phytol chain structures of Chl *b* 605 and 606 (nomenclature according to Liu et al. <sup>13</sup>) are not observed, while the other Chl phytol tails are resolved and are involved in stabilizing pigment-protein interactions within the complex. We thus conclude that the observed two sets of Chl phytol resonances in the  $J$ -based LHCII spectrum belong to the dynamic tails of Chls 605 and 606. Those Chls are close to V106, S110 and I111 that we classified as flexible sites based on analysis of the dipolar-based spectrum in the previous section. Figure 12 shows the LHCII structure with predicted protein and pigment  $J$  sites indicated in red. Notably, the N-terminal region around T16, (highlighted in the structure) and the C terminus stabilize Chl601 and the xanthophyll-cycle carotenoid Vio (violaxanthin, depicted in the structure) or Zea (zeaxanthin). Flexibility of those sites in isolated LHCII explains that carotenoids in this binding site are loosely bound and easily lost during protein isolation. The region around T35 contains the binding pocket of Lut2 (lutein 2) and flexibility in this site will influence the dynamics of Lut2 and its interaction with Chl601. A comparison of the  $J$ -based spectrum of LHCII and of the thylakoid membranes shows remarkable differences. The majority of the amino-acid signals in the spectrum of LHCII are not observed in the thylakoid spectrum, and no Chl resonances are observed. In accord with the analysis of the dipolar-based spectra that indicate that LHCII has reduced flexibility in native thylakoid membranes, the  $J$  analysis reveals that fast-amplitude motions in LHCII are significantly suppressed in the thylakoid membrane environment. We conclude that both small-amplitude motions in LHCII that reduce cross-polarization efficiency, and large-amplitude, segmental motions that enhance INEPT efficiencies, are significantly reduced in the native thylakoid

membranes compared to LHCII in reconstituted membranes. The predicted dynamic sites are close to the binding pockets of Vio or Zea and Lut2 in LHCII, inferring that those LHCII-associated carotenoids have decreased dynamics for LHCII in its native environment compared to LHCII in liposomes.

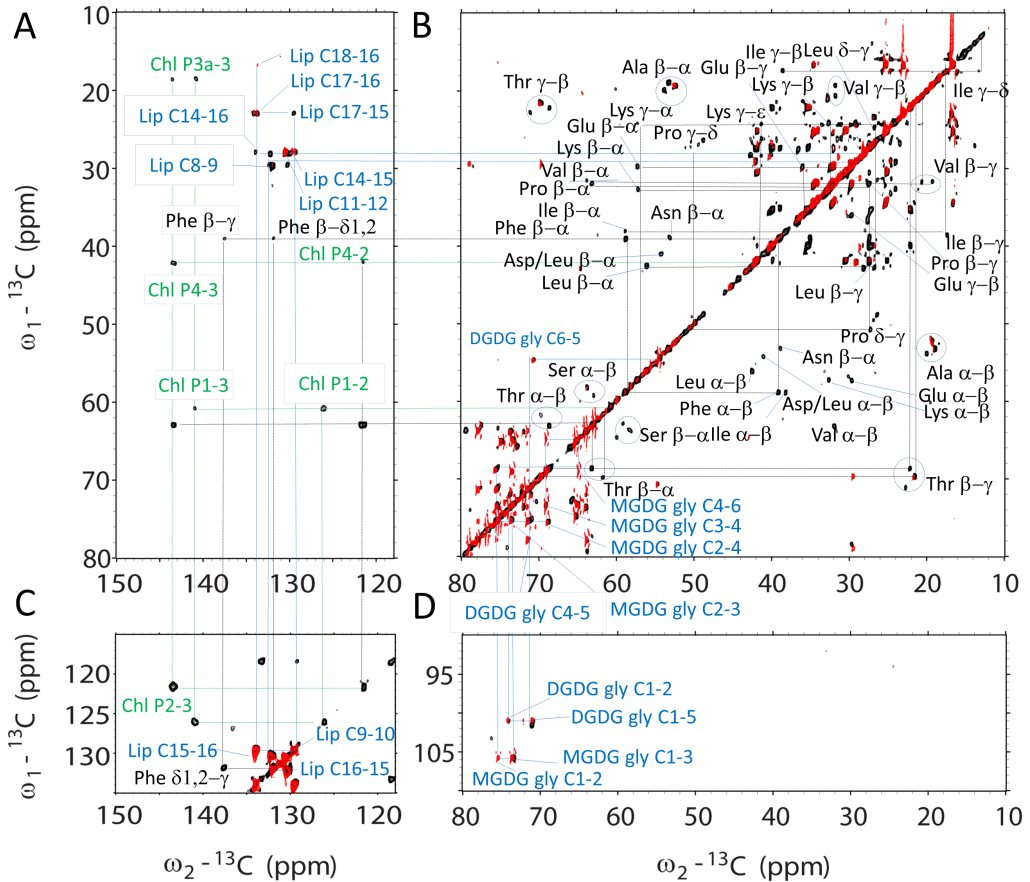


**Figure 11. A-D:** Overlay of the INEPT-TOBSY spectrum of *Cr.* LHCII (black) and of *Cr.* thylakoids (red). Protein assignments are indicated in black, Chl assignments in green and lipid assignments in blue.



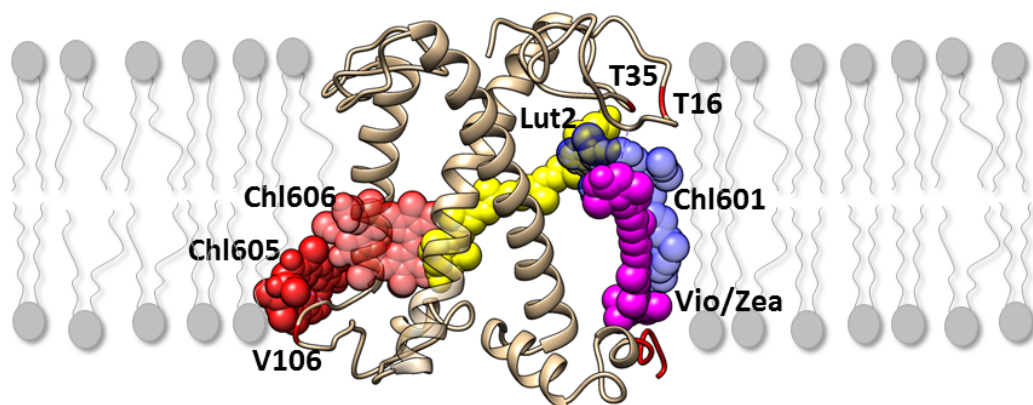


**Figure 12.** LHCII pigment-protein crystal structure, highlighting flexible protein sites and pigments that are in close vicinity.

Residue type	$C_{\alpha}$ [ppm]	$C_{\beta}$ [ppm]	$C_{\gamma}$ [ppm]	$C_{\delta}$ [ppm]	$C_{\epsilon}$ [ppm]
Ala	52.4	19.3			
	53.3	18.9			
	53.8	19.8			
Thr	61.9	69.7	21.5		
	63.2	68.6	22.2		
		71.1	22.8		
Ser	58.2	63.8			
	59.3	62.9			
	60.0	64.7			
Phe	58.8	39.1	137.5	131.9	
Ile	62.4	38.6	17.4	13.3	
Lys	57.2	32.7	24.2		41.4
Val	63.2	31.9	20.6	19.3	
Glu	57.3	29.7			
Asn	53.1	38.9			
Leu	56.1	42.5			
Pro	63.8	31.5	26.4	48.9	
			27.4	50.8	
			26.9	49.5	
Asp/Leu	54.2	41.0			

**Table 1.** Assignment of mobile amino-acid residue types detected in the *J*-based INEPT-TOBSY spectrum of membrane-reconstituted U- $^{13}\text{C}$ - $^{15}\text{N}$  LHCII.

Carbon atom	Chemical shift (ppm) Chl i [ppm]	Chl ii [ppm]
P1	60.8	62.9
P2	121.6	126.1
P3	140.8	143.5
P3a	18.4	18.4
P4	42.5	42.1

**Table 2.** Assignment of Chlorophyll tail  $^{13}\text{C}$  resonance signals detected in the  $J$ -based INEPT-TOBSY spectrum of membrane-reconstituted  $\text{U-}^{13}\text{C-}^{15}\text{N}$  LHCII.

### Dynamics of intrinsic lipids

The most abundant lipid types that are found in thylakoid membranes of *Cr.* are the glycolipids MGDG (monogalactosyldiacylglycerol), DGDG (digalactosyldiacylglycerol) and SQDG (sulfoquinovosyl diacylglycerol), and the phospholipid PG (phosphatidylglycerol). An important advantage of our NMR approach, where we investigate native membrane proteins, is that the labels are also incorporated in the membrane lipids, allowing us to identify the nature of lipid molecules that are co-purified with LHCII and to assess their dynamics. Note that the reconstituted lipids in the LHCII proteoliposomes are not isotope labeled and the probability of detecting  $^{13}\text{C-}^{13}\text{C}$  cross correlations of natural-abundance carbons is very low. The lipid  $^{13}\text{C}$  signals that are detected in CC spectra of membrane-reconstituted LHCII therefore must originate from intrinsic lipids that remained associated with the protein complex during the isolation procedure. For LHCII, a specific set of lipid signals attributed to PG was detected in the dipolar-based CC spectrum (Figure 3), indicating that a PG lipid molecule is strongly bound to the complex. LHCII complexes bind one PG lipid per monomer that is essential for ligating Chl611. Together with Chl612 and Chl610, these Chls form the terminal emitter domain of LHCII where excitations accumulate via downhill intra-protein energy-transfer. In the dissipative state, this site has been proposed to form a quenching domain<sup>18</sup>. A recent MD study on LHCII monomers suggested that the dynamic fluctuations of this lipid, which is stabilized by the N-terminal stretch, could modulate Chl611-Chl612 excitonic interactions with consequences for excitation quenching<sup>9</sup>. The appearance of strong lipid PG signals in the dipolar-based spectrum however are indicative of low dynamics. In contrast, multiple lipid signal resonances are observed in the  $J$ -based CC spectrum of LHCII that arise from glycolipid molecules (figure 9). Resonances of lipid galactosyl heads are

observed in the region between 50-106 ppm that can be assigned to MGDG and to DGDG or SQDG<sup>49</sup> and that are summarized in table 3. The glycolipids must also have been co-purified with LHCII indicating they are associated with the complex. However, their appearance in the INEPT spectrum reveals that they exhibit strong dynamics. We think that the intrinsic glycolipids may have exchanged with the (unlabeled) reconstituted lipids upon insertion of LHCII into the liposomes and are no longer protein bound. The high mobility of the MGDG head atoms does not support the hypothesis of Seiwert *et al.*, who suggested that specific hydrogen-bonding interactions might occur between LHCII and the MGDG galactosyl heads<sup>50</sup>.

Carbon atom	Chemical shift (ppm)	
	MGDG	DGDG
C1	105.9	101
C2	75.4	74.3
C3	73.4	-
C4	68.9	77.7
C5	-	71.1
C6	65	54.6
C7	-	-
C8	130.2	130.2
C9	132.1	132.1
C10	29.6	29.6
C11	27.9	27.9
C12	130.7	130.7
C13	-	-
C14	27.8	27.8
C15	129.6	129.6
C16	133.8	133.8
C17	23.1	23.1
C18	16.66	16.66

**Table 3.** Assignment of <sup>13</sup>C lipid resonance signals detected in the *J*-based INEPT-TOBSY spectrum of membrane-reconstituted U-<sup>13</sup>C-<sup>15</sup>N LHCII and in the spectrum of U-<sup>13</sup>C thylakoid membranes.

The lipid signatures in the NMR spectra of thylakoid membranes provide us with a molecular picture of lipid dynamics inside the membranes. Resonances of different lipid types are detected in both the thylakoid *J*- and the dipolar-based spectrum, showing that the thylakoid membrane contains mobile lipids with low segmental order and immobilized lipids with low dynamics. The results are in agreement with our recent 1D MAS-NMR studies on whole thylakoids and intact cells<sup>46 51</sup>. Owing to better peak separation in 2D spectra, we now can distinguish different

glycolipids on basis of their galactosyl head correlations, and to assign CH-CH<sub>2</sub> correlations of carbons in the unsaturated lipid tails. Because of the dense protein packing in the thylakoid membranes, we expect that the majority of the lipid molecules is constrained by lipid-protein interactions. However the CH-CH<sub>2</sub> correlation signals from the unsaturated glycolipid tails, resonating between 20-35 ppm in  $\omega_1$  and between 130-137 ppm in  $\omega_2$ , only appear in the INEPT spectrum. Seemingly, the unsaturated lipid chains are all mobile and disordered, despite the crowding and overall rigidity of the thylakoid membranes.

## Implications for the LHCII conformational switch *in vivo*

The NMR analysis clearly demonstrates that in thylakoid membranes *in vivo* at ambient temperature the conformational dynamics of LHCII are much more constrained than in thylakoid-mimicking liposome environments *in vitro* and that both fast, large-amplitude and slower motions are suppressed. The organization of LHCII in Photosystem II-LHCII (PSII-LHCII) supercomplexes, and the occurrence of three-dimensional membrane stacks that are not mimicked by the liposome membranes could cause restrained dynamics in LHCII in a thylakoid environment. *Cr.* thylakoid membranes form stacks of 2-3 membrane layers that are stabilized by transversal salt bridges between the stromal sites of LHCII complexes, and are mediated by divalent cations<sup>52</sup>. Moreover, specific arrangements of super complexes occur in the lateral plane of the membrane. According to the cryo-electron microscopy (cryo-EM) structures of *spinach* PSII-LHCII super complexes, Chl605 and the protein AC and EC loops of LHCII are in close contact with the minor antenna proteins CP29 or CP26<sup>17, 53</sup> and in the low-resolution structures of *Cr.* PSII-LHCII, *Cr.* LHCII trimers are also arranged next to CP29 and CP26<sup>44</sup>.

Our findings call to question whether or not spontaneous fluctuations of individual LHC proteins between different conformational states, as has been observed by single-molecules spectroscopy (SMS) and has been suggested by MD simulations, do occur *in vivo*. With SMS, dynamic transitions were detected for isolated LHCII and conformational fluctuations under those conditions were strong enough to occasionally cross the energetic barriers between different conformational states. According to our analysis, membrane-reconstituted LHCII contains distinct flexible sites that may undergo thermally-induced conformational transitions. LHCII in native, stacked thylakoid membranes however does not display this flexibility. This strongly suggests that *in vivo* under those conditions the LHCs are locked in their specific state, implying that an actinic response is required to temporarily reduce the energetic barriers by alterations in the physicochemical environment. Notably, the thylakoid sample was isolated from cells grown under moderate light conditions and we assume that the thylakoid-embedded LHCII structures represent the light-

harvesting conformation. Thus far this conformational state could only be assessed *in vitro* using isolated proteins in detergent solutions<sup>3-4, 8</sup> of which the dynamic features are not representative of their native states. In *Cr.* green algae, the LHC protein LHCSR is found to be involved in pH-induced non-photochemical quenching under excess light conditions. It is therefore noted here that under the growth conditions used for our experiments, no LHCSR is present in the cells.

## Conclusion

---

*In-cell* solid-state NMR is a rapid emerging field of research that is confronted with the major challenge of identifying signals from target proteins against the background of all other cell components. We demonstrate that the NMR signals of the major light-harvesting antenna LHCII can be detected of the protein within heterogeneous membranes that still contain the photosynthetic machinery. Moreover, lipid signals can be identified in parallel and signals are detected from different Lhcbm polypeptide types, which are not distinguished in crystallographic and cryo-EM structures. Selective Lhcbm mutants could be used in the future to further identify chemical shift contributions of the different polypeptide types<sup>45</sup>. Through our approach, we could compare the conformational dynamics in LHCII in native thylakoid membranes to its dynamics in reconstituted membranes. The significant differences that are observed underline the importance of molecular investigation of this pigment-protein complex in its native settings, and question whether spontaneous fluctuations between different fluorescent states occur for this protein *in vivo*. Our NMR approach now opens a route to compare the *in-situ* conformational dynamics of LHCII as function of phosphorylation, membrane state transitions and non-photochemical quenching conditions and determine the influence of thylakoid plasticity on the protein molecular conformational states.

## References

---

1. Kirchhoff, H., Structural changes of the thylakoid membrane network induced by high light stress in plant chloroplasts. *Philosophical Transactions of the Royal Society B: Biological Sciences* **2014**, *369* (1640), 20130225.
2. Horton, P.; Ruban, A., Molecular design of the photosystem II light-harvesting antenna: photosynthesis and photoprotection. *Journal of Experimental Botany* **2005**, *56* (411), 365-373.
3. Ruban, A.; Berera, R.; Iliaia, C.; van Stokkum, I. H. M.; Kennis, J. T. M.; Horton, P.; van Grondelle, R.; Pascal, A.; van Amerongen, H.; Robert, B., Identification of a mechanism of photoprotective energy dissipation in higher plants. *Nature* **2007**, *450* (7169), 575-578.

4. Kruger, T.; Ilioaia, C.; Johnson, M.; AV Ruban; Papagiannakis, E.; Horton, P.; Grondelle, R. v., Controlled Disorder in Plant Light-Harvesting Complex II Explains Its Photoprotective Role. *Biophysical journal* **2012**, *102* (11), 2669-2676.
5. Holt, N.; Zigmantas, D.; Valkunas, L.; Li, X.; Niyogi, K.; Fleming, G., Carotenoid cation formation and the regulation of photosynthetic light harvesting. *Science (New York, N.Y.)* **2005**, *307* (5708), 433-436.
6. Robert, B.; Horton, P.; Pascal, A.; Ruban, A., Insights into the molecular dynamics of plant light-harvesting proteins in vivo. *Trends in plant science* **2004**, *9* (8), 385-390.
7. Schlau-Cohen, G. S.; Yang, H.-Y.; Krüger, T. P. J.; Xu, P.; Gwizdala, M.; van Grondelle, R.; Croce, R.; Moerner, W. E., Single-Molecule Identification of Quenched and Unquenched States of LHCII. *The Journal of Physical Chemistry Letters* **2015**, *6* (5), 860-867.
8. Pandit, A.; Reus, M.; Morosinotto, T.; Bassi, R.; Holzwarth, A.; Holzwarth, A. R., An NMR comparison of the light-harvesting complex II (LHCII) in active and photoprotective states reveals subtle changes in the chlorophyll a ground-state electronic structures. *Biochimica et biophysica acta. Bioenergetics* **2013**, *1827* (6), 738-744.
9. Liguori, N.; Periole, X.; Marrink, S. J.; Croce, R., From light-harvesting to photoprotection: structural basis of the dynamic switch of the major antenna complex of plants (LHCII). *Sci Rep* **2015**, *5*, 15661.
10. Standfuss, A. C.; Terwisscha van Scheltinga, M.; Lamborghini, W.; Kühlbrandt, Mechanisms of photoprotection and nonphotochemical quenching in pea light-harvesting complex at 2.5 Å resolution. *EMBO journal* **2005**, *24* (5), 919-928.
11. Papadatos, S.; Charalambous, A. C.; Daskalakis, V., A pathway for protective quenching in antenna proteins of Photosystem II. *Scientific Reports* **2017**, *7* (1), 2523.
12. Miloslavina, Y.; Wehner, A.; Lambrev, P. H.; Wientjes, E.; Reus, M.; Garab, G.; Croce, R.; Holzwarth, A. R., Far-red fluorescence: A direct spectroscopic marker for LHCII oligomer formation in non-photochemical quenching. *FEBS Letters* **2008**, *582* (25-26), 3625-3631.
13. Liu, Z.; Yan, H.; Wang, K.; Kuang, T.; Zhang, J.; Gui, L.; An, X.; Chang, W., Crystal structure of spinach major light-harvesting complex at 2.72 Å resolution. *Nature* **2004**, *428* (6980), 287-292.
14. Fehr, N.; Dietz, C.; Polyhach, Y.; von Hagens, T.; Jeschke, G.; Paulsen, H., Modeling of the N-terminal Section and the Lumenal Loop of Trimeric Light Harvesting Complex II (LHCII) by Using EPR. *J Biol Chem* **2015**, *290* (43), 26007-20.
15. Crisafi, E.; Pandit, A., Disentangling protein and lipid interactions that control a molecular switch in photosynthetic light harvesting. *Biochim Biophys Acta* **2017**, *1859* (1), 40-47.
16. Natali, A.; Gruber, J. M.; Dietzel, L.; Stuart, M. C.; van Grondelle, R.; Croce, R., Light-harvesting Complexes (LHCs) Cluster Spontaneously in Membrane Environment Leading to Shortening of Their Excited State Lifetimes. *J Biol Chem* **2016**, *291* (32), 16730-9.
17. Wei, X.; Su, X.; Cao, P.; Liu, X.; Chang, W.; Li, M.; Zhang, X.; Liu, Z., Structure of spinach photosystem II-LHCII supercomplex at 3.2 Å resolution. *Nature* **2016**, *534*, 69.
18. Ruban, A.; Ruban, M.; Duffy, The photoprotective molecular switch in the photosystem II antenna. *Biochimica et biophysica acta. Bioenergetics* **2012**, *1817* (1), 167-181.
19. Ward, M. E.; Wang, S.; Munro, R.; Ritz, E.; Hung, I.; Gor'kov, Peter L.; Jiang, Y.; Liang, H.; Brown, Leonid S.; Ladizhansky, V., In Situ Structural Studies of Anabaena Sensory Rhodopsin in the E. coli Membrane. *Biophysical Journal* **2015**, *108* (7), 1683-1696.
20. Miao, Y.; Qin, H.; Fu, R.; Sharma, M.; Can, T.; Hung, I.; Luca, S.; Gor'kov, P. L.; Brey, W. W.; Cross, T. A., M2 Proton Channel Structural Validation from Full Length Protein Samples in Synthetic Bilayers and E. coli Membranes. *Angewandte Chemie (International ed. in English)* **2012**, *51* (33), 8383-8386.
21. Fu, R.; Wang, X.; Li, C.; Santiago-Miranda, A. N.; Pielak, G. J.; Tian, F., In situ structural characterization of a recombinant protein in native Escherichia coli membranes

with solid-state magic-angle-spinning NMR. *Journal of the American Chemical Society* **2011**, *133* (32), 12370-3.

22. Kaplan, M.; Narasimhan, S.; de Heus, C.; Mance, D.; van Doorn, S.; Houben, K.; Popov-Celeketic, D.; Damman, R.; Katrukha, E. A.; Jain, P.; Geerts, W. J. C.; Heck, A. J. R.; Folkers, G. E.; Kapitein, L. C.; Lemeer, S.; van Bergen En Henegouwen, P. M. P.; Baldus, M., EGFR Dynamics Change during Activation in Native Membranes as Revealed by NMR. *Cell* **2016**, *167* (5), 1241-1251 e11.

23. Renault, M.; Pawsey, S.; Bos, M. P.; Koers, E. J.; Nand, D.; Tommassen-van Boxtel, R.; Rosay, M.; Tommassen, J.; Maas, W. E.; Baldus, M., Solid-state NMR spectroscopy on cellular preparations enhanced by dynamic nuclear polarization. *Angew Chem Int Ed Engl* **2012**, *51* (12), 2998-3001.

24. Baker, L. A.; Sinnige, T.; Schellenberger, P.; de Keyzer, J.; Siebert, C. A.; Driessen, A. J. M.; Baldus, M.; Grunewald, K., Combined (1)H-Detected Solid-State NMR Spectroscopy and Electron Cryotomography to Study Membrane Proteins across Resolutions in Native Environments. *Structure (London, England : 1993)* **2017**.

25. Shi, P.; Li, D.; Chen, H.; Xiong, Y.; Wang, Y.; Tian, C., In situ (19)F NMR studies of an E. coli membrane protein. *Protein Science : A Publication of the Protein Society* **2012**, *21* (4), 596-600.

26. Kirchhoff, H.; Mukherjee, U.; Galla, H. J., Molecular architecture of the thylakoid membrane: lipid diffusion space for plastoquinone. *Biochemistry* **2002**, *41* (15), 4872-82.

27. Chua, N. H.; Bennoun, P., Thylakoid membrane polypeptides of *Chlamydomonas reinhardtii*: wild-type and mutant strains deficient in photosystem II reaction center. *Proceedings of the National Academy of Sciences of the United States of America* **1975**, *72* (6), 2175-2179.

28. Laemmli, U. K., Cleavage of Structural Proteins during the Assembly of the Head of Bacteriophage T4. *Nature* **1970**, *227*, 680-685.

29. Färber, A.; Jahns, P., The xanthophyll cycle of higher plants: influence of antenna size and membrane organization. *Biochim. Biophys. Acta* **1998**, *1363*, 47-58.

30. Jeffrey, S. W.; Mantoura, R. F. C.; Wright, S. W., Phytoplankton pigments in oceanography: guidelines to modern methods. *Monogr. Oceanogr. Methodol.* **1997**.

31. Pinest, A.; Gibbyt, M.G.; Waugh, J. S., Proton-enhanced NMR of dilute spins in solids. *The Journal of Chemical Physics* **1973**, *69* (2), 569-590.

32. Hartmann, S. R.; Hahn, E. L., Nuclear Double Resonance in the Rotating Frame. *Physical Review* **1962**, *128* (5), 2042-2053.

33. Baldus, M.; Petkova, A. T.; Herzfeld, J.; Griffin, R. G., Cross polarization in the tilted frame: assignment and spectral simplification in heteronuclear spin systems. *Molecular Physics* **1998**, *95* (6), 1197-1207.

34. Fung, B. M.; Khitrin, A. K.; Ermolaev, K. An Improved Broadband Decoupling Sequence for Liquid Crystals and Solids. *Journal of Magnetic Resonance* **2000**, *142*, 97-101.

35. Weingarth, M.; Demco, D. E.; Bodenhausen, G.; Tekely, P., Improved magnetization transfer in solid-state NMR with fast magic angle spinning. *Chemical Physics Letters* **2009**, *469* (4-6), 342-348.

36. Baldus, M., Correlation Experiments for Assignment and Structure Elucidation of Immobilized Polypeptides Under Magic Angle Spinning. *Prog. Nucl. Magn. Reson. Spectr* **2002**, *1-47* (1-2).

37. Baldus, M.; Meier, B. H., Total Correlation Spectroscopy in the Solid State. The Use of Scalar Couplings to Determine the Through-Bond Connectivity. *Journal of Magnetic Resonance, Series A* **1996**, *121* (1), 65-69.

38. Gareth, A. M.; Freeman, R., Enhancement of nuclear magnetic resonance signals by polarization transfer. *J. Am. Chem. Soc* **1979**, *101* (3), 760-762.

39. Goddard, T.; Kneller, D., SPARKY. *University of California, San Francisco*.

40. Arnold, K.; Bordoli, L.; Kopp, J.; Schwede, T., The SWISS-MODEL workspace: a web-based environment for protein structure homology modelling. *Bioinformatics* **2006**, *22* (2), 195-201.

41. Natali, A.; Croce, R., Characterization of the major light-harvesting complexes (LHCBM) of the green alga *Chlamydomonas reinhardtii*. *PLoS One* **2015**, *10* (2), e0119211.
42. Han, B.; Wishart, D. S.; Liu, Y.; Ginzinger, S. W., SHIFTX2: significantly improved protein chemical shift prediction. *J Biomol NMR* **2011**, *50*, 43-57.
43. Gradmann, S.; Ader, C.; Dittmann, M.; Engelhard, M.; Heinrich, I.; Cukkemane, A.; Baldus, M.; Nand, D.; Dijk, M. v.; Bonvin, A. M. J. J., Rapid prediction of multi-dimensional NMR data sets. *J Biomol NMR* **2012**, *54*, 377-387.
44. Drop, B.; Webber-Birungi, M.; Yadav, S. K. N.; Filipowicz-Szymanska, A.; Fusetti, F.; Boekema, E. J.; Croce, R., Light-harvesting complex II (LHCII) and its supramolecular organization in *Chlamydomonas reinhardtii*. *Biochimica et Biophysica Acta (BBA) - Bioenergetics* **2014**, *1837* (1), 63-72.
45. Ferrante, P.; Ferrante, P.; Ballottari, M.; Bonente, G.; Giuliano, G.; Bassi, R., LHCBM1 and LHCBM2/7 Polypeptides, Components of Major LHCII Complex, Have Distinct Functional Roles in Photosynthetic Antenna System of *Chlamydomonas reinhardtii*. *Journal of biological chemistry* **2012**, *287* (20), 16276-16288.
46. Azadi Chegeni, F.; Perin, G.; Sai Sankar Gupta, K. B.; Simionato, D.; Morosinotto, T.; Pandit, A., Protein and lipid dynamics in photosynthetic thylakoid membranes investigated by in-situ solid-state NMR. *Biochim Biophys Acta* **2016**, *1857* (12), 1849-1859.
47. Ward, M. E.; Ritz, E.; Ahmed, M. A.; Bamm, V. V.; Harauz, G.; Brown, L. S.; Ladizhansky, V., Proton detection for signal enhancement in solid-state NMR experiments on mobile species in membrane proteins. *J Biomol NMR* **2015**, *63* (4), 375-88.
48. Wang, Y.; Jardetzky, O., Investigation of the neighboring residue effects on protein chemical shifts. *Journal of the American Chemical Society* **2002**, *124* (47), 14075-84.
49. de Souza, L. M.; Iacomini, M.; Gorin, P. A.; Sari, R. S.; Haddad, M. A.; Sasaki, G. L., Glyco- and sphingophospholipids from the medusa *Phyllorhiza punctata*: NMR and ESI-MS/MS fingerprints. *Chem Phys Lipids* **2007**, *145* (2), 85-96.
50. Seiwert, D.; Witt, H.; Janshoff, A.; Paulsen, H., The non-bilayer lipid MGDG stabilizes the major light-harvesting complex (LHCII) against unfolding. *Scientific Reports* **2017**, *7* (1), 5158.
51. Azadi-Chegeni, F.; Schiphorst, C.; Pandit, A., In vivo NMR as a tool for probing molecular structure and dynamics in intact *Chlamydomonas reinhardtii* cells. *Photosynthesis Research* **2018**, *135* (1), 227-237.
52. Sculley, M. J.; Duniec, J. T.; Thorne, S. W.; Chow, W. S.; Boardman, N. K., The stacking of chloroplast thylakoids: Quantitative analysis of the balance of forces between thylakoid membranes of chloroplasts, and the role of divalent cations. *Archives of Biochemistry and Biophysics* **1980**, *201* (1), 339-346.
53. Su, X.; Ma, J.; Wei, X.; Cao, P.; Zhu, D.; Chang, W.; Liu, Z.; Zhang, X.; Li, M., Structure and assembly mechanism of plant C2S2M2-type PSII-LHCII supercomplex. *Science (New York, N.Y.)* **2017**, *357* (6353), 815-820.





# CHAPTER 4

---

**Conformational dynamics of zeaxanthin-binding LHCII in a lipid membrane**

---

## Abstract

---

Photosynthetic organisms have the challenging task to perform the conversion of light into chemical energy under fluctuating sunlight conditions. To cope with this challenge, they protect themselves from high light by dissipating excess energy as heat via the process called non-photochemical quenching (NPQ). Zeaxanthin (Zea) is essential for the full development of NPQ, but its role remains unclear. This chapter addresses the molecular effects of Zea on the structure and dynamics of Light Harvesting Complex II (LHCII). We applied solid state NMR spectroscopy on LHCII from the *npq2* mutant, which binds Zea in the V1 binding pocket, to investigate the effect of Zea on the protein conformational dynamics. Our results demonstrate that *npq2* LHCII have a different conformation than wildtype LHCII, from which we conclude that the protein fold and pigment-protein dynamics of LHCII depends on its oligomerization state and/or xanthophyll (Zea) binding. Moreover, we observe that, in contrast to wildtype LHCII, *npq2* LHCII contains a significant number of intrinsic galactolipids that are strongly bound. We conclude that Zea binding and monomerization influence lipid binding to LHCII and thereby could also influence structural arrangements and dynamics on the membrane level.

## Introduction

---

In excess light, the process of non-photochemical quenching (NPQ) is activated that causes heat dissipation of chlorophyll (Chl) excited-state energies in the Photosystem II (PSII) antenna. Two important components of NPQ are the pH-activated quenching of excitations in the light-harvesting antenna, known as qE, and zeaxanthin (Zea) dependent quenching, known as qZ, that is activated by the xanthophyll cycle which reversibly converts the carotenoid violaxanthin (Vio) into Zea via antheraxanthin. Molecular sites involved in qE and qZ are integrated in the Chl *a/b* binding light-harvesting antenna complexes of PSII, of which the most abundant ones are the LHCII. LHCII pigment-protein complexes are membrane proteins that bind various Chl *a* and *b* and different types of carotenoids in conserved binding pockets for lutein (L1 and L2), neoxanthin (N1) and violaxanthin (V1). In the xanthophyll cycle process, Vio in the V1 binding site of LHCII are replaced by Zea. Figure 1 presents the monomeric crystal structure of LHCII, highlighting the carotenoid binding sites.

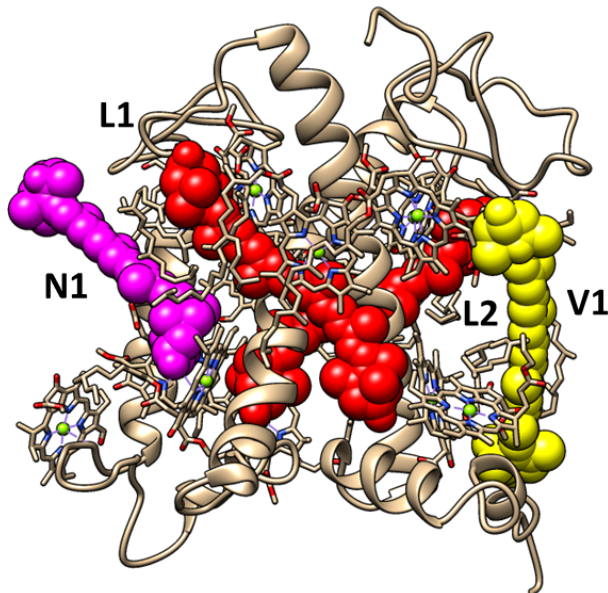


**Figure 1.** Crystal structure of monomeric LHCII indicating the carotenoid binding pockets. Neoxanthin (N1) is highlighted in purple, luteins (L1 and L2) are highlighted in red and violaxanthin (V1) in yellow.

The molecular effect of Zea replacement in LHCII is unclear. Zea might act directly with Chls in the antenna and quench excitations by Chl to Zea energy transfer or by forming charge-transfer states <sup>1</sup>. In its role as allosteric regulator of qE, Zea binding might promote a conformational change in LHCII due to its more hydrophobic nature <sup>2-3</sup>. Alternatively it has been proposed that Zea could be acting in between the complexes in the thylakoid membrane, to create a variety of quenching sites in the antenna complexes <sup>4</sup>. The presence of Zea appears to have a rigidifying effect on membrane fluidity and several experiments suggest that Zea binding rigidifies LHCII and stabilizes its quenched state <sup>5</sup>. However, structural data underpinning these structural effects are lacking.

The *npq2* mutants bind constitutively Zea in the V1 binding pocket of LHCII and provide an effective way to study the effect of Zea on structure and dynamics of LHCII. The *npq2* mutants lack the antheraxanthin enzyme to convert the Zea back to Vio in the V1 pocket, and also lack the carotenoid neoxanthin.

We performed a 2D dipolar based and INEPT based NMR analysis of Zea-containing LHCII complexes that were reconstituted in liposome membranes. <sup>13</sup>C-<sup>15</sup>N isotope-labeled LHCII complexes were isolated from the *npq2* strain of *Chlamydomonas reinhardtii* (*Cr.*). The liposomes for protein insertion were

composed of MGDG, DGDG, SQDG and PG. The lipid composition was chosen to mimic the lipid composition of native thylakoid membranes and a protein to lipid ratio of 1:55 (mol:mol) was chosen to mimic native protein packing densities <sup>6</sup>. These conditions are identical to those that we used in a study of WT LHCII proteoliposomes by NMR spectroscopy (Chapter 3). The collected <sup>13</sup>C-<sup>13</sup>C PARIS and <sup>13</sup>C-<sup>13</sup>C INEPT-TOBSY solid-state NMR spectra of Zea-LHCII proteoliposomes were compared to the previously collected spectra of wild type (WT) LHCII and show remarkable differences in structure, internal protein dynamics and lipid binding.

## Material and Methods

---

### LHCII extraction

*Cr.* Strains of *npq2* were grown under conditions as previously described for the WT cells in chapter 2. After thylakoid isolation, *Cr. npq2* thylakoids were re-suspended in buffer (50 mM Hepes-KOH pH 7.5, 5 mM MgCl<sub>2</sub> with 50% glycerol). For isolation of the LHCII fractions, thylakoid membranes corresponding to 3 mg/ml of total chlorophylls (based on the optical density at 680 nm) were washed with 50 mM EDTA and solubilized for 20 minutes on ice in 3 ml of 1.2%  $\alpha$ -DM in 10 mM Hepes (pH 7.5), after vortexing for 1 minute. The solubilized samples were centrifuged at 15000 $\times$ g for 30 minutes to eliminate any unsolubilized material and the supernatant with the photosynthetic complexes was then fractionated by ultracentrifugation in a 0–1 M sucrose gradient containing 0.06%  $\alpha$ -DM and 10 mM Hepes (pH 7.5), at 141000 $\times$ g for 40 hours at 4 °C. The green fraction corresponding monomeric *npq2* LHCII proteins was harvested with a syringe and the Chl concentration was adjusted to 2 mg/ml with buffer (50 mM HEPES, 5 mM MgCl<sub>2</sub>, pH 7.5).

### Preparation of liposomes

*Npq2* LHCII proteins solubilized in  $\alpha$ -DM were reconstituted in lipid membranes of which the lipid composition mimics the native thylakoid membrane. The proteoliposomes contained 47% MGDG, 12% SQDG, 14% PG and 27% DGDG at a protein-to-lipid ratio of 1:55 <sup>7</sup>. The chosen protein to lipid ratio is in the range of native protein packing densities in thylakoid membranes, where 70-80% of the membrane surface area is occupied by proteins <sup>6</sup>. The lipids were dissolved in chloroform and dried into a thin film using a rotary evaporator at 40 °C. The lipid film was hydrated by reconstitution buffer (50mM HEPES,

5mM MgCl<sub>2</sub>, pH=7.5 and 0.03%  $\beta$ -DM) and were exposed to 10 freeze-thaw cycles. After that, *npq2* LHCII was inserted into liposomes and detergent was removed by 72 hours of dialysis against detergent-free buffer. During the dialysis bio beads (SM-2, Bio Rad) were added to the buffer to speed up the dialysis process.

## Pigment analysis

The content of individual carotenoids of *npq2* LHCII was determined using high performance liquid chromatography (HPLC, Beckman System Gold), as described in <sup>8</sup>. The peaks of each sample were identified through the retention time and absorption spectrum <sup>9</sup>.

## UV/Visible spectroscopy

Absorption spectra were recorded on a Cary 60 UV–visible spectrophotometer (Agilent Technologies) with the wavelength range set from 350 to 750 nm using 0.5 cm cuvettes.

## Time-resolved fluorescence spectroscopy (TRF)

TRF measurements were performed using a FluoTime 300 (PicoQuant) time-correlated photon counter spectrometer. Samples were held in a 1x1 cm quartz cuvette that was kept at 20 °C with a thermostat and excited at 440 nm using a diode laser (PicoQuant). Fluorescence decay traces were fitted with multi-exponentials using a  $\chi^2$  least-square fitting procedure.

## NMR sample preparation

For the NMR samples, 18 ml of *npq2* LHCII proteoliposomes, containing approximately 6 mg LHCII and 1.5 mg Chl (as determined by OD<sub>680</sub> of the Chls), was pelleted by ultra-centrifugation (223000 $\times$ g, 4 °C, 90 min) and transferred to a thin-wall 3.2 mm solid-state NMR MAS (Magic Angle Spinning) rotor through centrifugation.

## Solid-State NMR experiments

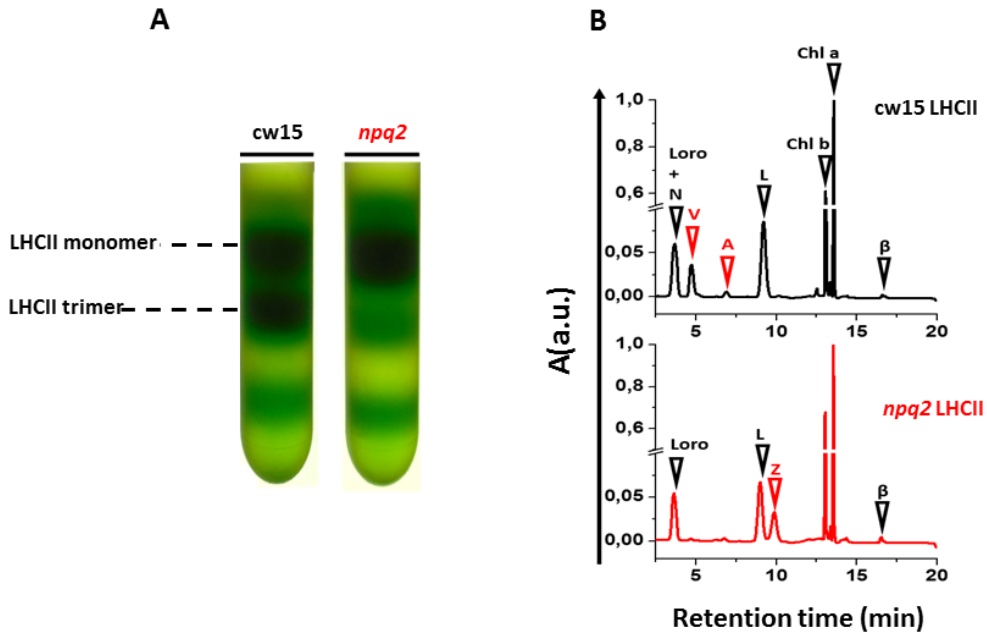
Solid-state NMR spectra were recorded with an ultra-high field 950-MHz <sup>1</sup>H Larmor frequency spectrometer (Bruker, Biospin, Billerica) equipped with a triple-channel <sup>1</sup>H, <sup>13</sup>C, <sup>15</sup>N 3.2 mm MAS probe. <sup>13</sup>C-<sup>13</sup>C PARIS and <sup>13</sup>C-<sup>13</sup>C INEPT on <sup>13</sup>C-<sup>15</sup>N *npq2* LHCII in lipid bilayers were recorded under the same MAS frequency, temperature and parameters as <sup>13</sup>C-<sup>15</sup>N WT LHCII in lipid bilayers (chapter 3). Typical  $\pi/2$  pulses were 3  $\mu$ s for <sup>1</sup>H, 5  $\mu$ s for <sup>13</sup>C, and 8  $\mu$ s for

$^{15}\text{N}$ . The  $^1\text{H}/^{15}\text{N}$  and  $^1\text{H}/^{13}\text{C}$  cross-polarization (CP)<sup>10</sup> contact times were 800  $\mu\text{s}$  and 1 ms, respectively, with a constant radio frequency (rf) field of 35 and 50 kHz on nitrogen and carbon, respectively, while the proton lock field was ramped linearly around the  $n=1$  Hartmann/Hahn condition<sup>11</sup>. The  $^{15}\text{N}/^{13}\text{C}$  SPECIFIC-CP transfer<sup>12</sup> was implemented with an optimized contact time of 4.2 ms with a constant lock field of  $2.5 \times \nu_r$  applied on  $^{15}\text{N}$ , while the  $^{13}\text{C}$  field was ramped linearly (10% ramp) around  $1.5 \times \nu_r$ .  $^1\text{H}$  decoupling during direct and indirect acquisition was performed using SPINAL64<sup>13</sup> with  $\sim 83$  kHz irradiation. The presented 2D  $^{13}\text{C}$ - $^{13}\text{C}$  PARIS<sup>14</sup> spectra were collected with a mixing time of 30 ms at 17 kHz MAS at a set temperature of  $-18$  °C. The  $J$ -coupling based 2D  $^{13}\text{C}$ - $^{13}\text{C}$  INEPT-TOBSY<sup>15-16</sup> experiments were recorded at  $-3$  °C with TOBSY mixing of 6 ms at 14 kHz MAS. Spectra were processed with Bruker TopSpin 3.2 (Bruker, Germany) with LPfr linear prediction and fqc mode for Fourier transformation. Spectra were analyzed by Sparky version 3.114<sup>17</sup> and MestReNova 11.0 (Mestrelab Research SL, Santiago de Compostela, Spain).

## Results

---

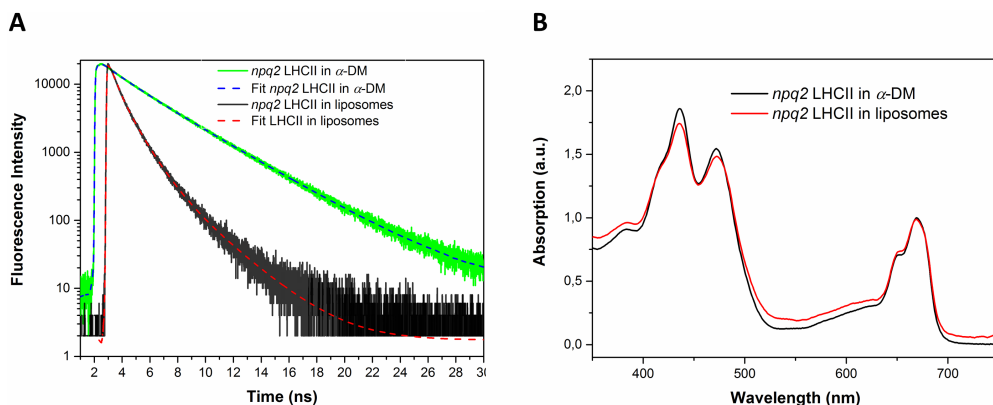
Biochemical analysis of *npq2* LHCII sucrose gradient analysis shows that the NPQ2 LHCII has a reduced trimeric content with respect to the WT (CW15) strain, as reported in literature<sup>18-21</sup>, and consequently monomeric fractions were collected. The inability to synthesize antheraxanthin, violaxanthin and neoxanthin and the constitutive accumulation of Zea in the Vx binding pocket was confirmed by high-pressure liquid chromatography (HPLC) analysis (see figure 2). The sucrose gradient analysis in figure 2A is also shown in chapter 2, figure 1, but is presented here again for discussion on the molecular properties of *npq2* LHCII. For comparison with the wild type LHCII, the *npq2* HPLC data is shown together with the HPLC chromatogram of wild type LHCII that was already presented in chapter 3, figure 3.



**Figure 2.** **A:** LHCII purification from sucrose gradients of thylakoid membranes from WT (CW15) and *npq2* *Cr.* cells. **B:** HPLC analysis of WT trimeric LHCII and *npq2* monomer LHCII fractions. Data of figure 2A has also been presented in Chapter 2, figure 1 and the HPLC chromatogram of the WT LHCII has also been presented in Chapter 3, figure 3.

In order to mimic the native lipid environment and to be consistent with conditions that were used for NMR analysis of WT LHCII, *npq2* LHCII was inserted into liposomes prepared from MGDG, DGDG, SQDG and PG lipids with a protein to lipid ratio of 1:55. Under these conditions, the LHCII complexes form aggregates inside the membranes and consequently the proteoliposomes are strongly fluorescence quenched, as shown in the time-resolved data in figure 3A. The *npq2* LHCII in  $\alpha$ -DM has an average life time of 3.2 ns, confirming that Zea binding to LHCII in itself does not induce a quenched state. The average lifetime is reduced to 1.1 ns after insertion into liposomes. The fluorescence characteristics are similar to those of the WT LHCII proteoliposomes that are reported in chapter 3 and that reveal similar strong fluorescence quenching which is attributed to aggregation of LHCII in the membranes. In addition, absorption spectra of the *npq2* LHCII were collected before and after insertion into the liposomes and are shown in figure 3B.

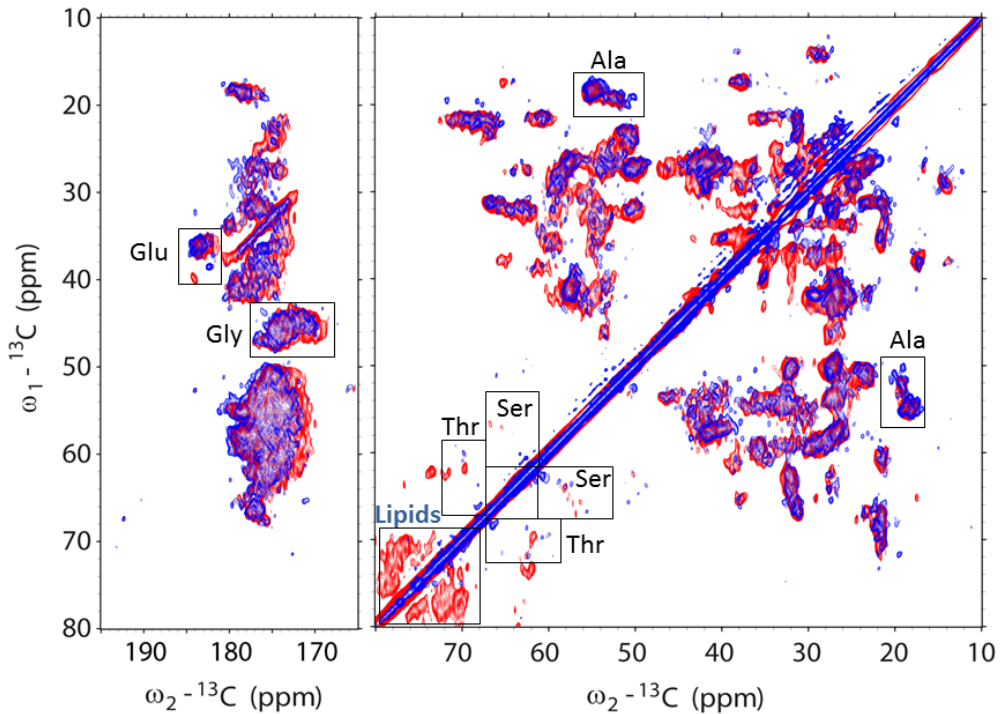




**Figure 3. A:** Time resolved fluorescence of *npq2* LHCII in  $\alpha$ -DM detergent (green) and *npq2* LHCII in liposomes (black). **B:** Absorption spectra of *npq2* LHCII in  $\alpha$ -DM detergent (black) and after inserting into liposomes (red).

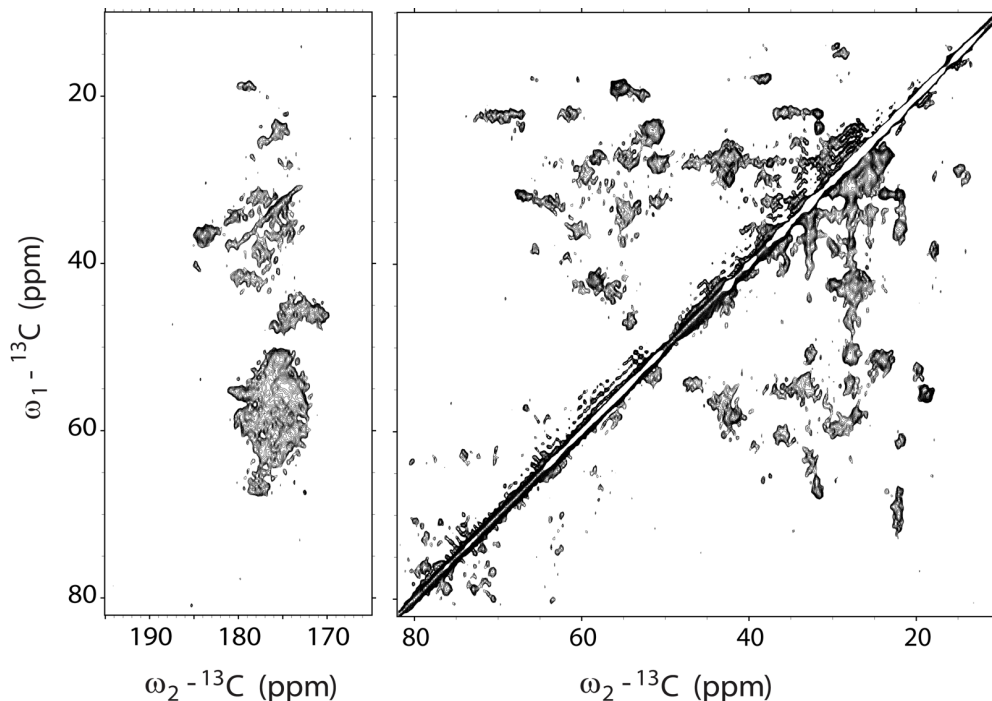
## Dipolar-based ssNMR experiments

Solid state NMR techniques were employed for investigation of the effect of Zea on the structure and dynamics of LHCII in lipid bilayers. First, 2D  $^{13}\text{C}$ - $^{13}\text{C}$  dipolar based PARIS spectra were collected on the  $^{13}\text{C}$ - $^{15}\text{N}$  *npq2* LHCII proteoliposomes under conditions described in the Materials and Methods section and results were compared to the spectra of  $^{13}\text{C}$ - $^{15}\text{N}$  WT LHCII proteoliposomes that were collected at identical experimental conditions.



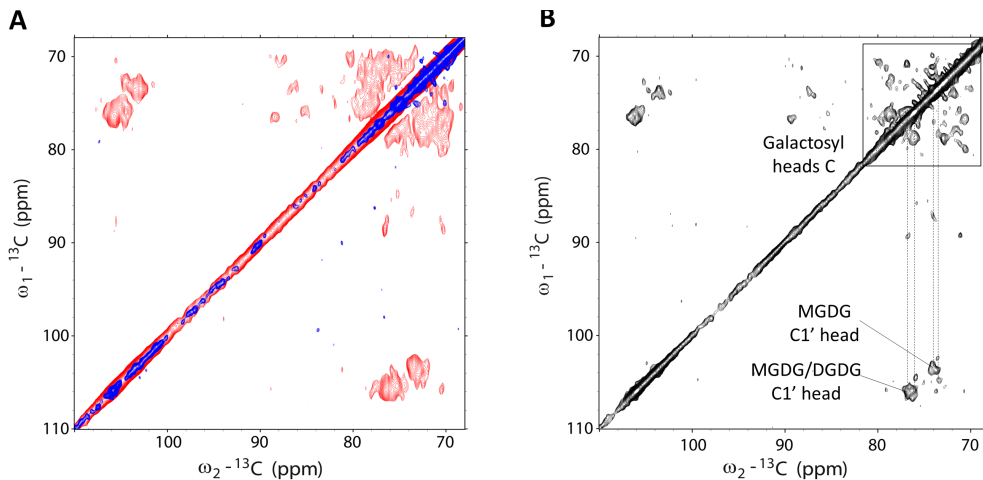
**Figure 4.** Overlaid  $^{13}\text{C}$ - $^{13}\text{C}$  PARIS spectra of WT LHCII (blue) and *npq2* LHCII (red). Spectra were collected at 255K and with 17 kHz MAS spinning.

Figure 4 shows the dipolar-based  $^{13}\text{C}$ - $^{13}\text{C}$  spectra of WT LHCII (blue) overlaid with *npq2* LHCII (red) that were collected and processed under identical conditions. The strong overlap of two spectra confirms that the overall fold of LHCII is preserved when Vio is replaced by Zea. However, the resonance peaks in the spectrum of *npq2* LHCII seem severely broadened. A readout temperature of 255K was applied for comparison with the WT LHCII spectrum under matching conditions. The CC PARIS experiments on *npq2* LHCII were repeated at 270K, which significantly improved the spectral resolution in the lipid region (figure 5 and 6).



**Figure 5.**  $^{13}\text{C}$ - $^{13}\text{C}$  PARIS spectra of *npq2* LHCII at 270 K and 17 kHz MAS spinning.

Another clear difference between the *npq2* and the WT LHCII spectrum as shown in the figure 4 and 6A, is the presence of strong signals resonating between 70-80 and 105 ppm in the spectrum of *npq2* LHCII that are from signals from the galactolipid heads. Since the liposome lipids are not isotope-labeled and the probability for detecting  $^{13}\text{C}$ - $^{13}\text{C}$  correlations among natural abundance  $^{13}\text{C}$  carbons is very low, lipid signals must arise from intrinsic thylakoid lipids that remained associated with LHCII upon its purification. According to galactolipid head chemical-shift assignments, signals around 105-107 ppm originate from the galactosyl C1' carbon of MGDG or DGDG, correlating with C2', C3' or C4' around 73-77 ppm. DGDG molecules should give additional signals from the second ring with chemical shifts of C1'' around 101 ppm. Because no additional correlations are observed, we tentatively attribute the strong lipid galactosyl signals to MGDG molecules that are strongly bound to Zea-LHCII and must be non-annular lipids that do not exchange on NMR time scales (*i.e.*  $< 10^4 \text{ s}^{-1}$ ).



**Figure 6. A:** Close up of lipid signals in  $^{13}\text{C}$ - $^{13}\text{C}$  PARIS spectrum of WT (blue) and *npq2* (red) LHCII at 255K. **B:**  $^{13}\text{C}$ - $^{13}\text{C}$  PARIS spectrum of *npq2* LHCII at 270K.

For further analysis of the *npq2* LHCII backbone structure, we take a closer inspection of selective spectral regions. The backbone  $C_\alpha$  and  $C_\beta$  chemical-shift signals of Ala, Thr and Ser residues accumulate in distinct spectral regions that are separated from the correlations of other amino acid residues. Comparing the Ala, Ser and Thr backbone chemical shifts of *npq2* LHCII to the shifts of the WT LHCII, significant differences are observed. Three clear Ala  $C_\alpha$ - $C_\beta$  correlations in the WT LHCII spectrum are lacking in the *npq2* LHCII spectrum as indicated in figure 7B. These three peaks in the spectrum of WT LHCII do not match with any predicted chemical-shift correlations that were produced using *Cr* LHCII structure homology models (chapter 3). The homology models are built from the plant LHCII X-ray structures that lack the first 14 residues in the N terminus and therefore the three peaks could be from Ala residues in the N-terminal stretch. Also in the Thr and Ser coil regions of  $C_\alpha$ - $C_\beta$  correlations, dramatic changes are observed (figure 7B). While the Thr and Ser coil signals in the WT spectrum are rather weak, multiple strong signals are observed in the *npq2* spectrum. In addition, interesting changes in the chemical shift pattern of Ser residues are observed (figure 7A). According to the crystal structure, LHCII consists of three transmembrane helices together with large flexible loops and tails. However, several Ser residues of *npq2* LHCII appear to have strand conformations according to the PARIS NMR spectrum. This suggests that *npq2* LHCII folds into strands in some parts of the protein. Thr and Ser residues in the coil area are highlighted in red in the crystal structure of LHCII (figure 8).

Furthermore, in the CO region of the spectrum, we observe a clear change in the NMR signal of a Glu COO<sup>-</sup> carboxyl side chain that indicates a change in one of the Glu residues in the *npq2* LHCII (figure 7C).

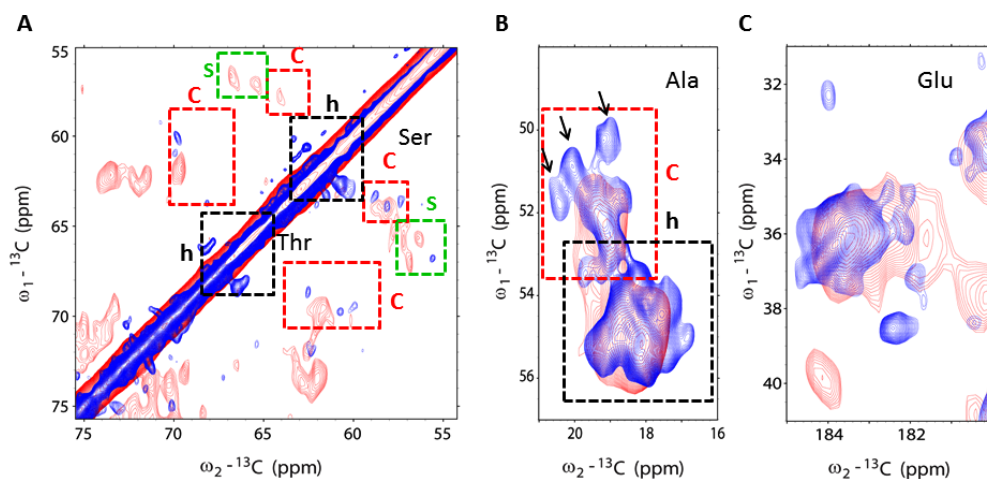


**Figure 7.** **A:** The Ser and Thr regions in the  $^{13}\text{C}$ - $^{13}\text{C}$  PARIS spectra of WT (blue) and *npq2* (red) LHCII. Helix, coil and  $\beta$  strands contribution are presented with black, red and green boxes. **B:** The Ala region. Arrows indicate extra resonances that are observed in the spectrum of WT LHCII. **C:** Glu COO region.

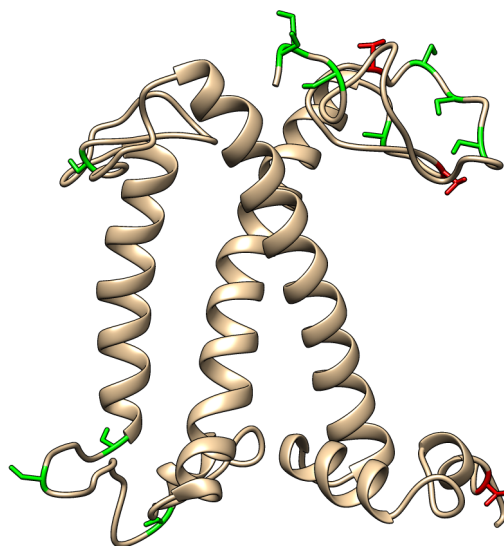


**Figure 8.** Crystal structure of LHCII highlighting the Thr (red) and Ser (green) residues in coil regions.

Several carotenoid and Chl pigment correlations can easily be identified in the spectra because they accumulate in a spectral region where no protein signals occur, including the carotenoid conjugated-chain CH<sub>3</sub>-CH correlations and correlations of the Chl *a* C8<sup>1</sup>/8<sup>2</sup>- 8/9 macrocycle side chains (figure 9). By comparison with NMR data of U-<sup>13</sup>C-lutein LHCII (Crisafi *et al.*, in progress), we are able to attribute the most upfield shifted carotenoid CH chemical shifts below 132 ppm to Zea. In the *npq2* mutant, the only carotenoids that are present are lutein and Zea. In WT spectra the chemical shift changes are observed for Chl *a* C8<sup>1</sup>/8<sup>2</sup>- 8/9 resonances, however in *npq2* spectra the signals appear shifted to upfield. According to the crystal structure of LHCII, Chl *a* 614 is close proximity to the Zea molecule and close interaction between Zea and Chl *a* 614 might explain the different Chl *a* shift pattern compared to the spectrum of WT LHCII.

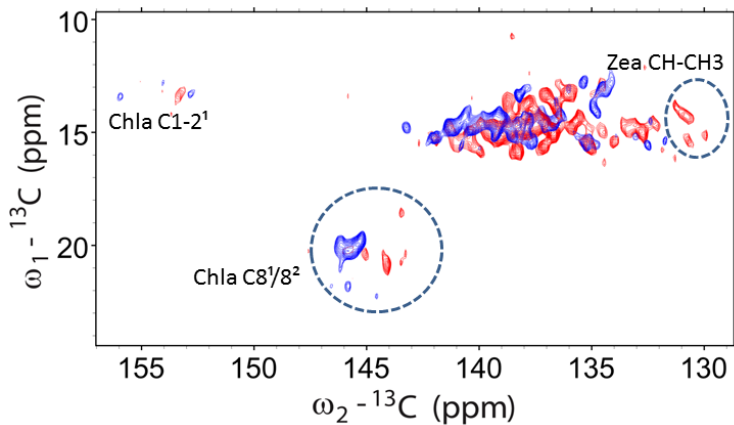


**Figure 9.** Pigment region of the <sup>13</sup>C-<sup>13</sup>C PARIS spectrum of WT (blue) and *npq2* (red) LHCII. Circles indicate the upfield shifted of carotenoid and Chl *a* signals.

## J-coupling based ssNMR experiments

The conformational dynamics of *npq2* LHCII is further investigated by a 2D <sup>13</sup>C-<sup>13</sup>C INEPT-TOBSY experiment that was collected at 270K. In this experiment polarization transfer is based on *J*-coupling interactions and that is selective for molecules that undergo strong ns or sub-ns motions. Selective protein signals are observed in the *npq2* INEPT spectrum that overlap with the INEPT-TOBSY spectrum of the WT (figure 10). However, for a Phe and two Thr residues, and two Chl phytol chains, signals are observed in the WT INEPT spectrum but not in the INEPT spectrum of *npq2* LHCII. The Chl tails were predicted to belong to

Chl605 and Chl606 that of which the tails are not resolved in the X-ray structures and the Phe residue was predicted to be located in the LHCII C terminus (chapter 3). In addition, few other protein signals are few shifted or missing in the *npq2* spectrum compared to the WT spectrum as indicated by circles in figure 10. Furthermore, the *npq2* spectrum shows resonances of lipid galactosyl heads that are also observed in the WT spectrum. These signals are attributed to lipids that have been co-purified with LHCII, but are not strongly bound and may have exchanged with bulk lipids upon reconstitution of LHCII in the liposomes.

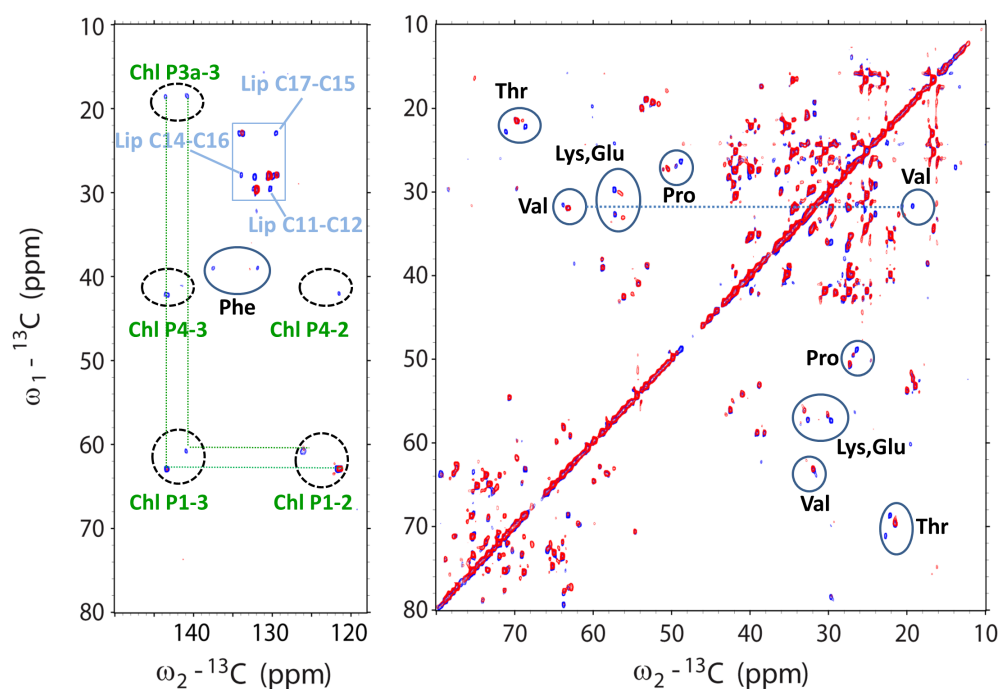


**Figure 10.** Overlaid  $^{13}\text{C}$ - $^{13}\text{C}$  INEPT-TOBSY spectra of WT (blue) and *npq2* (red) LHCII. Spectra were collected with a spinning frequency of 14 kHz at 270K. Resonance signals of residues which are missing or shifted in the *npq2* spectra are indicated with circles.

## Discussion

The analyzed *npq2* LHCII complex differs in three ways from the WT complex: (i) Vio is replaced by Zea, (ii) the Neo carotenoid that points outwards the complex is lacking, and (iii) due to destabilization of the trimers in *npq2*

membranes, the *npq2* LHCII complexes were collected as monomers. The strong signals in the CP-based NMR spectrum of non-annular galactolipids associated with *npq2* LHCII contrast with the picture of lipids associated with WT LHCII. For the WT complexes only a small number of associated galactolipids were detected, and only in INEPT-based spectra, indicating that those lipids were not tightly bound and likely are annular lipids (chapter 3) <sup>22</sup>. The difference may be explained by the monomerization of *npq2* LHCII. Compared to trimers, LHCII monomers will have more membrane-exposed hydrophobic protein sites that form potential lipid binding sites. Another possible explanation is that *Zea* increases the affinity of LHCII for lipids, owing to its more hydrophobic nature compared to *Vio*. It is not clear if the LHCII are already present as monomers in the *npq2* thylakoid membranes or that lower stability of *npq2* LHCII trimers caused their monomerization during purification. For WT LHCII, light-induced trimer to monomer transitions have been observed <sup>23</sup> and it has been reported that high light induces monomerization of LHCII trimers in plant leaves, leading to more quenching and less efficient transfer of excitations to the reaction center <sup>24</sup>. The monomeric state of LHCII, or oligomers formed from LHCII monomers, thus represents a state that may also be present under stress conditions *in vivo*. The recently obtained cryo-EM LHCII-PSII supercomplex structures reveal well-defined lipid molecules that contribute to interactions between the LHCII and PSII core <sup>25</sup>. Increased lipid binding to monomeric *Zea* LHCII could play a role in modulating LHCII-PSII interactions, or the interactions among the antenna proteins. Moreover, it has been reported that elevated levels of *Zea* associated with LHCII oligomers enhances resistance to photooxidative stress by a lipid-protective mechanism <sup>26</sup>. Increased affinity of lipids for *Zea*-containing LHCII could also serve as a way to protect thylakoid lipids under light stress conditions.

It is very interesting to note that also 2D CP-PARIS NMR spectra of *Cr. npq2* whole thylakoids from which the *npq2* LHCII were isolated differ from WT thylakoid spectra by containing strong signals of immobilized galactolipid heads (chapter 2) <sup>22</sup>. This suggests that also inside the original *npq2* thylakoid membranes galactolipids are strongly associated with *Zea* LHCII. We speculate that those lipids bound to *Zea* LHCII count for the additional fraction of immobilized lipids that is observed in *npq2* thylakoids compared to WT thylakoids <sup>22</sup> and may contribute to the overall rigidity of *Zea*-containing thylakoid membranes as has been described in chapter 2 and by various other reports <sup>18, 27</sup>.

In INEPT spectra of WT LHCII proteoliposomes, Chl phytol tail signals are detected that were attributed to Chl *b* 605 and 606. The 605 and 606 Chls are located at the periphery of the complexes and have Chl tails that will protrude



into the surrounding lipid bilayer. Dynamic Chl tails are only detected for WT and not for *npq2* LHCII, indicating that WT LHCII has a less tight packing in the proteoliposome membranes. Other dynamic sites that are detected for WT but not for *npq2* LHCII involve two Thr and one Phe residue. In our previous study, we predicted that these dynamic amino acids are located in the C terminus, which site is involved in stabilizing the V1 carotenoid. The reduced dynamics of this site in *npq2* LHCII suggests that Zea in the V1 pocket rigidifies the LHCII protein structure. This notion is further confirmed by strong Thr and Ser coil and strand signals that appear in the *npq2* spectrum, while the Thr and Ser coil signals in the CP-PARIS spectrum of WT LHCII are very weak.

The three coil Ala peaks in the LHCII WT spectrum that are not found in the *npq2* spectrum could originate from the N terminal stretch, which would suggest that the N terminal stretch adopts a more ordered structure in WT LHCII. Furthermore, the LHCII crystal structures do not contain strand segments, while the NMR spectrum of *npq2* LHCII contains Ser signals in the predicted region for strand conformations. These differences clearly indicate that the LHCII pigment-protein complex has sites with structural plasticity that refold upon xanthophyll exchange and/or monomerization.

## Conclusion

---

In summary, our results provide converging evidence for structural plasticity in LHCII. The same protein matrix adopts a different fold depending on its trimerization state, and on Zea binding in the V1 pocket. Both elements also have a strong effect on the lipid affinity of LHCII and may affect the overall membrane fluidity or supramolecular organization by changes in lipid-protein interactions.

## References

---

1. Holt, N. E.; Zigmantas, D.; Valkunas, L.; Li, X.; Niyogi, K.; Fleming, G. R., Carotenoid Cation Formation and the Regulation of Photosynthetic Light Harvesting. *Science* **2005**, *307*, 433-436.
2. Ruban, A.; Ruban, M.; Duffy, The photoprotective molecular switch in the photosystem II antenna. *Biochimica et biophysica acta. Bioenergetics* **2012**, *1817* (1), 167-181.

3. Horton, P.; Ruban, A. V.; Wentworth, M., Allosteric regulation of the light-harvesting system of photosystem II. *Philos Trans R Soc Lond B Biol Sci* **2000**, *355* (1402), 1361-70.
4. Xu, P.; Tian, L.; Kloz, M.; Croce, R., Molecular insights into Zeaxanthin-dependent quenching in higher plants. *Scientific Reports* **2015**, *5*, 13679.
5. Schlau-Cohen, G. S.; Yang, H. Y.; Kruger, T. P.; Xu, P.; Gwizdala, M.; van Grondelle, R.; Croce, R.; Moerner, W. E., Single-Molecule Identification of Quenched and Unquenched States of LHCII. *J Phys Chem Lett* **2015**, *6* (5), 860-7.
6. Kirchhoff, H.; Mukherjee, U.; Galla, H. J., Molecular architecture of the thylakoid membrane: lipid diffusion space for plastoquinone. *Biochemistry* **2002**, *41* (15), 4872-82.
7. Crisafi, E.; Pandit, A., Disentangling protein and lipid interactions that control a molecular switch in photosynthetic light harvesting. *Biochim Biophys Acta* **2017**, *1859* (1), 40-47.
8. Färber, A.; Jahns, P., The xanthophyll cycle of higher plants: influence of antenna size and membrane organization. *Biochim. Biophys. Acta* **1998**, *1363*, 47-58.
9. Jeffrey, S. W.; Mantoura, R. F. C.; Wright, S. W., Phytoplankton pigments in oceanography: guidelines to modern methods. *Monogr. Oceanogr. Methodol.* **1997**.
10. Pinest, A.; Gibbyt, M.G.; Waugh, J. S., Proton-enhanced NMR of dilute spins in solids. *The journal of Chemical Physics* **1973**, *69* (2), 569-590.
11. Hartmann, S. R.; Hahn, E. L., Nuclear Double Resonance in the Rotating Frame. *Physical Review* **1962**, *128* (5), 2042-2053.
12. Baldus, M.; Petkova, A. T.; Herzfeld, J.; Griffin, R. G., Cross polarization in the tilted frame: assignment and spectral simplification in heteronuclear spin systems. *Molecular Physics* **1998**, *95* (6), 1197-1207.
13. Fung, B. M.; Khitrin, A. K.; Ermolaev, K. An Improved Broadband Decoupling Sequence for Liquid Crystals and Solids. *Journal of Magnetic Resonance* **2000**, *142*, 97-101.
14. Weingarth, M.; Demco, D. E.; Bodenhausen, G.; Tekely, P., Improved magnetization transfer in solid-state NMR with fast magic angle spinning. *Chemical Physics Letters* **2009**, *469* (4-6), 342-348.
15. Baldus, M.; Meier, B. H., Total Correlation Spectroscopy in the Solid State. The Use of Scalar Couplings to Determine the Through-Bond Connectivity. *Journal of Magnetic Resonance, Series A* **1996**, *121* (1), 65-69.
16. Morris, G. A.; Freeman, R., Enhancement of nuclear magnetic resonance signals by polarization transfer. *J. Am. Chem. Soc* **1979**, *101* (3), 760-762.
17. Goddard, T.; Kneller, D., SPARKY. *University of California, San Francisco*.
18. Tardy, F.; Havaux, M., Thylakoid membrane fluidity and thermostability during the operation of the xanthophyll cycle in higher-plant chloroplasts. *Biochimica et biophysica acta* **1997**, *1330* (2), 179-93.
19. Lokstein, H.; Tian, L.; Polle, J. E. W.; DellaPenna, D., Xanthophyll biosynthetic mutants of *Arabidopsis thaliana*: altered nonphotochemical quenching of chlorophyll fluorescence is due to changes in Photosystem II antenna size and stability. *Biochimica et Biophysica Acta* **2002**, *1553*, 309-319.
20. Havaux, M.; Dall'Osto, L.; Cuine, S.; Giuliano, G.; Bassi, R., The effect of zeaxanthin as the only xanthophyll on the structure and function of the photosynthetic apparatus in *Arabidopsis thaliana*. *J Biol Chem* **2004**, *279* (14), 13878-88.
21. Dall'Osto, L.; Caffarri, S.; Bassi, R., A mechanism of nonphotochemical energy dissipation, independent from PsbS, revealed by a conformational change in the antenna protein CP26. *Plant Cell* **2005**, *17* (4), 1217-32.
22. Azadi Chegeni, F.; Perin, G.; Sai Sankar Gupta, K. B.; Simionato, D.; Morosinotto, T.; Pandit, A., Protein and lipid dynamics in photosynthetic thylakoid membranes investigated by in-situ solid-state NMR. *Biochim Biophys Acta* **2016**, *1857* (12), 1849-1859.

23. Garab. G1; Cseh. Z; Kovács. L; Rajagopal. S; Várkonyi. Z; Wentworth. M; Mustárdy. L; Dér. A; Ruban. A.V; Papp. E; Holzenburg. A; P., H., Light-Induced Trimer to Monomer Transition in the Main Light-Harvesting Antenna Complex of Plants: Thermo-Optic Mechanism. *Biochemistry* **2002**, *41*, 15121-15129.
24. Bielczynski, L. W.; Schansker, G.; Croce, R., Effect of Light Acclimation on the Organization of Photosystem II Super- and Sub-Complexes in *Arabidopsis thaliana*. *Front Plant Sci* **2016**, *7*, 105.
25. Lu, S.; Cao, Y.; Fan, S. B.; Chen, Z. L.; Fang, R. Q.; He, S. M.; Dong, M. Q., Mapping disulfide bonds from sub-micrograms of purified proteins or micrograms of complex protein mixtures. *Biophys Rep* **2018**, *4* (2), 68-81.
26. Johnson, M. P.; Havaux, M.; Triantaphylides, C.; Ksas, B.; Pascal, A. A.; Robert, B.; Davison, P. A.; Ruban, A. V.; Horton, P., Elevated zeaxanthin bound to oligomeric LHCII enhances the resistance of *Arabidopsis* to photooxidative stress by a lipid-protective, antioxidant mechanism. *J Biol Chem* **2007**, *282* (31), 22605-18.
27. Havaux, M., Carotenoids as membrane stabilizers in chloroplasts. *trends in plant science* **1998**, *3*, 147-151.

# CHAPTER 5

---

***In-vivo* NMR as a tool for probing molecular structure and dynamics in intact *Chlamydomonas reinhardtii* cells**

---

This work is published as: Azadi-Chegeni F., Schiphorst C. & Pandit A.  
Photosynthesis research (2018), 135(1-3): 227-237

## Abstract

---

We report the application of NMR dynamic spectral editing for probing the structure and dynamics of molecular constituents in fresh, intact cells and in freshly prepared thylakoid membranes of *Chlamydomonas reinhardtii* (*Cr.*) green algae. For isotope labeling, wild type *Cr.* cells were grown on  $^{13}\text{C}$  acetate-enriched minimal medium. 1D  $^{13}\text{C}$   $J$ -coupling based and dipolar-based MAS NMR spectra were applied to distinguish  $^{13}\text{C}$  resonances of different molecular components. 1D spectra were recorded over a physiological temperature range and whole-cell spectra were compared to those taken from thylakoid membranes, evaluating their composition and dynamics. A theoretical model for NMR polarization transfer was used to simulate the relative intensities of direct,  $J$ -coupling and dipolar-based polarization from which the degree of lipid segmental order and rotational dynamics of the lipid acyl chains were estimated. We observe that thylakoid lipid signals dominate the lipid spectral profile of whole algae cells, demonstrating that with our novel method, thylakoid membrane characteristics can be detected with atomistic precision inside intact photosynthetic cells. The experimental procedure is rapid and applicable to fresh cell cultures, and could be used as an original approach for detecting chemical profiles, and molecular structure and dynamics of photosynthetic membranes *in vivo* in functional states.

## Introduction

---

The plasticity of oxygenic photosynthetic membranes is tightly connected with plant fitness in fluctuating environments and their capability to respond to stress in excess light or drought conditions. Regulation of photosynthetic light harvesting is controlled by flexibility of the light-harvesting antenna from atomistic to supra molecular scale. Short and long-term adaptation results in structural, dynamical changes varying from atomic-scale pigment and protein alterations to mesoscopic membrane rearrangements<sup>1-4</sup>. Fast membrane remodeling is required to cope with sunlight fluctuations, while photosynthetic organisms may adjust their membrane compositions in adaptation to varying seasons or climates. The underlying regulation mechanisms have to be understood to the molecular level to gather central knowledge that can be used to increase plant stress tolerance or design algae species with improved solar-to-biomass conversion.

Essential here is the parallel development of suitable tools and methodology that can analyze molecular composition, structure and plasticity of intact photosynthetic membranes of plants and cells grown under various environmental conditions or in different functional states. Fluorescence techniques have been developed for functional analysis of whole membranes, cells, or leaves, probing the dynamic nature of light harvesting *in vivo* in molecular detail <sup>5-8</sup>. Complementary techniques that can resolve conformational structures and dynamics at the molecular level inside physiological membranes or whole cells are still challenging. With Fourier-Transform Infra-Red (FTIR) spectroscopy, molecular information of protein carbonyls and lipids can be obtained from heterogeneous membranes, but has to be extracted from band fitting of broad FTIR absorbance spectra. The technique has been applied to determine the dynamics of protein and lipid moieties in *Synechocystis* cells and in higher-plant thylakoid membranes <sup>9-10</sup>. Resonance Raman (RR) spectroscopy can report on the conformations and H-bonding patterns of chromophores in intact systems and through this technique, it was discovered that light stress induces *in-vivo* and *in-vitro* changes in the conformation of neoxanthin (Neo) <sup>11</sup>. Fluorescence Recovery After Photobleaching (FRAP) was used to investigate the lateral mobility of light-harvesting complexes in cyanobacteria and in plant thylakoid membranes <sup>12</sup>. Thylakoid membrane fluidity has been investigated by measuring the rotational dynamics of externally added fluorescence or Electron Spin Resonance (ESR) spin probes <sup>4</sup>. The latter techniques, however, do not report on the intrinsic, molecular dynamics of the membrane components. <sup>31</sup>P NMR and fluorescence studies using fluorolipid probes have been applied to detect mesoscopic phase transitions in functional thylakoid membranes, and detected a transition from bilayer to inverted hexagonal states at high temperature <sup>13-14</sup>. The advantage of <sup>31</sup>P NMR is that no external probes are added and no isotope enrichment is required, the disadvantage is however that only the phases of the phospholipids are followed, which in thylakoids only form ~10% of the total lipid composition. Recent multi-scale modeling simulations have provided molecular insight in thylakoid lipid lateral organization and dynamics <sup>15</sup> and predicted the molecular dynamics of Photosystem II embedded in a thylakoid membrane <sup>16-17</sup>. These studies have not been matched by experimental approaches, which would require detection of protein and lipid dynamics with atomistic resolution in native thylakoids, or atomic-level structural analysis of isolated pigment-protein complexes reconstituted in thylakoid lipid membranes.

Herein we describe the use of dynamic spectral-editing NMR as a new tool to analyze molecular composition and dynamics of thylakoid membranes or whole cells. Arnold et al. demonstrated that lipid and saccharide constituents could be identified in whole microalgae cells using NMR dynamic spectral-editing to

improve spectral resolution<sup>18</sup>. Topgaard and Sparr developed polarization transfer solid-state NMR into a method that allowed them to detect molecular mobility in intact skin<sup>19</sup> and to determine surfactant phase transitions<sup>20</sup>. In chapter 2, we elaborated on these approaches to separate rigid and mobile thylakoid constituents in *Chlamydomonas reinhardtii* (*Cr.*) thylakoids<sup>21</sup> and demonstrated that protein and lipid molecules in zeaxanthin (*Zea*)-accumulating *npq2* thylakoids display differential dynamics compared to WT (CW15) membranes, providing a molecular explanation for reported increased rigidity in *Zea*-rich membranes.

In this chapter, we demonstrate that our approach can be applied directly to fresh *Cr.* cells, circumventing isolation procedures and the need for sample storage. By simulating the polarization transfer efficiencies, we show that lipid acyl-chain rotational dynamics and their degree of segmental order can be estimated within a certain range, in a quantitative way. Comparison of intact *Cr.* cells and freshly isolated thylakoid membranes show very similar NMR lipid spectral profiles, demonstrating that the thylakoid lipids dominate and implying that their molecular conformation and dynamics can be determined inside intact cells.

## Material & Methods

---

### Cell culturing and <sup>13</sup>C isotope labeling

Wild-type *Cr.* cells (*strain* CC-124) were grown mixotrophically on Tris-Acetate-Phosphate (TAP) medium in a home-built set up, under continuous illumination with cool white LEDs (~50  $\mu\text{mol}/\text{m}^2 \text{ s}$ ) and constant temperature of 25°C. For isotope-label incorporation, the acetic acid was replaced by <sup>13</sup>C- acetate (Cambridge Isotopes).

### Pigment analysis

Chlorophyll and carotenoid concentrations were determined based on<sup>22</sup>, using a home-written Javascript web application that performs a non-negative least-square fitting procedure based on Lawson and Hanson<sup>23</sup> and Bro and de Jong<sup>24</sup>. In addition, pigment extracts were analyzed by High-Performance Liquid Chromatography (HPLC).

## Thylakoid extraction

The isolation of thylakoids was performed according to Chua and Bennoun<sup>25</sup> with some modifications. Cells were harvested in the exponential growth phase, centrifuged and resuspended in 0.2 volumes of MgCl<sub>2</sub> buffer (1mM MgCl<sub>2</sub>, 0.1 M HEPES, pH 7.5/KOH, 10% sucrose). Cells were ruptured by sonication on a 2500 Watt sonicator at 10%, using 15 cycles of 1s on/10s off followed by 30 cycles of 2s on/10s off. Thylakoid membranes were isolated using a discontinuous sucrose gradient. The disrupted cells were overlaid with 3mL of 1.8M sucrose in EDTA buffer, 1ml of 1.3M sucrose EDTA buffer, 1 ml of 0.5M sucrose EDTA buffer and 5ml of EDTA buffer without sucrose. The gradients were ultra-centrifuged for one hour at 4 °C in a SW41 swing rotor (Beckmann) at 24000 rpm (100000×g).

## Solid-state NMR

NMR spectra were recorded with a Bruker Advance-III 750 MHz wide bore NMR spectrometer. NMR samples were prepared by mild centrifugation of fresh cell or thylakoid suspensions into a 4mm NMR rotor that was used with a top insert. For cell samples, approximately 50mL of cell culture was used and concentrated into the rotor, from which we estimate that samples contained about 0.5mg of Chl. Magic Angle Spinning was performed at 5 kHz for whole cells and at 13 kHz for thylakoid extractions. Cross polarization (CP) experiments were performed with a 2ms CP contact time ( $\tau_{CP}$ ), 5s recycle delay and 20ms acquisition time,  $\omega_1^C/2\pi$  of 40.3 kHz and <sup>1</sup>H nutation frequency linearly ramped from 80 to 100 kHz. Insensitive Nucleus Enhanced Polarization Transfer (INEPT) experiments were performed with two delays of 1.25ms and an acquisition time of 80ms. For direct polarization (DP) experiments, the delay was set at 5s and the acquisition time was set to 43ms. The dead time after pulse excitation before acquisition was 4.5 microseconds. Data were processed and analyzed in TopSpin3.2 and MNova. Temperature were calibrated analyzing <sup>207</sup>Pb NMR chemical shifts of lead nitrate (Pb(NO<sub>3</sub>)<sub>2</sub>)<sup>26</sup>.

## Simulation of INEPT and CP intensities

CP and INEPT intensities relative to DP as function of rotational correlation time  $\tau_c$  and order parameter  $S$  were estimated by using the following equations taken from<sup>27-28</sup>:



$$\frac{I_{CP}}{I_{DP}} = \frac{\gamma_H}{\gamma_C} \frac{\exp\left(-\frac{\tau_{CP}}{T_{1\rho}^H}\right) - \exp\left(-\frac{\tau_{CP}}{T_{CH}}\right)}{1 - \frac{\tau_{CH}}{T_{1\rho}^H}}, \quad (1)$$

in which the gyromagnetic ratios of  $^1\text{H}$  and  $^{13}\text{C}$  are equivalent to 267.5 ( $10^6 \text{ rad S}^{-1} \text{ T}^{-1}$ ) and 67.2 ( $10^6 \text{ rad S}^{-1} \text{ T}^{-1}$ ), respectively,  $T_{1\rho}^H$  is the  $^1\text{H}$  spin-lattice relaxation time in the rotating frame,  $T_{CH}$  is the time constant for cross-polarization and  $\tau_{CP}$  is the contact time for cross polarization.

$$\frac{I_{INEPT}}{I_{DP}} = \frac{\gamma_H}{\gamma_C} n \sin(2\pi J_{CH}\tau) \sin(2\pi J_{CH}\tau') \cos^{n-1}(2\pi J_{CH}\tau') \exp\left(-\frac{2\tau}{T_2^H} - \frac{2\tau'}{T_2^C}\right), \quad (2)$$

in which  $n$  is the bond multiplicity,  $J_{CH}$  is the  $^1\text{H}$ - $^{13}\text{C}$  through bond scalar coupling constant, and  $T_2^H$  and  $T_2^C$  are the effective  $^1\text{H}$  and  $^{13}\text{C}$  transverse dephasing times. The DP intensities in the equation are the theoretical intensities assuming that total polarization relaxation occurs after each pulse. The coherence evolution times  $\tau=1/4J_{CH}$  and  $\tau'=1/6J_{CH}$  are delays between the radio frequency (rf) pulses in the INEPT sequence.  $T_2^H$ ,  $T_2^C$ ,  $T_{1\rho}^H$  and  $T_{CH}$  values were estimated from a rotational correlation function that describes time-averaged fluctuations of the local magnetic field due to chemical-bond vector reorientations, depending on  $\tau_c$  and  $S$  (see <sup>20</sup> and <sup>28</sup>). Experimental parameters that were used as input for the simulations were  $\tau_{CP}=2\text{ms}$ ,  $J_{CH}=133.3 \text{ Hz}$ ,  $\omega_1^C/2\pi=86 \text{ kHz}$ ,  $\omega_1^H/2\pi=40.3 \text{ kHz}$ ,  $\omega_0^C/2\pi=86 \text{ MHz}$ ,  $\omega_0^H/2\pi=188 \text{ MHz}$ ,  $\tau_S=1 \text{ ms}$ ,  $\omega_R=5 \text{ kHz}$  for cells and  $13 \text{ kHz}$  for isolated thylakoid membranes. Curves of the relative INEPT intensities as function of rotational correlation time  $\tau_c$  and order parameter  $S$  were generated using MathCad 15.0.

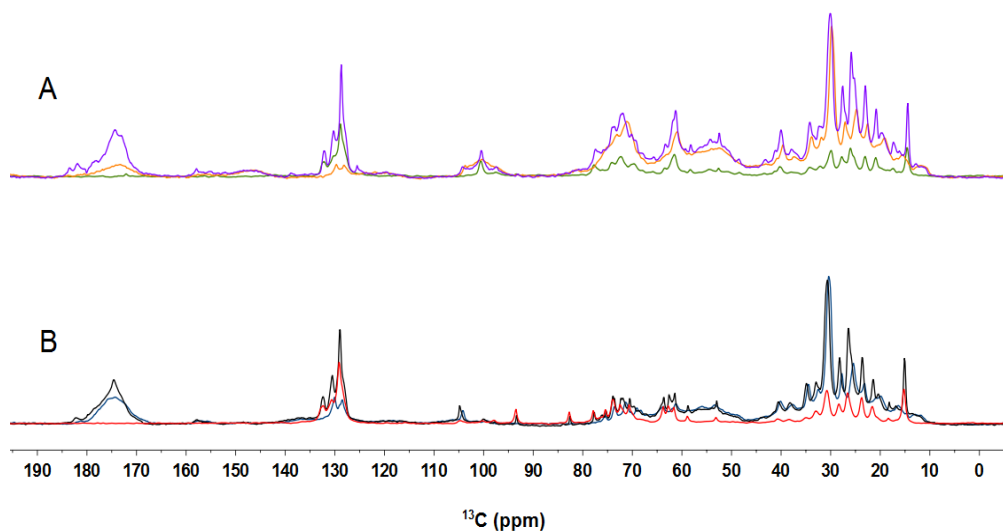
## Results and Discussion

---

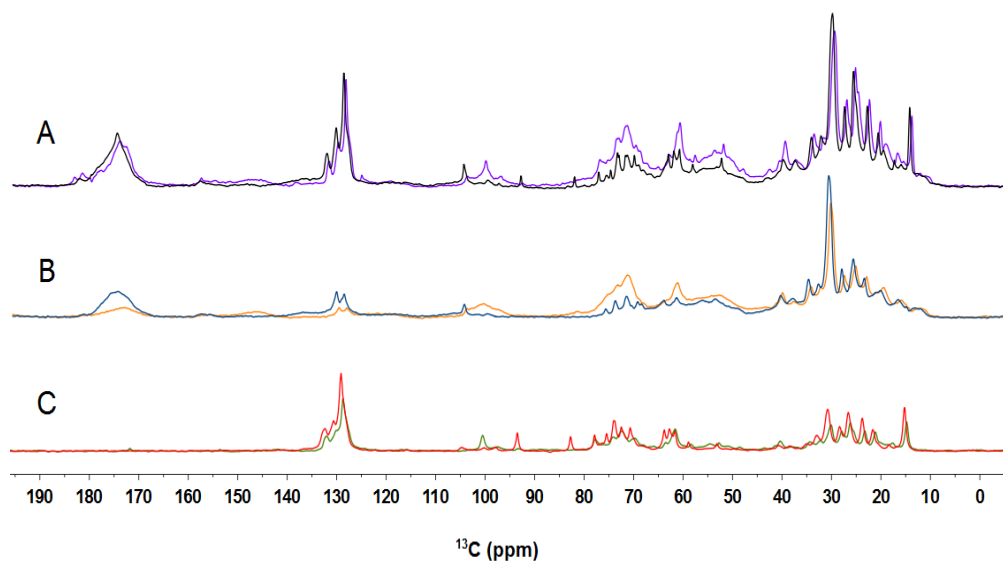
### Spectral editing and assignment of molecular constituents in *Cr.* intact cells

Figure 1A presents a DP, CP and INEPT  $^{13}\text{C}$  spectrum of *Cr.* cells. We performed an assignment of the most prominent peaks in the  $^{13}\text{C}$  spectra. Most of the assignments are based on the following references and are summarized in table 1 <sup>18, 29-32</sup>. Many assignments are ambiguous and peaks correspond with reported NMR resonances of more than one possible carbon atom type, as indicated. *Cr.* lipid composition consists of monogalactosyldiacylglycerol (MGDG), digalactosyldiacylglycerol (DGDG), sulfoquinovosyldiacylglycerol (SQDG), diacylglyceryltrimethylhomo-Ser (DGTS), phosphatidylglycerol (PG) and phosphatidylethanolamine (PE) in descending order of abundance, and in case of overlapping peaks we only specify fatty acid (FA) chain length and degree

of unsaturation, based on <sup>30</sup>. The region 10-40 ppm contains the protein side chain resonances that accumulate in a broad peak, together with the lipid FA CH<sub>2</sub> and CH<sub>3</sub> signals, which are the sharp peaks superimposed. The protein C<sub>α</sub> signals are visible between 50-70 ppm and partly overlap with carbohydrate signals that are visible in the region 70-100 ppm. The region 125-135 ppm contains the signals of the aromatic protein side chains and double-bonded CH signals of the lipid FA. The protein backbone carbonyl signals accumulate between 170-180 ppm. Chl and xanthophyll signals are relative weak and coincide with other peaks. Figure 1 presents DP, CP and INEPT <sup>13</sup>C spectra of *Cr.* whole cells (1A) and of thylakoid membranes (1B) and in figure 2 the spectrum of thylakoids and those of whole cells are superimposed for each type of NMR experiment. The lipid patterns in the aliphatic region (10-40 ppm) and aromatic region (125-135 ppm) are remarkably similar for both types of samples, which indicates that in whole cells, most of the lipids belong to the thylakoids. As expected, the signals from cell-wall components, starch or DGTS are absent in the spectra of thylakoids. The thylakoid membranes were purified with sucrose gradients, and signals in the region 70-100 ppm could originate from galactosyl lipid head groups but also from natural-abundant <sup>13</sup>C of the sucrose present in the buffer. Between 135-140 ppm a weak shoulder of the xanthophylls becomes visible in the DP and CP spectra of thylakoids. The protein carbonyl band has more intensity in the CP spectrum of thylakoids than in whole cells. This is because thylakoids contain membrane proteins that are relatively rigid and enhanced in CP, whereas intact cells contain a mixture of membrane and soluble proteins with higher mobility. The CH peaks of the unsaturated CH<sub>3</sub> fatty acids (FA) have much higher intensities in INEPT than in CP and the 132 ppm peak of the C16 carbons towards the FA end-tail are absent in CP, indicating that the majority of the CH<sub>3</sub> FA chains have low segmental ordering and highly dynamic FA tails.



**Figure 1.** **A:** Overlaid  $^{13}\text{C}$ -DP (purple),  $^{13}\text{C}$ -CP (orange) and  $^{13}\text{C}$ -INEPT (green) spectra of whole cells recorded at 13.5 °C. **B:** Overlaid  $^{13}\text{C}$ -DP (black),  $^{13}\text{C}$ -CP (blue) and  $^{13}\text{C}$ -INEPT (red) spectra of isolated thylakoids recorded at 13.5 °C.



**Figure 2.** Overlaid DP, CP and INEPT spectra of whole cells and thylakoids recorded at 13.5°C. **A:** DP spectra of whole cells (purple) and thylakoids (black). **B:** CP spectra of whole cells (orange) and thylakoids (blue). **C:** INEPT spectra of whole cells (green) and thylakoids (red).

Chemical shift (ppm)	Assignment	INEPT	CP	Reference
12.6	Ile C $\alpha$ ; xanth 9/13-Me		×	31, 33
14.6	lipid CH <sub>3</sub>	×		30, 34
21.0	lipid ( $\omega$ -1) CH <sub>2</sub> 18:3	×	×	30
23.2	Lipid ( $\omega$ -1) CH <sub>2</sub> 16:1/16:0	×	×	30
26.0	lipid C3	×	×	30,18
27.8	lipid C8 18:3	×	×	30
30.2	lipid $n$ CH <sub>2</sub>	×	×	34
32.5	lipid C14 16:1/16:0	×	×	30
34.5	lipid C2; Lut/Neo C1	×	×	30, 31
37.6	Chl P7/11 phy; glycoprotein C3; xanth C1	×	×	32, 31
40.1	Chl phytols P8/10/12; xanth C4	×	×	32, 31
52.6	glycoprotein C; PC C $\gamma$	×	×	18
61.7	Glyc C1/C3; glycoprotein C2	×	×	18, 34
63.5	Glyc C1/C3	×		18, 34
71.5	MGDG G3		×	18, 34
72.5	lipid G2/3/5, starch C2/5	×		18
73.6	lipid G2/3		×	18, 34
74.3	starch C3	×	×	18
78.0	glycoprotein C4	×		18
98.0	SQDG/DGDG G1	×	×	18, 34
100.5	DGDG G1, starch C1	×	×	18
104.2	MGDG G1; cell wall C1	×	×	18, 34
128.6	lipid C10 18:3	×	×	30
130.1	lipid C9/12/13 18:3	×	×	30, 31
132.0	lipid C16 18:3	×		30, 31
157.7	Arg C $\zeta$			33
171.9	lipid C1/CO	×		18
172.6	DGTS C1/CO			18
174.2	PG C1			18
181.7	Glu/Asp COO $\cdot$		×	33
183.1	Glu/Asp COO $\cdot$		×	33

**Table 1.** Chemical shift assignments. Crosses indicate that the peak is observed in the <sup>13</sup>C INEPT, resp. CP spectrum. Xanth: xanthophyll; Phy: Chl phytol chain; Lut: lutein; Neo: neoxanthin; Glyc: glycerol.

## Temperature dependence

The dynamic behavior of protein and lipid components was further explored by varying the temperature in a physiological range. For thylakoid membranes, the temperature was not raised above 23.3 °C to make sure that no irreversible damage would occur. For whole cells, the temperature was raised to 37.8 °C. To check if heating caused irreversible changes, the temperature was raised and lowered again after which samples were re-measured, verifying that no heating-induced changes had taken place (*data not shown*). We noticed a decrease of

signal intensity in DP spectra over time, which could be caused by the effect of magic-angle spinning, slowly sedimenting the cells at the rotor walls and changing the filling factor. To correct for time-dependent intensity changes, the CP and INEPT intensities were divided by the DP intensities of the respective peaks. Figure 3 presents the temperature-dependent CP over DP and INEPT over DP signal intensities of whole-cell spectral components and figure 4 presents the temperature curves obtained from thylakoid spectra. The intensities are normalized with respect to the intensity at 3 °C for better comparison. The thylakoid INEPT-observed components (4C) show an increase with temperature that seems to stabilize for around 20 °C for the CH and FA end-tail carbons. The thylakoid CP-observed components (4A, B) show a decrease of CP efficiencies with temperature except for the  $n\text{CH}_2$  carbons. Because INEPT signals are sensitive for highly mobile components and CP signals are enhanced for more rigid molecules, this behavior is in line with expected increase of mobility at higher temperatures. The whole-cell CP-observed components (3A, B) also show an overall decrease of CP efficiencies with temperature, but unexpectedly the INEPT-observed intensities (4C, D) only increase up to 13.5°C and stabilize or decrease at higher temperatures, suggesting that their dynamics is reduced.

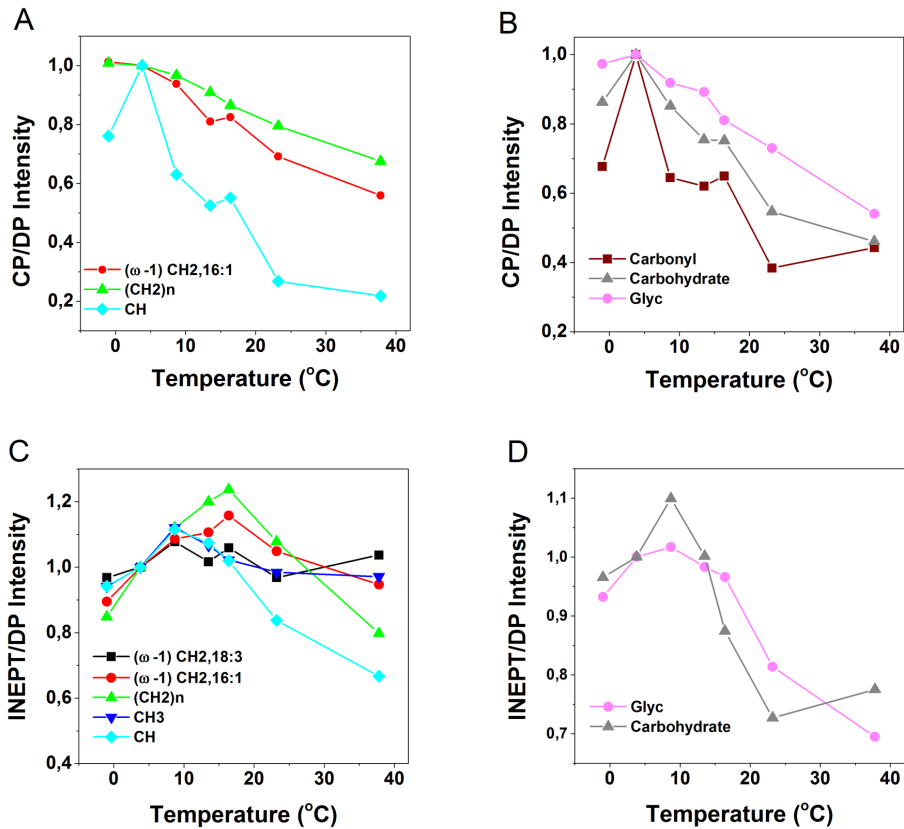


**Figure 3.** <sup>13</sup>C CP and INEPT intensities of whole-cell components as a function of temperature. The intensities are normalized at T=3 °C. **A:** CP intensities of fatty acids. Red circles: (ω-1) CH<sub>2</sub> of 16:1; green triangles: nCH<sub>2</sub>; light-blue squares: CH. **B:** CP intensities of protein carbonyls and carbohydrates. Dark-red squares: carbonyl; gray triangles: galactosyl and glycerol carbons (Galac) of glycerolipids; pink circles: glycoprotein and glycerol C1/C3 carbons (Glyc). **C:** INEPT intensities of fatty acids. Black squares: (ω-1) CH<sub>2</sub> of 18:3; red circles: (ω-1) CH<sub>2</sub> of 16:1; green triangles: nCH<sub>2</sub>; dark blue triangles: CH<sub>3</sub>; light blue squares: CH. **D:** INEPT intensities of protein carbonyls and carbohydrates. Grey triangles: galactosyl and glycerol carbons of glycerolipids; pink circles: glycoprotein and glycerol C1/C3 carbons

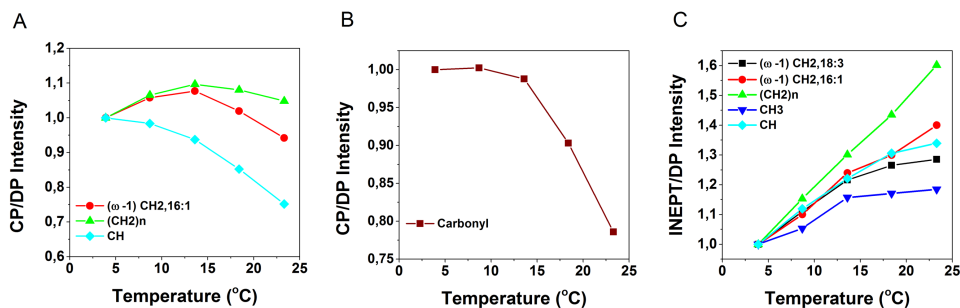


**Figure 4:**  $^{13}\text{C}$  CP-MAS and INEPT intensities of thylakoids as a function of temperature. **A:** CP intensities of fatty acids. Red circles:  $(\omega-1)$   $\text{CH}_2$  of 16:1; green triangles:  $n\text{CH}_2$ ; light-blue squares: CH. **B:** CP intensities of protein carbonyls. **C:** INEPT intensities of fatty acids. Black squares:  $(\omega-1)$   $\text{CH}_2$  of 18:3; red circles:  $(\omega-1)$   $\text{CH}_2$  of 16:1; green triangles:  $\text{CH}_2$ ; dark-blue triangles:  $\text{CH}_3$ ; light-blue squares: CH.

## Simulated INEPT and CP efficiencies

To gain more insight how the experimentally obtained INEPT and CP intensities related to molecular dynamics and segmental ordering, we simulated the INEPT and CP intensities as function of rotational correlation time  $\tau_C$  and order parameter  $S$ , using our experimental NMR parameters as input. In figure 5, we show the theoretical INEPT polarization transfer efficiency for a CH segment. Figure 5A and B present  $I_{\text{INEPT}}/I_{\text{DP}}$  as a function of correlation time ( $\tau_C$ ) and of order parameter ( $S$ ) at MAS frequency of 13 kHz (simulating the thylakoid experiment), and 5C and D present  $I_{\text{INEPT}}/I_{\text{DP}}$  calculated for a MAS frequency of 5 kHz (simulating the whole-cell experiment). At both MAS frequencies, INEPT starts to be effective for correlation times below 0.1  $\mu\text{s}$  ( $\tau_C < 0.1 \mu\text{s}$ ) and approaches a maximum ( $I_{\text{max}}$ ) at  $\tau_C < 1$  ns. In the sub-nanosecond dynamics range, the INEPT intensities only depend on the segmental order parameter  $S$ . At 13 kHz MAS, INEPT becomes effective at  $S < 0.2$ , while at 5 kHz, INEPT becomes effective at  $S < 0.05$ , and has a lower  $I_{\text{max}}$ . We performed the same analysis for  $\text{CH}_2$  and  $\text{CH}_3$  segments and summarized the results in table 2.

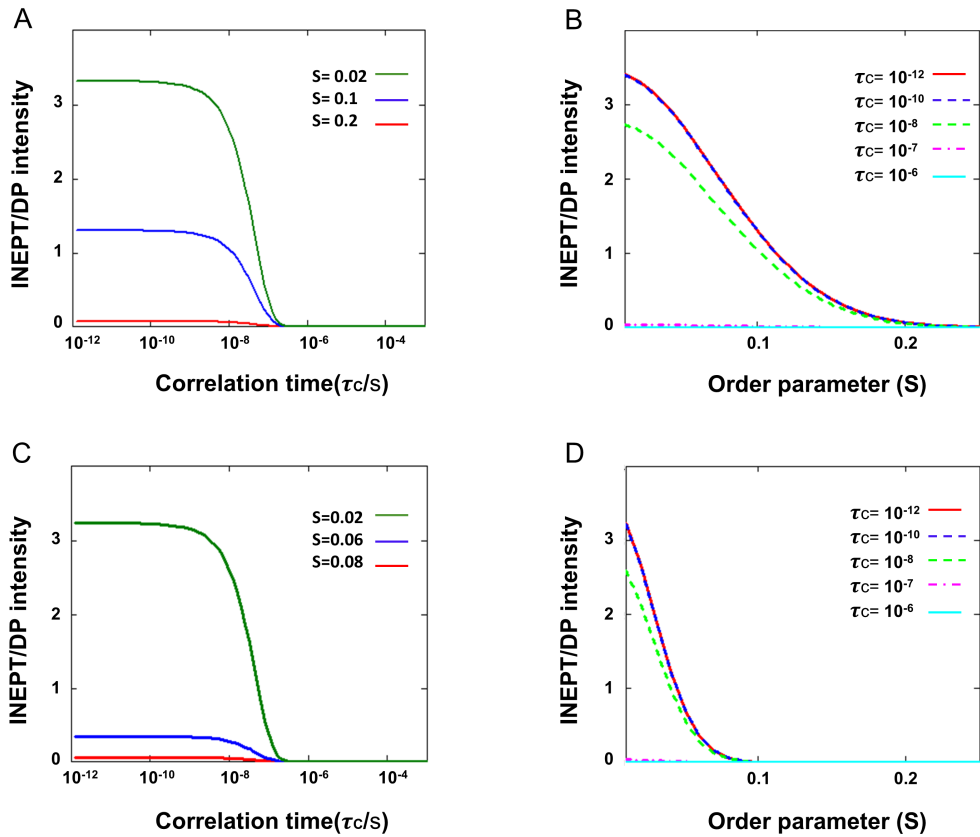


**Figure 5.** Simulated INEPT/DP intensities as a function of order parameter  $S$  and rotational correlation time  $\tau_C$  for a CH segment. **A:** INEPT/DP intensities for  $\omega_R=13$  kHz as function of  $\tau_C$  at  $S=0.2, 0.1$  and  $0.02$ . **B:** INEPT/DP intensities for  $\omega_R=13$  kHz as a function of  $S$  at  $\tau_C=10^{-12}, 10^{-10}, 10^{-8}, 10^{-7}$  and  $10^{-6}$  seconds. **C:** INEPT/DP intensities for  $\omega_R=5$  kHz as a function of  $\tau_C$  at  $S=0.08, 0.06$  and  $0.02$ . **D:** INEPT/DP intensities for  $\omega_R=5$  kHz as a function of  $S$  at  $\tau_C=10^{-12}, 10^{-10}, 10^{-8}, 10^{-7}$  and  $10^{-6}$  seconds.



Spinning frequency ( $\omega_R$ )		Correlation time ( $\tau_c$ )	Order parameter ( $S$ )
5kHz	CH	<0.1 $\mu$ s	<0.08
	CH <sub>2</sub>	<0.05 $\mu$ s	<0.05
	CH <sub>3</sub>	<0.05 $\mu$ s	<0.1
13kHz	CH	<0.1 $\mu$ s	<0.2
	CH <sub>2</sub>	<0.05 $\mu$ s	<0.1
	CH <sub>3</sub>	<0.05 $\mu$ s	<0.03

**Table 2.** Theoretical conditions for observing INEPT intensities at 5 kHz (simulating the whole-cell experiments) and 13 kHz (simulating the thylakoid experiments)

Figure 6 presents the theoretical  $I_{CP}/I_{DP}$  intensities as a function of correlation time for a CH segment. The predicted CP intensities were identical for 5 kHz and 13 kHz. Figure 6 shows that CP is effective for correlation times between nanoseconds and seconds, except for a gap in the microsecond range in which CP gives no signal. The same behavior as function of the correlation time is observed for different order parameter values ( $S=0.05, 0.1$  and  $0.5$ ) except that for  $S \geq 0.5$ , CP has non-zero intensity for sub-nanosecond  $\tau_c$  values. Hence, CP is effective for oriented molecules with restricted motions, even if they exhibit very fast dynamics.

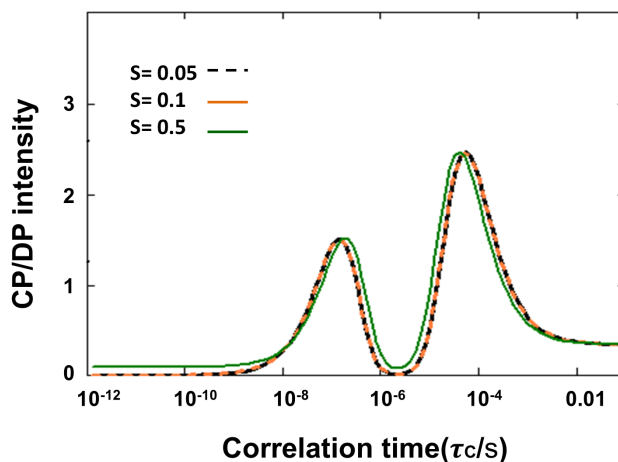


**Figure 6.** Simulated CP/DP intensities as a function of rotational correlation time  $\tau_c$  for  $S = 0.05, 0.1$  and  $0.5$ .

## Dynamics of *Cr.* cell and thylakoid molecular components

We used the simulations to estimate the dynamics of *Cr.* cell constituents, in particular of the lipids, of which signals are observed both in INEPT and CP. The simulated intensity ratios use  $I_{DP}$  assuming that DP is effective over the whole frequency range. The experimentally observed DP intensities however depend on  $T_1$  and on the delay time  $t_d$  between scans, so that  $I_{DP}/I_{DP}^{\text{theory}} = 1 - \exp(-t_d/T_1^C)$ . With our experimental settings we assume that DP intensities are attenuated for components with  $\tau_c > 1\mu\text{s}$ . Since the DP spectra show significant intensity for most of the cell and thylakoid components, we presume that these have dynamics in the sub-microsecond range. Comparing the spectral profiles of whole-cells and thylakoids (figure 2), we conclude that the whole-cell INEPT spectrum is dominated by the signals of the thylakoid lipids. The higher intensities observed for the thylakoid INEPT spectrum compared to the whole-cell INEPT spectrum, relative to the DP intensities (figure 1A and B) can be explained by the increased MAS frequency used for the thylakoid experiments that renders INEPT more efficient, as illustrated in the model. The largest  $n\text{CH}_2$  lipid peak at 30 ppm has similar intensity in CP and DP for both whole cells and thylakoids (figure 1A and B), conforming to  $I_{CP/DP} \sim 1$  in our model. Focusing on the sub-microsecond regime where DP is effective,  $I_{CP/DP} \sim 1$  matches with  $\tau_c$ 's in the order of 50 ns. In contrast to the  $n\text{CH}_2$  carbons, the CH carbons have much larger signals in INEPT than in CP, implying that they have conformational dynamics with  $\tau_c < 10$  ns and a large degree of disorder ( $S < 0.05$  for whole cells). The lipid CH carbons are the bended, lower part of the unsaturated FA chains, while the  $n\text{CH}_2$  FA carbons are located toward the lipid head groups. The lipid FA chains of the unsaturated lipids thus become more dynamic towards the end tails, which are disordered and undergo fast motions.

In the temperature profiles of the intact cells (figure 3), we observe overall a decay of the CP intensities for lipid (3A), and protein backbone and cell wall (3B) components at higher temperatures, indicating that the cell components have increased molecular motions. The lowest temperature point in the curves in figure 3 was close to zero Celsius, which could have led to non-linear temperature effects, and might explain the observed increase instead of decrease of CP signal between the two lowest temperature points. The INEPT-observed lipid signals (3C) increase for temperatures up to  $\sim 13$  °C, indicating that the lipid segments increase their conformational dynamics, or become more disordered. Above this temperature, the signals remain constant for the end-tail carbons, suggesting that their conformational dynamics enter the sub-nanosecond regime where INEPT becomes insensitive to further changes in dynamics, and that there is no change in lipid disorder. Interestingly, the INEPT-observed  $n\text{CH}_2$ , CH (3C) and galactosyl/glycerol (3D) signals clearly

decline at higher temperatures, suggesting that conformational dynamics of mobile lipid head groups and FA segments are suppressed. The lipid spectral profiles do not change with temperature and from analysis of lipid peak intensities we exclude significant changes in lipid unsaturation or isomerization. The reduced lipid dynamics at high temperatures could be associated with a phase transition in the membrane. The INEPT temperature curves suggest that there is a mechanism (phase transition or other) that effectively protects the photosynthetic membranes against extreme membrane fluidity at high temperatures, unrelated to lipid saturation or isomerization, which would be of interest to further explore.

The temperature profiles of the thylakoid sample (figure 4) cannot directly be compared to the whole-cell sample, because of the increased sensitivity for INEPT detection in the thylakoid experiment due to higher MAS frequency that was used, and because of the limited temperature range over which the thylakoid preparations could be recorded without thermal damage. In the overlapping temperature range, the overall dynamic behavior is similar. The relative INEPT intensities of the lipid signals in the thylakoid spectrum in this work (4C) are higher than observed in the study in chapter 2<sup>21</sup>, where we concluded that the major lipid fraction did not display fast dynamics, and only a small fraction of lipids had mobile FA tails. In chapter 2 we also observed larger effect of lipid isomerization with temperature. Here we observe only small effect of isomerization and find that the majority of the lipids have very flexible end tails. A difference in sample conditions was that in the former study the water content of the rotor sample preparations was lower, which could have reduced the lipid conformational dynamics. In addition, the thylakoid preparations studied in chapter 2 were from different strains and had been stored at -80°C before use, using glycerol as a cryo-protectant, whereas the thylakoid preparation in this study contained sucrose and was freshly prepared.

## Conclusion

---

We demonstrate that <sup>13</sup>C NMR spectral editing can identify lipid, protein, sugar and cell wall constituents and resolve and quantify molecular dynamics of different cellular components, in particular lipid FA, in intact photosynthetic cells. Sample preparation typically involved growing a 50ml *Cr.* culture for 2-3 days and using 1,2-<sup>13</sup>C acetate as a carbon source, which is very feasible both in terms of labor and label expenses. The presented spectra were each recorded with 64 scans, which typically takes about 10 minutes for scan accumulation.

However, we noticed that after rotor insertion, spectral changes occurred during MAS in the first 30-60 minutes, presumably due to slow sedimentation of cells on the rotor walls. Thus, the samples need to be spun for at least one hour in the rotor at the set spinning frequency before starting the measurements. MAS spinning did not break the cells at 5 kHz spinning frequency, which was checked afterward using an ordinary light microscope.

## References

---

1. Betterle, N.; Ballottari, M.; Zorzan, S.; de Bianchi, S.; Cazzaniga, S.; Dall'osto, L.; Morosinotto, T.; Bassi, R., Light-induced Dissociation of an Antenna Hetero-oligomer Is Needed for Non-photochemical Quenching Induction. *Journal of biological chemistry* **2009**, *284* (22), 15255-15266.
2. Cruz, J.; Avenson, T.; Kanazawa, A.; Takizawa, K.; Edwards, G.; Kramer, D., Plasticity in light reactions of photosynthesis for energy production and photoprotection. *Journal of experimental botany* **2005**, *56* (411), 395-406.
3. Erickson, E.; Wakao, S.; Niyogi, K. K., Light stress and photoprotection in *Chlamydomonas reinhardtii*. *Plant J* **2015**, *82* (3), 449-65.
4. Tardy, F.; Havaux, M., Thylakoid membrane fluidity and thermostability during the operation of the xanthophyll cycle in higher-plant chloroplasts. *Biochimica et biophysica acta* **1997**, *1330* (2), 179-93.
5. Lambrev, P. H.; Nilkens, M.; Miloslavina, Y.; Jahns, P.; Holzwarth, A. R., Kinetic and Spectral Resolution of Multiple Nonphotochemical Quenching Components in Arabidopsis Leaves. *Plant Physiology* **2010**, *152* (3), 1611-1624.
6. Włodarczyk, L. M.; Snellenburg, J. J.; Ihalainen, J. A.; van Grondelle, R.; van Stokkum, I. H.; Dekker, J. P., Functional Rearrangement of the Light-Harvesting Antenna upon State Transitions in a Green Alga. *Biophysical Journal* **2015**, *108* (2), 261-271.
7. Ünlü, C.; Drop, B.; Croce, R.; van Amerongen, H., State transitions in *Chlamydomonas reinhardtii* strongly modulate the functional size of photosystem II but not of photosystem I. *Proceedings of the National Academy of Sciences* **2014**, *111* (9), 3460-3465.
8. Amarnath, K.; Zaks, J.; Park, S. D.; Niyogi, K. K.; Fleming, G. R., Fluorescence lifetime snapshots reveal two rapidly reversible mechanisms of photoprotection in live cells of *Chlamydomonas reinhardtii*. *Proceedings of the National Academy of Sciences* **2012**, *109* (22), 8405-8410.
9. Kóta, Z.; Horváth, L. I.; Droppa, M.; Horváth, G.; Farkas, T.; Páli, T., Protein assembly and heat stability in developing thylakoid membranes during greening. *Proceedings of the National Academy of Sciences of the United States of America* **2002**, *99* (19), 12149-12154.
10. Szalontai, B.; Nishiyama, Y.; Gombos, Z.; Murata, N., Membrane dynamics as seen by Fourier transform infrared spectroscopy in a cyanobacterium, *Synechocystis* PCC 6803: The effects of lipid unsaturation and the protein-to-lipid ratio. *Biochimica et Biophysica Acta (BBA) - Biomembranes* **2000**, *1509* (1-2), 409-419.
11. Ruban, A. V.; Berera, R.; Ilioaia, C.; van Stokkum, I. H. M.; Kennis, J. T. M.; Pascal, A. A.; van Amerongen, H.; Robert, B.; Horton, P.; van Grondelle, R., Identification of a mechanism of photoprotective energy dissipation in higher plants. *Nature* **2007**, *450* (7169), 575-578.

12. Mullineaux, C. W.; Sarcina, M., Probing the dynamics of photosynthetic membranes with fluorescence recovery after photobleaching. *Trends in Plant Science* **7** (6), 237-240.
13. Krumova, S. B.; Koehorst, R. B. M.; Bóta, A.; Páli, T.; van Hoek, A.; Garab, G.; van Amerongen, H., Temperature dependence of the lipid packing in thylakoid membranes studied by time- and spectrally resolved fluorescence of Merocyanine 540. *Biochimica et Biophysica Acta (BBA) - Biomembranes* **2008**, *1778* (12), 2823-2833.
14. Krumova, S. B.; Dijkema, C.; de Waard, P.; Van As, H.; Garab, G.; van Amerongen, H., Phase behavior of phosphatidylglycerol in spinach thylakoid membranes as revealed by <sup>31</sup>P-NMR. *Biochimica et Biophysica Acta (BBA) - Biomembranes* **2008**, *1778* (4), 997-1003.
15. van Eerden, F. J.; de Jong, D. H.; de Vries, A. H.; Wassenaar, T. A.; Marrink, S. J., Characterization of thylakoid lipid membranes from cyanobacteria and higher plants by molecular dynamics simulations. *Biochimica et Biophysica Acta (BBA) - Biomembranes* **2015**, *1848* (6), 1319-1330.
16. van Eerden, F. J.; van den Berg, T.; Frederix, P. W. J. M.; de Jong, D. H.; Periolo, X.; Marrink, S. J., Molecular Dynamics of Photosystem II Embedded in the Thylakoid Membrane. *The Journal of Physical Chemistry B* **2017**, *121* (15), 3237-3249.
17. Ogata, K.; Yuki, T.; Hatakeyama, M.; Uchida, W.; Nakamura, S., All-Atom Molecular Dynamics Simulation of Photosystem II Embedded in Thylakoid Membrane. *Journal of the American Chemical Society* **2013**, *135* (42), 15670-15673.
18. Arnold, A. A.; Genard, B.; Zito, F.; Tremblay, R.; Warschawski, D. E.; Marcotte, I., Identification of lipid and saccharide constituents of whole microalgal cells by (1)(3)C solid-state NMR. *Biochim Biophys Acta* **2015**, *1848* (1 Pt B), 369-77.
19. Pham, Q. D.; Topgaard, D.; Sparr, E., Tracking solvents in the skin through atomically resolved measurements of molecular mobility in intact stratum corneum. *Proceedings of the National Academy of Sciences* **2017**, *114* (2), E112-E121.
20. Nowacka, A.; Mohr, P. C.; Norrman, J.; Martin, R. W.; Topgaard, D., Polarization Transfer Solid-State NMR for Studying Surfactant Phase Behavior. *Langmuir* **2010**, *26* (22), 16848-16856.
21. Azadi Chegeni, F.; Perin, G.; Sai Sankar Gupta, K. B.; Simionato, D.; Morosinotto, T.; Pandit, A., Protein and lipid dynamics in photosynthetic thylakoid membranes investigated by in-situ solid-state NMR. *Biochimica et Biophysica Acta (BBA) - Bioenergetics* **2016**, *1857* (12), 1849-1859.
22. Porra, R.J.; Thompson, w. A.; Kriedemann, P. E., Determination of accurate extinction coefficients and simultaneous equations for assaying chlorophylls a and b extracted with four different solvents: verification of the concentration of chlorophyll standards by atomic absorption spectroscopy *Biochimica et biophysica acta* **1989**, *975*, 384-394.
23. Lawson, C. L.; Hanson, R. J., *Solving least squares problems*. SIAM: 1995; Vol. 15.
24. Bro, R.; De Jong, S., A fast non-negativity-constrained least squares algorithm. *Journal of Chemometrics* **1997**, *11* (5), 393-401.
25. Chua, N. H.; Bennoun, P., Thylakoid membrane polypeptides of *Chlamydomonas reinhardtii*: wild-type and mutant strains deficient in photosystem II reaction center. *Proceedings of the National Academy of Sciences of the United States of America* **1975**, *72* (6), 2175-2179.
26. Guan, X.; Stark, R. E., A general protocol for temperature calibration of MAS NMR probes at arbitrary spinning speeds. *Solid State Nucl Magn Reson* **2010**, *38* (2-3), 74-6.
27. Nowacka, A.; Mohr, P. C.; Norrman, J.; Martin, R. W.; Topgaard, D., Polarization transfer solid-state NMR for studying surfactant phase behavior. *Langmuir* **2010**, *26* (22), 16848-56.

28. Nowacka, A.; Bongartz, N. A.; Ollila, O. H. S.; Nylander, T.; Topgaard, D., Signal intensities in  $1\text{H}$ - $^{13}\text{C}$  CP and INEPT MAS NMR of liquid crystals. *Journal of Magnetic Resonance* **2013**, *230*, 165-175.
29. Castro, V.; Dvinskikh, S. V.; Widmalm, G.; Sandström, D.; Maliniak, A., NMR studies of membranes composed of glycolipids and phospholipids. *Biochimica et Biophysica Acta (BBA) - Biomembranes* **2007**, *1768* (10), 2432-2437.
30. Coddington, J. M.; Johns, S. R.; Leslie, D. R.; Willing, R. I.; Bishop, D. G.,  $^{13}\text{C}$  Nuclear magnetic resonance studies of the composition and fluidity of several chloroplast monogalactosyldiacylglycerols. *Biochimica et Biophysica Acta (BBA) - Lipids and Lipid Metabolism* **1981**, *663* (3), 653-660.
31. Moss, G. P., Carbon-13 NMR Spectra of Carotenoids. In *Pure and Applied Chemistry*, 1976; Vol. 47, p 97.
32. Lötjönen, S.; Hynninen, P. H., Carbon-13 NMR spectra of chlorophyll a, chlorophyll a', pyrochlorophyll a and the corresponding pheophytins. *Organic Magnetic Resonance* **1983**, *21* (12), 757-765.
33. Markley, J. L.; Ulrich, E. L.; Berman, H. M.; Henrick, K.; Nakamura, H.; Akutsu, H., BioMagResBank (BMRB) as a partner in the Worldwide Protein Data Bank (wwPDB): new policies affecting biomolecular NMR depositions. *J Biomol NMR* **2008**, *40* (3), 153-5.
34. de Souza, L. M.; Iacomini, M.; Gorin, P. A.; Sari, R. S.; Haddad, M. A.; Sasaki, G. L., Glyco- and sphingophosphonolipids from the medusa *Phyllorhiza punctata*: NMR and ESI-MS/MS fingerprints. *Chem Phys Lipids* **2007**, *145* (2), 85-96.



# CHAPTER 6

---

General discussion and future prospects

---



Photosynthetic light harvesting complexes from plant and algae have the crucial role to capture the sunlight and transfer it to reaction centers for biochemical productions. Fluctuation in sunlight intensity is a challenge that plants face every day. To cope with this challenge, they develop complex protective mechanisms to protect themselves from photo-damage. The PhD research described in this thesis aimed to understand how the structural flexibility of photosynthetic light harvesting complex II effects on its function and how this can be controlled by membrane environments. In this light, obtaining atomic-level structures of these complexes under physiological conditions and in native environments is an essential step towards understanding the molecular mechanisms that regulate the excitation energy flow.

NMR spectroscopy has the advantage over crystallography that it is capable of studying conformational dynamics of membrane proteins in their native environments. *In-situ* and *in-cell* NMR spectroscopy allow to the researcher to simultaneously have an overview of membrane or cell chemical compositions and conformations (lipid isomers, degree of unsaturation). While *in-cell* or *in-situ* NMR spectroscopy for structure characterization is very challenging, several studies have been reported, for example solid-state NMR of recombinant-expressed PagL in *E. coli* whole cells and cell envelopes, *in-situ* NMR of the Chl-binding CsmA protein and Dynamic Nuclear Polarization NMR of proteins in native cellular membranes<sup>1-3</sup>. The *in-situ* NMR experiments reported in this thesis may serve as a steppingstone toward structural characterization of LHC pigment-protein complexes in their native environments.

## Dynamics of LHCII and the role of the membrane environment: from protein and lipids to cell

---

### *In-vitro*: LHCII

The conformational dynamics of LHCII is mainly studied via the spectroscopic characteristics of the pigments that are taken as reporters, resulting in lack of information on the dynamics of the protein helices and loops. However, with our NMR approach we obtained simultaneously a direct view of the protein, pigment, associated intrinsic lipids of LHCII and their dynamics.

Combining the NMR results together, we could detect flexible sites of LHCII that have not been resolved by crystallography and cryo-EM, including residues of the N-terminus and 2 Chl tails (**Chapter 3**). Our findings in **Chapter 3** of a flexible N terminus are in agreement with a reported MD study on membrane-

embedded LHCII and with an EPR-spin label study <sup>4</sup>. Interestingly, the suggested flexible sites in our study are in close proximity to carotenoid and Chl sites that have been proposed to be involved in excitation quenching <sup>5-9</sup>. The NMR signals of different Lhcbm polypeptides could be distinguished in our NMR study, which could not be distinguished in X-ray or cryo-EM studies (chapter 3). Selective Lhcbm mutants may be used in future to identify chemical shift contributions of the different polypeptide types <sup>10</sup>.

Moreover, we present the first study of the effect of Zea binding on the conformation and dynamics of LHCII (**Chapter 4**). Our NMR results on Zea binding LHCII from the *npq2* mutant reconstituted in a lipid bilayer reveal that Zea-LHCII binds many lipids that are immobilized and that protein dynamics is reduced compared to wildtype LHCII. In addition, evidences for structural change have been observed revealing that some parts of the Zea-containing LHCII folds into strands. Our novel results of reduced dynamics and strong lipid binding of Zea LHCII might be correlated with the reduced fluidity of Zea-accumulating thylakoid membranes that was observed in **Chapter 2**. Although our approach, where we did not perform a sequence-specific NMR assignment revealed interesting results on the conformational dynamics of LHCII in lipid environments, a sequential assignment will help to reveal site-specific structure and dynamics. This would require selective labeling of native LHCII that are extracted from *Cr.* or selective labeling of recombinant LHCII that is overexpressed in *E. coli*. However, for both approaches there are number of challenges. For *E. coli*, selective labeling methods are well established, however for *Cr.* selective labeling strategies would first have to be established. A challenge that recombinant expression of LHCII faces is the refolding of recombinant LHCII. The LHCII proteins expressed from *E. coli* come as inclusion bodies and should be refolded with pigments, and further purified to separate the refolded proteins from free pigments and unfolded proteins. Hence, obtaining NMR quantities (milligrams) of refolded LHCII may lead to long sample preparation time.

The conformational dynamics studies in **Chapter 3** and **4** were performed on proteoliposomes in conditions where the LHCII proteins were strongly fluorescence quenched due to the high protein to lipid ratio. An interesting study would be to investigate the conformational dynamics of LHCII under mild quenched conditions. Fluorescence quenching of LHCII in our preparations is induced by protein self-aggregation in liposomes <sup>11</sup>. Therefore dilution of the LHCII complexes in proteoliposomes would reduce the quenched state. This requires at least 10 times dilutions of protein content compared to the condition described in the **Chapter 3** and **4**. Therefore, the concentration might not be enough for the 2D <sup>13</sup>C-<sup>13</sup>C NMR measurements. However 1D CP and INEPT or

$^1\text{H}$ - $^{13}\text{C}$  HETCOR still could provide information on the effect of the protein to lipid ratio on the conformational dynamics of LHCII.

### ***In-situ*: thylakoid membrane**

We show that polarization transfer solid state NMR and biosynthetic isotope labeling methods have the ability for assessing protein and lipid molecular dynamics in native heterogeneous photosynthetic membranes, providing a microscopic picture on molecular components of thylakoid membranes (**Chapter 2**). Separation of the rigid and mobile components is possible by combining CP and INEPT based experiments. Our method has provided detailed information on molecular dynamics of protein, lipid and xanthophyll molecules in thylakoid membranes as a function of temperature and comparing wildtype and *Zea* accumulating membranes. Moreover, we demonstrate that the NMR signals of LHCII can be detected within native thylakoid membranes, which allowed us to explore the role of the native environment on the conformational dynamics of LHCII by comparing LHCII in native thylakoid membranes and in liposome membranes (**Chapter 3**). Our NMR results reveal that the dynamics of LHCII flexible sites are significantly suppressed in native thylakoid membranes. Current models for excitation migration assume that individual antenna proteins fluctuate between quenched and unquenched states. Our observation that the intrinsic dynamics of LHCII is constrained in native membranes raises questions by this view and suggests that environmental changes are necessary to enable their conformational switching.

For the purpose of studying active membranes on which only rapid, 1D experiments can be performed in order to maintain their states, a limitation is the lack of sensitivity for detection of specific proteins. In that respect, FRAP is more selective for study of light-harvesting protein mobility, but has limited spatial resolution since lateral diffusion is measured over long distances, while NMR detects rotational diffusion of molecules with atomistic resolution. Our *in-situ* NMR approach can be further exploited by integration with selective mutation or labeling strategies. *In-situ* NMR studies that are aimed at structural characterization of a target protein generally rely on genetic manipulation to reduce the background signals of other cellular or membrane components. Recently, a chloroplast biosynthesis induction/repression system was reported to create minimal cells with stripped thylakoid membranes containing LHCII as the only Chl-binding protein <sup>12</sup>. Such a system could be used to more selectively probe the dynamic behavior of LHCII in a membrane or cellular environment. Selective  $^{13}\text{C}$  *in-vivo* labeling of Chls could be achieved by addition of  $\delta$ -aminolevulinic acid to the cell growth medium <sup>13</sup>, which would amplify the Chl signals with respect to the lipid and membrane background. Another interesting direction would be to perform *in-situ* NMR on LHCII,

comparing thylakoid membranes of cells grown under different light conditions to study the effect of environmental conditions at the protein level.

Furthermore, our NMR method can be combined with other spectroscopic techniques such as fluorescence, EPR, electron microscopy and Raman as complementary methods for quantitative analysis of protein and lipids structure and dynamics.

### ***In-cell*: thylakoid membrane dynamics in intact *Cr.* algae**

Polarization transfer NMR was successfully extended to whole cells (**Chapter 5**) providing a molecular picture of cell components in intact *Cr.* cells. Intact *Cr.* cells and isolated thylakoid membranes share very similar NMR lipid spectral profiles, demonstrating that the lipid NMR profiles in the spectra of *Cr.* cells are dominated by thylakoid lipids. This suggests that their molecular conformation and dynamics can be determined inside intact cells. The intrinsic dynamics of protein and lipid constituents was measured over a physiological temperature range. An overall increase of mobility was observed for the cell components with increasing temperature up to 13 °C Celsius. However, at higher temperatures, the dynamics of the lipids decreased or stabilized, which may suggest the existence of a protective mechanism in the membrane that prevents the membrane from extreme fluidity. In addition to the temperature dependence NMR analysis, simulated INEPT and CP NMR intensities provided quantitative information on values or ranges of order parameters and rotational correlation times of the lipid components, which may provide input for coarse-grain and molecular dynamics simulations.

In this thesis, cells were grown on a moderate light using acetic acid as carbon source, however different growth conditions such as high light, different CO<sub>2</sub> concentrations or salt stress could be tested in future to investigate the effect of various environmental conditions on dynamics of cell components.

For the *in cell* NMR experiments, the stability and physiological state of cells during the measurements has to be controlled. Controlling the physiological states of *Cr.* cells during NMR experiments could be a problem since without light and oxygen, the cells can switch on fermentation<sup>14</sup>. Further research is required to test and verify under which conditions *in-cell* NMR can best be performed.

## References

---

1. Renault, M.; Tommassen-van Boxtel, R.; Bos, M. P.; Post, J. A.; Tommassen, J.; Baldus, M., Cellular solid-state nuclear magnetic resonance spectroscopy. *Proceedings of the National Academy of Sciences* **2012**, *109* (13), 4863-4868.
2. Kulminskaya, N.; Miller, M.; Pedersen, M.; Bjerring, M.; Underhaug, J.; Pedersen, M.; Bjerring, M.; Underhaug, J.; Nielsen, N.; Frigaard, N.-U.; Nielsen, J., In Situ Solid-State NMR Spectroscopy of Protein in Heterogeneous Membranes: The Baseplate Antenna Complex of *Chlorobaculum tepidum*. *Angewandte Chemie (International ed.)* **2012**, *51* (28), 6891-6895.
3. Yamamoto, K.; Caporini, M.; Im, S.-C.; Waskell, L.; Ramamoorthy, A., Cellular solid-state NMR investigation of a membrane protein using dynamic nuclear polarization. *Biochimica et biophysica acta. Biomembranes* **2015**, *1848* (1 Pt B), 342-349.
4. Fehr, N.; Dietz, C.; Polyhach, Y.; von Hagens, T.; Jeschke, G.; Paulsen, H., Modeling of the N-terminal Section and the Luminal Loop of Trimeric Light Harvesting Complex II (LHCII) by Using EPR. *J Biol Chem* **2015**, *290* (43), 26007-20.
5. Park, S.; Fischer, A. L.; Steen, C. J.; Iwai, M.; Morris, J. M.; Walla, P. J.; Niyogi, K. K.; Fleming, G. R., Chlorophyll-Carotenoid Excitation Energy Transfer in High-Light-Exposed Thylakoid Membranes Investigated by Snapshot Transient Absorption Spectroscopy. *J Am Chem Soc* **2018**, *140* (38), 11965-11973.
6. Bode, S.; Quentmeier, C. C.; Liao, P.-N.; Hafi, N.; Barros, T.; Wilk, W.; Bittner, F.; Walla, P. J., On the regulation of photosynthesis by excitonic interactions between carotenoids and chlorophylls. *PNAS* **2009**, *106*, 12311-12316.
7. Ruban, A. V.; Berera, R.; Iliaia, C.; van Stokkum, I. H.; Kennis, J. T.; Pascal, A. A.; van Amerongen, H.; Robert, B.; Horton, P.; van Grondelle, R., Identification of a mechanism of photoprotective energy dissipation in higher plants. *Nature* **2007**, *450* (7169), 575-8.
8. Holt, N. E.; Zigmantas, D.; Valkunas, L.; Li, X.; Niyogi, K.; Fleming, G. R., Carotenoid Cation Formation and the Regulation of Photosynthetic Light Harvesting. *Science* **2005**, *307*, 433-436.
9. Barros, T.; Royant, A.; Standfuss, J.; Dreuw, A.; Kuhlbrandt, W., Crystal structure of plant light-harvesting complex shows the active, energy-transmitting state. *EMBO J* **2009**, *28* (3), 298-306.
10. Ferrante, P.; Ferrante, P.; Ballottari, M.; Bonente, G.; Giuliano, G.; Bassi, R., LHCBM1 and LHCBM2/7 Polypeptides, Components of Major LHCII Complex, Have Distinct Functional Roles in Photosynthetic Antenna System of *Chlamydomonas reinhardtii*. *Journal of biological chemistry* **2012**, *287* (20), 16276-16288.
11. Crisafi, E.; Pandit, A., Disentangling protein and lipid interactions that control a molecular switch in photosynthetic light harvesting. *Biochim Biophys Acta* **2017**, *1859* (1), 40-47.
12. Dinc, E.; Ramundo, S.; Croce, R.; Rochaix, J. D., Repressible chloroplast gene expression in *Chlamydomonas*: A new tool for the study of the photosynthetic apparatus. *Biochimica et biophysica acta. Bioenergetics* **2014**, *1837* (9), 1548-1552.
13. Janssen, G. J.; Daviso, E.; van Son, M.; de Groot, H. J. M.; Alia, A.; Matysik, J., Observation of the solid-state photo-CIDNP effect in entire cells of cyanobacteria *Synechocystis*. *Photosynthesis Research* **2010**, *104* (2-3), 275-282.
14. Mus, F.; Dubini, A.; Seibert, M.; Posewitz, M. C.; Grossman, A. R., Anaerobic acclimation in *Chlamydomonas reinhardtii*: anoxic gene expression, hydrogenase induction, and metabolic pathways. *J Biol Chem* **2007**, *282* (35), 25475-86.

# APPENDICES

---

Summary

Samenvatting

Curriculum vitae

Publications

Acknowledgement

---

## Summary

---

Light-Harvesting Complex II (LHCII) is responsible for light absorption and excitation energy transfer in plants and photosynthetic algae, while in high light it undergoes conformational changes by which it quenches excitations to prevent photodamage. The underlying molecular picture of these conformational changes has not yet been resolved. The main target of the research described in this thesis is to address the conformational dynamics of photosynthetic Light Harvesting Complex II and the role of the membrane environment. Hereto, I explored NMR-based methods that could eventually probe the molecular structure and dynamics of photosynthetic components *in-vivo* in functional membranes or cell systems.

In **Chapter 1**, a general introduction to photosynthetic antenna complexes and photoprotection mechanisms is presented. I further describe the methodological background of Nuclear Magnetic Resonance (NMR) spectroscopy and cross polarization (CP) and insensitive nuclei enhanced by polarization transfer (INEPT) based NMR dynamic spectral editing methods.

CP and INEPT polarization transfer solid-state NMR methods complemented with biosynthetic isotope labeling and NMR relaxation methods are successfully employed in **Chapter 2** for determining protein and lipid molecular dynamics in native thylakoid membranes. Our results provide a microscopic dynamic picture of thylakoid membranes of wild-type (WT) and the zeaxanthin (Zea)-accumulating *npq2* mutant of *Chlamydomonas reinhardtii* (*Cr.*). For both WT and *npq2* thylakoid membranes a larger fraction of ordered lipids than of mobile lipids is observed, which indicates that the majority of the lipids are immobilized within or between supercomplexes. In addition, lipid isomerization from all-trans to trans-gauche configurations is detected at higher temperatures for both WT and *npq2* thylakoid membranes. It is found that *npq2* membranes have more rigid xanthophylls and contain a fraction of rigid proteins and ordered lipids that are less sensitive to temperature changes than for the WT. This suggests an overall rigidity of the thylakoid membranes due to Zea accumulation, and the xanthophyll thus plays a role in membrane stabilization.

To investigate the plasticity of LHCs and the role of the thylakoid environment in controlling their light-harvesting function, it is essential to study their dynamic behavior in their native membrane environments. In **Chapter 3**, 2D CP and INEPT based experiments are employed to obtain detailed insight into conformational dynamics of LHCII in reconstituted membranes and in native thylakoid membranes. Interestingly, the NMR responses of LHCII can be detected within native thylakoid membranes and chemical shifts of selective spin systems can be partially assigned. Moreover, lipid signals and signals from

different Lhcbm polypeptides are identified by comparing the 2D  $^{13}\text{C}$  NMR spectra of LHCII reconstituted in lipid bilayers and of whole thylakoid membranes. Different protein-associated glycolipids are distinguished based on their galactosyl head  $^{13}\text{C}$ - $^{13}\text{C}$  correlation signals. It is found that LHCII has significantly reduced flexibility in native thylakoid membranes compared to reconstituted membranes, emphasizing the importance of the native membrane environment. Membrane-reconstituted LHCII contains flexible sites located in the N- or C-terminus and, based on its flexibility, may undergo thermally-induced conformational transitions, allowing reversible switching between light-harvesting and quenched states. However, since LHCII has significantly reduced flexibility in native, stacked thylakoid membranes, the occurrence of spontaneous transitions *in vivo* is questionable. The detected dynamic sites in LHCII are in close proximity to the xanthophyll-cycle carotenoid and lutein 2 molecules, which have been proposed to be involved in excitation quenching in the photoprotective state.

In chapter 2, the effect of *Zea* accumulation on thylakoid membrane dynamics is described. The effect of *Zea* exchange on LHCII internal molecular dynamics is further explored in **Chapter 4** by comparing monomeric *Zea*-containing LHCII of *npq2* with WT trimeric LHCII. Interestingly, on a protein level, *Zea* exchange leads to an overall reduced dynamics of the protein and to binding of many lipids. Moreover, it was observed that *npq2* LHCII containing *Zea* adopts a different fold than WT LHCII in a lipid bilayer. Several Ser residues fold into strands and the NMR spectra of *npq2* LHCII lack three Ala signals that are attributed to the Ala in the N-terminus, suggesting that either the presence of *Zea* or the effect of monomerization changes the N-terminal fold. These results suggest that conformational changes of LHCII upon *Zea* binding may cause the overall rigidity of thylakoid membranes that is reported in chapter 2.

The polarization-transfer dynamic spectral editing NMR approaches are extended for screening of photosynthetic cell components in **Chapter 5**. We succeeded in distinguishing the signals from lipid head-groups,  $\text{CH}_2$  and  $\text{CH}$  carbons of the lipid tails, protein backbone and side chain, and carbohydrates of cell wall components. Remarkable similarities are observed between the lipid NMR signals in  $^{13}\text{C}$  spectra of thylakoid membranes and the lipid response in spectra of whole *Cr.* cells. This suggests that the majority of the cellular lipids are incorporated in the thylakoid membranes and that those can be detected against the background of other cellular components, which enabled us to perform an *in-vivo* analysis of the thylakoid lipid properties. Insights in membrane thermodynamics have been obtained by collecting spectra over a physiological temperature range. Quantitative analysis of the molecular dynamics of thylakoid components and cellular constituents are provided by



comparing the experimentally recorded NMR spectra of *Cr.* cells and thylakoid membranes with simulated INEPT and CP intensities as function of order parameter and rotational correlation times.

Finally, in **Chapter 6**, a general discussion on the results is presented in the context of existing literature, and perspectives for future research are presented.

## Samenvatting

---

*Light-Harvesting Complex II* (LHCII) is verantwoordelijk voor lichtabsorptie en excitatie-energieoverdracht in planten en fotosynthetische algen, maar bij te veel licht ondergaat het conformationele veranderingen waardoor het excitaties dissipeert om zo lichtschade te voorkomen. Het onderliggende moleculaire beeld van deze conformationele veranderingen is nog niet opgehelderd. Het doel van het onderzoek beschreven in dit proefschrift is om de conformationele dynamica van het fotosynthetische *Light Harvesting Complex II* en de rol van de membraanomgeving te onderzoeken. Hiertoe heb ik NMR-gebaseerde methoden verkend die uiteindelijk de moleculaire structuur en dynamica van de fotosynthetische componenten *in vivo* kunnen meten in functionele membranen of celsystemen.

In **Hoofdstuk 1** wordt een algemene introductie gegeven over fotosynthetische antennecomplexen en fotoprotectiemechanismen. Ik beschrijf verder de methodologische achtergrond van kernspin resonantie (*Nuclear Magnetic Resonance*, NMR) spectroscopie en de op *cross polarization* (CP) en INEPT (insensitive nuclei enhanced by polarization transfer) gebaseerde NMR dynamische spectrale bewerkingsmethoden.

CP en INEPT polarisatieoverdracht vaste-stof NMR-methoden aangevuld met biosynthetische isotopen verrijking en NMR-relaxatiemethoden worden met succes toegepast in **Hoofdstuk 2** voor het bepalen van eiwit- en lipide moleculaire dynamica in natieve thylakoïde membranen. Onze resultaten bieden een microscopisch dynamisch beeld van thylakoïde membranen van wildtype (WT) en van de zeaxanthine (*Zea*)-accumulerende *npq2* mutant van *Chlamydomonas reinhardtii* (*Cr.*). Voor zowel WT als *npq2* thylakoïde membranen wordt een grotere fractie van geordende lipiden dan van mobiele lipiden waargenomen, wat aangeeft dat de meerderheid van de lipiden binnen of tussen supercomplexen is geïmmobiliseerd. Bovendien is het mogelijk om lipide-isomerisatie te detecteren van all-trans naar trans-gauche configuratie bij hogere temperaturen, voor zowel WT als *npq2* thylakoïde membranen. Daarnaast is gevonden dat *npq2* membranen meer rigide xanthofylen en een fractie van rigide eiwitten bevatten alsmede geordende lipiden die minder gevoelig zijn voor temperatuurveranderingen. Dit suggereert een algehele stijfheid van de thylakoïde membranen als gevolg van *Zea* accumulatie, en dit xanthofyl speelt dus een rol bij membraanstabilisatie.

Om de plasticiteit van LHC's en de rol van de thylakoïde omgeving in het controleren van hun functie om licht te oogsten te onderzoeken, is het essentieel om hun dynamisch gedrag in hun eigen membraanomgevingen te bestuderen. In **Hoofdstuk 3** worden 2D CP- en INEPT-gebaseerde experimenten gebruikt

om gedetailleerd inzicht te verkrijgen in conformationele dynamica van LHCII in gereconstitueerde membranen en in natieve thylakoïde membranen. Interessant is dat de NMR-signalen van LHCII kunnen worden detecteerd in natieve thylakoïde membranen en dat de chemische verschuivingen in selectieve spin-systemen gedeeltelijk kunnen worden toegekend. Bovendien kunnen lipide signalen en signalen van verschillende Lhcbm-polypeptiden worden geïdentificeerd door vergelijking van de 2D  $^{13}\text{C}$  NMR-spectra van LHCII gereconstitueerd in een lipide bilaag en van gehele thylakoïde membranen. Verschillende eiwit-geassocieerde glycolipiden worden onderscheiden op basis van hun galactosyl  $^{13}\text{C}$ - $^{13}\text{C}$  correlatiesignalen. De flexibiliteit van LHCII in natieve thylakoïde membranen is aanzienlijk verminderd in vergelijking met LHCII in gereconstitueerde membranen, wat het belang van de natuurlijke membraanomgeving benadrukt. Membraan-gereconstitueerde LHCII bevat flexibele delen gelokaliseerd in de N- of C-terminus. Het zou, op basis daarvan, thermisch geïnduceerde conformationele overgangen kunnen ondergaan, waardoor reversibel schakelen tussen licht-oogstende en licht-dovende staten mogelijk is. LHCII heeft echter aanzienlijk minder flexibiliteit in natieve, gestapelde thylakoïde membranen, waardoor het de vraag is of spontane overgangen plaatsvinden *in vivo*. De gedetecteerde dynamische sites in LHCII bevinden zich in de nabijheid van de xantofyl-cyclus carotenoïde en van luteïne 2,, waarvan is voorgesteld dat ze betrokken zijn bij licht uitdoving in de fotoprotectie toestand.

In hoofdstuk 2 wordt het effect van *Zea* accumulatie op thylakoid membraan dynamica beschreven. Het effect van *Zea* uitwisseling op de interne moleculaire dynamica van LHCII wordt verder onderzocht in **Hoofdstuk 4** door monomere *Zea*-houdend LHCII van *npq2* te vergelijken met WT trimere LHCII. Interessant is dat *Zea* uitwisseling op eiwitniveau leidt tot een algeheel verminderde dynamiek van het eiwit en tot binding van veel lipiden. Bovendien is waargenomen dat *Zea*-houdend *npq2* LHCII anders gevouwen is dan WT LHCII in een lipide bilaag. Verschillende Ser residuen vouwen tot strengen en de NMR spectra van *npq2* LHCII missen drie Ala signalen die worden toegeschreven aan de Ala in de N-terminus, wat suggereert dat ofwel de aanwezigheid van *Zea* danwel het effect van monomerisatie de vouwing van de N terminus verandert. Deze resultaten suggereren dat conformationele veranderingen van LHCII na het binden van *Zea* algehele stijfheid van thylakoïde membranen zoals beschreven in hoofdstuk 2 kunnen veroorzaken.

De op polarisatie-overdracht gebaseerde dynamische spectrale bewerkings-NMR experimenten worden uitgebreid voor het screenen van fotosynthetische cel-componenten in **Hoofdstuk 5**. We zijn erin geslaagd om de signalen van lipide kopgroepen,  $\text{CH}_2$ - en  $\text{CH}$ -koolstofatomen van de lipide staarten, eiwit

backbone en zijketens, en koolhydraten van celwand componenten te onderscheiden. Opmerkelijke overeenkomsten worden waargenomen tussen de lipide NMR-signalen in  $^{13}\text{C}$  spectra van thylakoïde membranen van gehele *Cr.* cellen. Dit suggereert dat de meerderheid van de cellulaire lipiden is opgenomen in de thylakoïde membranen en dat deze kunnen worden gedetecteerd tegen de achtergrond van andere cellulaire componenten, wat ons in staat stelt om thylakoïde lipide-eigenschappen te analyseren *in vivo*. Inzichten in membraan thermodynamica zijn verkregen door spectra op te nemen over een fysiologisch temperatuurbereik. Kwantitatieve analyse van de moleculaire dynamica van thylakoïde componenten en van cellulaire bestanddelen is verkregen door vergelijking van de experimenteel bepaalde NMR spectra met gesimuleerde INEPT- en CP- NMR intensiteiten als functie van de orde parameter en van rotationele correlatietijden.

Ten slotte wordt in **Hoofdstuk 6** een algemene discussie over de resultaten gepresenteerd in de context van bestaande literatuur, en worden perspectieven voor toekomstig onderzoek gepresenteerd.

## Curriculum vitae

---

I was born and grown up in the mountain city of Khorramabad in Iran where I completed schooling. After the high school period, I decided to pursue my university studies in the field of Physics. In 2011, I received my master degree in Solid State Physics from Iran University of Science and Technology (IUST) in Tehran. Following the completion of my master program, I taught a wide range of theoretical and practical bachelor courses as a guest lecturer at Azad University of Parand in Tehran province. In 2013, I moved to Germany to perform research on Raman microscopy and spectroscopy on nanosystems in the group of Prof. Peter Lemmens at the Technical University of Braunschweig. A year later, in 2014, I joined the Solid-State NMR group in the Leiden Institute of Chemistry to work on the doctoral project described in this thesis under supervision of Dr. Anjali Pandit and Prof. Huub de Groot.

During my PhD program, my research was selected for oral presentations at several scientific conferences including the Light-Harvesting satellite meeting of the 17<sup>th</sup> International Congress on Photosynthesis Research (Egmond aan Zee, 2016), CHAINS (Veldhoven, 2016), 52<sup>th</sup> NMR-DG meeting (Geleen, 2017) and round-table discussions at 10<sup>th</sup> Alpine conference on Solid-State NMR (France, 2017). During the Alpine conference, I had the opportunity to chair two round table discussions. My research has also been presented as posters at the Dutch Biophysics meetings (Veldhoven, 2014 and 2018), 5<sup>th</sup> EBSA Solid-State NMR school (Munich, 2014), CHAINS (Veldhoven, 2015), EUROMAR (Prague, 2015), International school of Pure and Applied Biophysics “Molecular and Biophysical Aspects of Photosynthesis” (Venice, 2016), 17<sup>th</sup> International Congress on Photosynthesis Research (Maastricht, 2016) and the 50<sup>th</sup> and 51<sup>th</sup> NMR-DG meetings (Utrecht, 2015 and Wageningen, 2016). In addition, in 2017, I was awarded an ISMAR student travel stipend to participate and present my research at the 20<sup>th</sup> ISMAR conference in Quebec, Canada.

## Publications

---

- 1) **Azadi Chegeni. F, Faizabadi. E**, Quantum conductance of three-terminal nanoring in the presence of Rashba interaction, *International Journal of Applied Physics and Mathematics* (2011), 1 (3), 155.
- 2) **Azadi-Chegeni. F, Perin. G, Simionata. D, Morosinoto. T, Pandit. A**, Protein and lipid dynamics in photosynthetic thylakoid membranes investigated by *in-situ* solid-state NMR, *(BBA) Bioenergetics* (2016), 1857 (12), 1849-1859.
- 3) **Azadi-Chegeni. F, Schiphorst. C, Pandit. A**, *In-vivo* NMR as a tool for probing molecular structure and dynamics in intact *Chlamydomonas reinhardtii* cells, *Photosynthesis Research* (2017), 135 (1-3), 227-237.
- 4) **Azadi-Chegeni. F, Ward. E. M, Perin. G, Simionata. D, Morosinoto. T, Baldus. M, Pandit. A**, Conformational dynamics of a light-harvesting complex in native thylakoid membranes. *bioRxiv*, 288860.
- 5) **Azadi-Chegeni. F, Ward. E. M, Perin. G, Morosinoto. T, Baldus. M, Pandit. A**, Effect of zeaxanthin on ligh-harvesting complex II in a lipid bilayer, In preparation.

## Acknowledgment

---

PhD is a journey. Now, I have arrived at the end of this journey and, of course, this achievement could not have been possible without the aid and support of many people.

First and foremost, I would like to express my sincere gratitude to Dr. Anjali Pandit for providing me the opportunity to complete my PhD in her group, and also for her dedication, guidance, and support during this period. I also thank Prof. Huub de Groot for promoting my PhD and for his insightful comments on my PhD thesis.

I am profoundly grateful to my collaborators Dr. Tomas Morosinoto, Dr. Giorgio Perin, and Dr. Diana Simionata from University of Padova, and Prof. Marc Baldus and Dr. Meaghan Ward from Utrecht University for their contribution to my research projects and valuable discussions.

My special gratitude to the SSNMR members. Karthick, I still remember the first days of my PhD, I think you do too, you helped me make a smooth transition into a new field. Our discussions and chats about food and news during NMR experiments are memorable. Brijith, Emanuela, Rubin and Maithili, thank you for being great officemates and friends, for all discussions and for the fun we have had together over the last years. Liesbeth, you are truly the heart of our group and always friendly and helpful. Vidya, Zhongwu, Franco, Fons, Yohan, Ximmeng, Yang, Yuliya, Jan Paul, Faezeh, Agur, Remco, Christo, Alia, Laura, Lijin, Dieuwertje, Jessica, Adriano, Thomas, and Robin, thank you all.

I was fortunate to have many friends outside the university who shed more light on my life. I want to thank my amazing friends in the “Gezellig” group, you are important to me. Elham, you are like a sister. Behrouz, your positive energy is always inspiring, keep it up. Special thanks to my Dutch teacher and classmates, I have had many happy moments because of being with you.

Heartfelt thanks go to my parents and siblings. Thank you for supporting me throughout my life. There are no words to convey how much I am grateful for your love and encouragement.

Khosrow, thank you for giving me your unfailing love and thank you for being my best friend and a supportive husband. You always helped me and stood by my side to get through this period.

Fatemeh Azadi Chegeni

January 2019